NASA Contractor Report 4131

Integrated Autopilot/Autothrottle Based on a Total Energy Control Concept: Design and Evaluation of Additional Autopilot Modes

Kevin R. Bruce

CONTRACT NAS1-16300
APRIL 1988

NASA

NASA Contractor Report 4131

Integrated Autopilot/Autothrottle Based on a Total Energy Control Concept: Design and Evaluation of Additional Autopilot Modes

Kevin R. Bruce
Boeing Commercial Airplane Company
Seattle, Washington

Prepared for
Langley Research Center
under Contract NAS1-16300

National Aeronautics
and Space Administration

Scientific and Technical
Information Division

1988

CONTENTS

LIST OF TABLES

LIST OF FIGURES

LIST OF FIGURES (Continued)

1.0 SUMMARY

An integrated autopilot/autothrottle system was designed using a total energy control design philosophy. This system was designed around a fixed inner loop configuration that controls flightpath angle (FPA) and velocity using elevator and thrust. Each vertical control mode:

1) Glideslope control
2) Vertical path control
3) Altitude control
4) FPA and go-around control
5) Speed profile control
6) Mach control
7) CAS control
8) Angle-of-attack control
9) Groundspeed control
10) Flare mode
11) Velocity vector control column steering (vel-CCS)

generates an FPA and velocity command that are compatible with the inner loop.

The system design uses a "total energy control concept" which ensures that the system can differentiate between maneuvers requiring a change in thrust to accomplish a net energy change (e.g., an increase in velocity or height) and those maneuvers that only require elevator control to redistribute energy (e.g., speed/altitude exchange).

Previous work under Boeing and NASA funding developed the linear design of the inner loop configuration and basic outer loops. From this linear model, a nonlinear simulation model was developed and the system was evaluated on a flight simulator.

This report covers the further development of the system, in particular:

1) Engine EPR controller redesign
2) Flare mode and go-around
3) Vel-CCS

A summary of simulation results have been included to illustrate the performance of the various modes.

The overall system design has been achieved with reduced complexity as compared with conventional autopilot/autothrottle systems, and yet is more versatile and achieves better performance.

All modes of operation (except go-around) satisfy the basic performance criteria:

1) Less than 1-kn speed error for any flightpath maneuver
2) Less than 20-ft height error for any speed maneuver
3) Not greater than 0.1g normal acceleration (except go-around)

The system was designed for maximum safety. In particular, the angle-of-attack mode was designed to prevent stall in all conditions including full extension or retraction of flaps.

2.0 INTRODUCTION

The objective of the total energy control system (TECS) design was to develop all longitudinal control modes for the autopilot/autothrottle and flight management system using a common, generalized flightpath and speed control algorithm, thereby eliminating unnecessary control law replication and providing a flight management system (FMS) simplification.

This algorithm provides full-time thrust and elevator control coordination for all modes and flight conditions, thus eliminating speed deviation due to flightpath maneuvers and flightpath deviations due to speed maneuvers.

The TECS was designed to provide a full complement of longitudinal FMS modes, including a properly prioritized and integrated stall, and engine overboost protection. These provisions have been designed to be foolproof. A maximum thrust stall, as happened on a Mexicana DC-10 during climbout, would not be possible. In addition, speed control has been prioritized during descent to prevent overspeeding when the throttle goes to idle. Present autothrottles cannot provide these operational safeguards.

A significant aim of this work was to develop a total longitudinal system that takes care of all control requirements simultaneously, thereby providing a significant reduction in software and hardware coupled with an improvement in overall performance.

The total energy control concept requires that thrust be used to control the total energy requirements of the aircraft while the elevator is used to distribute the energy between the flightpath and speed objectives.

The system design approach is to:

1) Develop an energy rate error ($\dot{E}_\epsilon$) which is the sum of longitudinal acceleration error ($\dot{V}_\epsilon$) and FPA error (γ_ϵ) (i.e., $\dot{E}_\epsilon = \dot{V}_\epsilon + g\gamma_\epsilon$ where g = gravitational constant).

2) Develop an energy rate distribution error ($\dot{E}_\delta$) which is the difference between $\dot{V}_\epsilon$ and γ_ϵ (i.e., $\dot{E}_\delta = \dot{V}_\epsilon - g\gamma_\epsilon$).

The energy rate error is used to develop thrust commands, whereas the energy rate distribution error is used to develop elevator commands. The commanded values γ_c and $\dot{V}_c$ are developed by normalization of the particular flightpath and speed control signals for each individual mode.

Control of thrust based on total energy error also means that maneuvers involving mainly energy exchange are executed by the elevator and unnecessary throttle activity are eliminated.

This report documents the development of TECS and covers:

1) A redesign of the engine controller to reduce steady-state gain and bandwidth variation over a wide range of aerodynamic conditions and to prevent engagement transients.

2) Design of a flare law and go-around mode.

3) Design of vel-CCS.

4) A performance evaluation to illustrate the current system capabilities and highlight the unique features of TECS (including the improvements to existing modes: (a) altitude select mode, (b) velocity select mode, and (c) AOA mode, and demonstrate the prioritizing of speed in double maneuvers that cause limiting of the throttle.

3.0 SYMBOLS AND ABBREVIATIONS

AOA	Angle of attack
ACSL	Advanced continuous simulation language
ALFREF	Angle-of-attack reference value
ALTCMD	Commanded altitude
ALW	Wing angle of attack
AZ, AZCG, A_z	Longitudinal acceleration (through center of gravity)
CAS	Calibrated airspeed
CAS_{SEL}	Selected CAS
CCS	Control column steering
CG, cg	Center of gravity
CMD	Commanded signal
DCOL	Column deflection
DELCAS	Error in CAS
DEPRO	Input to engine control loop
DFM	Flap angle
$\dot{E}_\delta$	Energy rate distribution error
$\dot{E}_\epsilon$	Energy rate error
EAS	Equivalent airspeed
ELEV	Elevator angle
EPR	Engine pressure ratio
EPR_C, EPR_{CMD}	Commanded EPR
EPR_{IC}	Initial EPR
EPR_{IDL}	Idle EPR
EPR_{OUT}	Measured EPR

3.0 SYMBOLS AND ABBREVIATIONS (Continued)

FL	Flap angle
FLEPRE	Go-around engagement indication (1 = engage)
FMS	Flight management system
F_{N_C}	Net thrust command
FPA	Flightpath angle
$FPA_{L1,L2}$	FPA for leg 1 of maneuver, leg 2 of maneuver
G	Engine gain (throttle command to EPR)
G_1	Engine gain (XSA to EPR)
g	Gravitational constant
GAINT	Gain within engine loop, identical to Kp
GAINV	γ_{CMD} for unit stick deflection
GAMDED	Commanded flightpath angle (deg)
GAMEPS	Flightpath angle error
GAMMA	Flightpath angle
GAMMAD	Flightpath angle (in deg)
GEAR	Landing gear position (1 = down, 0 = up)
G(s)	Forward path transfer function
GSE, GSERR	Glideslope error
H, h	Height
$\dot{h}$	Height rate
$\ddot{h}$	Vertical acceleration
$\dot{h}_B$, h_{baro}	Barometric height
h_c, h_{CMD}	Commanded height
H_D, H_{DOT}	Height rate

3.0 SYMBOLS AND ABBREVIATIONS (Continued)

H_{dtcmd}	Commanded height rate
H_{dtcml}	Limited commanded height rate
H_{dtrl}	Rate limited height rate
H_{ERR}, H_{ERROR}	Height error
h_I	Inertial height
h_o	Initial height
h_oL1	Initial height for leg_1 of flight
h_R	Radar altimeter measurement, height above runway
h_{ref}	Reference height
h_{sel}	Selected height
$\dot{h}_{TD}$	Height rate at touchdown
h_ϵ	Height error
ICTIC	Engine loop integrator initial condition
KAEPR	Controller gain equivalent to G
KALFBS	Bias for computation of K_α
K_p	Forward path engine controller gain identical to GAINT
MACSEL	Selected Mach number
MCP	Mode control panel
RADALT	Radio altimeter measurements
RAND1	Range rate
RL	Rate limiter
SD	Standard deviation
SX	Touchdown along runway

3.0 SYMBOLS AND ABBREVIATIONS (Continued)

T	Time
t	Time, time from start of flare
TAS	True airspeed
TCAB1	Hardware throttle position
TECS	Total energy control system
TH,THPOS,THR	Throttle position
THBIAS	Throttle bias
THCM	Throttle command
THETAD	Attitude angle
THMAX	Maximum throttle angle
THMIN	Minimum throttle angle
THTRM	Throttle trim position
TOTT	Total air temperature
u_g	Longitudinal gust velocity
V_{CAS}, V_{CASEL}	Calibrated airspeed, selected CAS
V_{CMD}, $\dot{V}_{CMD}$	Commanded velocity, velocity rate
$\dot{V}_{CMD}FL$	Commanded velocity rate during flare
$\dot{V}_d$	Derived velocity rate
Vel-CCS	Velocity vector control column steering
V_{err}, V_{error}	Velocity error
V_G, V_{GO}	Groundspeed, initial
V_{G1}	Smoothed groundspeed
$\dot{V}_{HF}$	High-frequency component of velocity rate
$\dot{V}_{LF}$	Low-frequency component of velocity rate

3.0 SYMBOLS AND ABBREVIATIONS (Continued)

V_P	True airspeed
V_{ref}	Reference velocity
V_T	True airspeed
$\dot{V}_\epsilon$	Error in velocity rate
W	Weight
W_g	Vertical gust velocity
X	Distance along runway from glideslope intersection point
XSA, XSHARG	Cross-shaft angle
α	Angle of attack
α_{ref}	Reference angle of attack
α_{vane}, α_w	Wing angle of attack
γ_c, γ_{cmd}	Commanded FPA
γ_I	Inertial FPA
γ_{SYNT}	Synthesized FPA
γ_ϵ	FPA Error
$\Delta h_{G/s}$	Height error off glideslope
ΔM_c	Change in commanded Mach number
ΔT	Change in throttle position
ΔV_c	Change in commanded velocity
$\Delta\gamma_{SEL}$	Change in selected FPA
δ	Pressure ratio
δ_{COL}	Column deflection
δ_e	Change in elevator angle
δ_{ec}	Change in commanded elevator angle

3.0 SYMBOLS AND ABBREVIATIONS (Continued)

ϵ	Energy
ζ	Damping ratio
θ	Attitude angle
σ_h, σ_v	Standard deviation of height rate, velocity
σ_{δ_e}, $\sigma_{\delta_{TH}}$	Standard deviation of elevator angle, throttle position
τ	Time constant of engine loop, or steady state CCS lag
τ_E	Time constant of engine
τ_F	Time constant of flare
τ_{GA}	Time constant of go-around filter
τ_o	Initial system time constant
$\tau_{\dot{V}}$	Time constant of V complementary filter
ω_n	Natural frequency

4.0 DESIGN AND PERFORMANCE REQUIREMENTS

1) Integrate all longitudinal and vertical control modes to use a single generalized flightpath and speed control algorithm that provides simultaneous thrust and elevator commands.

2) Provide full-time elevator and throttle control coordination to limit speed coupling errors due to flightpath maneuvers to 1 kn and limit flightpath coupling errors due to speed maneuvers to 20 ft.

3) Eliminate throttle response to flightpath perturbations.

4) Minimize throttle response in cases of desired altitude/speed trades.

5) Provide capability to limit normal acceleration during vertical maneuvers to preselected value (i.e., 0.1 g).

6) For step command inputs the response should be smooth and overshoot free. The damping ratio of dominant poles should be greater than 0.7. There should be a consistent response over the whole aerodynamic envelope.

7) Control mode switching should be transient free.

8) The design should incorporate foolproof safeguards to prevent stall and overboost of the engine for all modes and flight conditions.

9) For final approach, the system should be optimized for flightpath and speed tracking, and commensurate with acceptable throttle/elevator activity in turbulence.

10) For cruise, the system should be optimized for minimal throttle/elevator activity and commensurate with acceptable speed and path tracking in turbulence and windshear.

11) The flare mode should achieve an overall longitudinal touchdown dispersion $\sigma_x < 125$ ft and a sinkrate dispersion $\sigma_{\dot{h}} < 1$ ft/s, while exhibiting no appreciable sensitivity to approach terrain and runway slope.

12) For the velocity vector steering mode the requirements are that:

    a) The response lag between the pilot input and the displayed control variable (through which the pilot closes the short-term control loop) must be small enough to allow smooth and positive control.

    b) With the pilot out of the loop, the automatic control must track the control command close enough to avoid pilot intervention for the purposes of short-term airplane stabilization.

    c) During manual maneuvering, the automatic system must not in any way interfere with the pilot's control task, but rather should provide the necessary command and stability augmentation to yield good handling qualities reflected in control column sensitivity, responsiveness, and damping.

5.0 ENGINE CONTROL

5.1 ENGINE CONTROL OBJECTIVES

Previous autothrottle systems have employed a simple throttle lever position servo control. The problems with this type of control were: 1) significant backlash between the throttles and the engine that resulted in limit cycling, and 2) widely varying engine static gain and response over the flight envelope which resulted in poor system performance.

The TECS computes the total net thrust required to execute both flightpath and speed commands, basically for a nominal weight aircraft. The new thrust command is then scaled for the actual aircraft weight, which is presumed to be available from the flight management computer. To avoid the problems described above, the engine should be controlled to deliver directly the total required net thrust. However, the available engine control parameter is engine pressure ratio (EPR). Therefore, the new incremental thrust command must first be converted to an EPR command (EPR_c). This is done by conversion of net thrust command F_{N_C} to normalized net thrust command F_{N_C}/δ using the dividing factor $\delta = p/p_0$.

Next, the normalized net thrust command F_{N_C}/δ is converted to EPR_c using the gain KEPR. This gain is derived from Figure 1, which shows the relationship between EPR and F_N/δ for the JT8D engine adjusted for dual engines. This F_{N_C}/δ EPR relationship is Mach dependent; nevertheless, the Mach effect is small for this type of engine and the relationship may be approximated by an averaged constant.

5.2 EARLIER ENGINE CONTROL USING FIXED-GAIN EPR LOOP

In the earlier TECS engine control design, (ref. 1), control of net thrust was achieved by conversion of the thrust command into a corresponding EPR command with the use of a fixed-gain EPR feedback loop around the basic throttle position loop (fig. 2). Assuming zero throttle position corresponds to the desired engine idle, the bias EPRIDL must be subtracted from the EPR feedback to obtain proper trim. This design approach reduced the effect of throttle to engine backlash and variation in engine dynamics. It was satisfactory for the low-speed approach flight condition. However, tests on the flight simulator revealed other flight conditions where a mismatch existed between the computed throttle command and the throttle position (THTRM) calculated in trim mode. This caused transients at the start of simulation runs. Table 1 shows the calculated throttle command (THCM) and throttle position (THTRM) with Case 3 showing a 13-deg mismatch. In addition, engine characteristics were found to vary with flight conditions causing variation in loop bandwidth and steady-state gain between EPR command and EPR. Since this variation in steady-state gain was excessive, it was necessary to redesign the engine loop gains to reduce this variation.

Table 1. Initial Throttle Command and Trim Value

CASE NO.	AERODYNAMICS CONDITIONS		THROTTLE COMMAND	THROTTLE TRIM VALUE	EPR (initial condition)	EPR (at idle)
	Altitude (ft)	EAS (kn)	THCM (deg)	THTRM (deg)	EPRIC	EPRIDL
1	5,000	150	20.18	21.02	1.386	1.025
2	10,000	150	25.1	22.5	1.484	1.036
3	20,000	150	40.1	27.7	1.775	1.004
4	20,000	250	20.5	20.2	1.436	0.925
5	30,000	250	32.7	24.4	1.68	0.97

5.3 ANALYSIS OF SYSTEM

To gain a better understanding of the problem, the system was analyzed using linear techniques. However, since the JT8D-9 turbofan engine has a highly nonlinear response caused by variable rate limiting during spool up and spool down, it should be noted that any meaningful conclusions drawn from the linear analysis must bear these factors in mind.

5.3.1 First Order System

An earlier analysis of TECS using a linear system assumed that the dominant response of the engine can be modeled using a simple lag with a time constant (τ_E) of 1 sec. This approximation was substantiated by studies which obtained favorable comparisons between linear simulation results of the full system and simulations using the flight simulator which employs the detailed JT8D-9 model. (ref. 1).

It appears logical to start a linear analysis of the EPR command loop by assuming that the engine can be modeled using a lag with $\tau_E = 1$ sec. In this case, the effect of the lag of the throttle servo will be ignored.

For the system shown in Figure 2, the closed loop transfer function (CLTF) between EPR command and EPR is given by:

$$\frac{\Delta EPR}{\Delta EPR_{CMD}} = \frac{KEPRP.G}{(1 + KEPRP.G.KEFB)} + \tau_E s \tag{1}$$

where G is the engine gain, throttle position (deg) to EPR. By inspection, it can be seen that by defining

$$KEPRP = \frac{K_p}{G} \tag{2}$$

Equation (1) can be simplified to:

$$\frac{\Delta EPR}{\Delta EPR_{CMD}} = \frac{K_p}{(1 + K_p.KEFB) + \tau_E s} \tag{3}$$

For this system, it is required that the steady-state gain (SSG) $\Delta EPR/\Delta EPR_{CMD}$ is 1.

Therefore,

$$\underset{(s\rightarrow 0)}{SSG} = 1 = \frac{K_p}{1 + K_p.KEFB} \tag{4}$$

Dividing top and bottom of the RHS of Equation (3) by

$$(1 + K_pKEFB)$$

yields an expression for the time constant (τ) of the loop

$$\tau = \frac{\tau_E}{1 + K_p.KEFB} \tag{5}$$

Rearranging Equation (5):

$$\frac{\tau_E}{\tau} = (1 + K_pKEFB) \tag{6}$$

and substituting in Equation (4):

$$K_p = \frac{\tau_E}{\tau} \tag{7}$$

from Equation (6) and rearranging gives an expression for the feedback gain:

$$KEFB = (1 - \frac{1}{K_p}) \tag{8}$$

or using Equation (7):

$$KEFB = (1 - \frac{\tau}{\tau_E}) \tag{9}$$

Knowing the time constant of the engine lag, the forward and feedback gains of the EPR loop are dictated by the required overall time constant of the loop (i.e., equations (7) and (9).

For an engine time constant (τ_E) of 1 sec:

$$K_p = \frac{1}{\tau} \tag{10}$$

Hence from Equations (2) and (9):

$$KEPRP = \frac{1}{G\tau} \tag{11}$$

$$KEFB = (1 - \tau) \tag{12}$$

5.3.2 Second-Order System

A study of the simulation JT8D-9 model used with the flight simulator showed that although rate limiting effects dominate, the linear response to very small perturbations is modeled by a lag of $\tau_E = 0.2$ sec. This time constant is the same order of magnitude as the throttle servo, and therefore the effect of the servo should be considered in providing a comparison with the first order analysis.

In addition, it is convenient to redefine the gain of the engine as:

$$G_1 = \frac{\Delta EPR}{\Delta XSA} \tag{13}$$

where XSA = cross-shaft angle.

The relationship between throttle (T) and XSA is approximated (in the linear region) by

$$\Delta XSA = 0.9\Delta T \tag{14}$$

Therefore,

$$G = \frac{\Delta EPR}{\Delta T} = \frac{\Delta XSA}{\Delta T} \cdot \frac{\Delta EPR}{\Delta XSA} = 0.9\, G_1 \tag{15}$$

This provides a more precise analysis and is convenient in that all figures given later in this section show engine gain (G_1) as $\Delta EPR/\Delta XSA$.

The transfer function for this system is given by

$$\frac{\Delta EPR}{\Delta EPR_{CMD}} = \frac{\dfrac{KEPRP \cdot 0.9 \cdot G_1}{(1+.15s)(1+\tau_E s)}}{1 + \dfrac{0.9 \cdot (KEPRP \cdot G_1 \cdot KEFB)}{(1+0.15s)(1+\tau_E s)}} \tag{16}$$

Redefining $KEPRP = K_p/G_1$, for the second order system analysis and multiplying by $(1+0.15s)(1+\tau_E s)$.

Then

$$\frac{\Delta EPR}{\Delta EPR_{CMD}} = \frac{0.9\, K_p}{(1+0.15s)(1+\tau_E s) + 0.9\, K_p KEFB} \tag{17}$$

$$= \frac{0.9\, x\, K_p/0.15\tau_E}{s^2 + \dfrac{\tau_E + 0.15\, s}{0.15\tau_E} + \dfrac{1+0.9K_pK_{EFB}}{0.15\tau_E}}$$

We require the SSG to be 1, therefore

$$1 = \frac{0.9K_p}{1 + 0.9K_pKEFB} \tag{18}$$

$$K_{EFB} = (1 - \frac{1}{0.9K_p}) \tag{19}$$

The elimination of engine gain from Equation (17) and the use of Equations (18) and (19) shows that SSG can be maintained at unity over the whole flight regime provided the feedback gain is selected as a function of forward path gain.

The general equation for a second-order system is:

$$\frac{\omega_n^2}{s^2 + 2\zeta\omega_n s + \omega_n^2} \tag{20}$$

where

ω_n = natural frequency (bandwidth)

ζ = damping ratio

Comparison of this equation with Equation (17) yields

$$2\zeta\omega_n = \frac{\tau_E + 0.15}{0.15\tau_E} \tag{21}$$

$$\omega_n^2 = \frac{1 + 0.9K_pKEFB}{0.15\tau_E} \tag{22}$$

Using Equations (21) and (22), it is possible to calculate the required forward and feedback gains K_p, K_{EFB} for selected values of damping and engine time constant τ_E to satisfy Equation (18). These results are shown in Table 2.

Table 2. Results of Second-Order Analysis

CASE	ζ	τ_E	ω_n	K_p	K_{EFB}	LOOP GAIN 0.9 K_p K_{EFB}
1	1.0	0.2	5.8	1.135	0.02	0.020
2	0.7	0.2	8.3	2.316	0.52	1.08
3	1.0	1.0	3.8	2.44	0.55	1.20
4	0.7	1.0	5.5	5.0	0.78	3.50

Conversely, Table 2 shows that by selecting $K_p = 2.37$ and $K_{EFB} = 0.52$ (loop gain 1.23), the engine time constant can vary from 0.2 to 1.0 while damping will only change from 1 to 0.7. A 5-to-1 variation in engine time constant is reduced to a 2-to-1 variation in overall loop bandwidth.

5.3.3 Compensation for Variation of Engine Gain G

A simplified diagram of the JT8D-9 engine is shown in Figure 3. The gain (G) across the engine (EPR/ΔT) is defined as:

$$G = 0.9 \times \frac{\Delta(EPR)}{\Delta(XSA)} \tag{23}$$

The relationship between EPR and XSA is given in Figure 4. It can be seen that gain G is a function of total air temperature (TOTT), Mach number, and bleed valve position. Figure 5 shows that the major factor in gain variation is TOTT. This dependency of G on TOTT has been plotted as gain factor KAEPR in Figure 6 for closed bleed valve and median Mach number as determined from Figure 4.

Thus, to maintain unity steady-state gain of the transfer function

$$\frac{\Delta EPR}{\Delta EPR_{CMD}}$$

and minimize loop bandwidth change with variation of the engine response time constant, the gains K_p (= KEPRP.G) and K_{EFB} must be maintained constant. This requires that the forward path gain KEPRP be varied inversely with the variation of KAEPR. Thus,

$$KEPRP = \frac{2.37}{KAEPR}$$

Further, it can be seen in Figure 4 that for small throttle angles 0 to 7 deg (or XSA between 38 and 45 deg) the engine gain

$$\frac{\Delta EPR}{\Delta XSA}$$

is very nonlinear. Therefore, to achieve satisfactory closed-loop performance, it was decided to use a lower throttle position limit of 7 deg and thus determine EPRIDL by taking the steady-state EPR at 45-deg cross-shaft angle from Figure 4. EPRIDL is programmed as a function of Mach number only. At the same time, a 7-deg bias is added to the throttle command to provide proper trim of the control loop. The resulting revised engine control loop is shown in Figure 7.

Comparison of Figures 2 and 7 shows that DEPRO corresponds to δEPR_{CMD} in Figure 2. The output of the thrust integrator ("A") corresponds to the nominal net incremental thrust command computed by the TECS control algorithm. This signal is scaled by the airplane weight factor (W/W_o) and the atmospheric pressure ratio ($1/\delta = p_o/p$) to generate the normalized net thrust command (F_{N_C}/δ), which is converted into the equivalent δEPR_{CMD} using the gain

KEPR. This gain KEPR is determined from Figure 1, using half the averaged slope for varying Mach number. Half the averaged slope is used to account for two engines producing thrust.

5.3.4 Thrust Control Command Initialization

It is necessary to initialize the thrust integrator ("A") to develop a ΔEPR_{CMD} (DEPRO) corresponding to existing engine trim at engagement of the system. On the flight simulator, trim thrust and throttle position (THTRM) are calculated by the trim routine. This throttle position may be used to calculate the initial value ICTIC of the thrust integrator ("A").

From Figure 7 throttle command:

$$THCM = THBIAS + KEPRP\,(DEPRO - KEFB\,(EPROUT - EPRIDL)) \quad (24)$$

During trim then:

$$THCM = THTRM \quad (25)$$

Rearranging Equation (24):

$$DEPRO = \frac{THTRM - THBIAS}{KEPRP} + KEFB\,(EPROUT - EPRIDL) \quad (26)$$

From Figure 7 (during trim):

$$DEPRO = ICTIC.KD.KEPR \quad (27)$$

Therefore,

$$ICTIC = \frac{DEPRO}{KD.KEPR} \quad (28)$$

Substituting in for DEPRO:

$$ICTIC = (THTRM - THBIAS + KEFB\,(EPROUT - EPRIDL)\,KEPRP$$

$$ICTIC = \frac{THTRM - THBIAS + KEFB\,(EPROUT - EPRIDL)\,KEPRP}{KEPRP.KD.KEPR} \quad (29)$$

This provides a convenient method of calculating the integrator IC (ICTIC) utilizing the throttle trim value.

5.3.5 Thrust Limiting

To prevent engine overboost, the computed ΔEPR command is combined with the EPR_{IDL} signal to form the total EPR command signal. This signal is used to form EPR error signals relative to the maximum and minimum allowable EPR values. If the EPR command exceeds the limit, the error signal is fed back through a high gain into the thrust integrator, thereby preventing the EPR command from exceeding the EPR limit significantly (fig 7).

Likewise, the throttle position command is checked against upper and lower limits, and in the case of exceedance of the limits, the error is fed back through a high gain.

5.4 RESULTS OBTAINED FROM THE HARRIS SIMULATOR

The linear analysis results shown in Table 2 (Case 2) were used as a starting point for the evaluation of the system on the flight simulator. This simulation included throttle servo and cable system nonlinearities. These nonlinearities caused a deterioration of the damping of the EPR control loop. To improve the damping, the loop gain $0.9K_p$.KEFB was reduced to 0.5, yielding for the forward path gain ($0.9\ K_p = 1.5$) and the feedback path gain (KEFB = 0.333). As a result

$$\text{KEPRP} = \frac{1.5}{\text{KAEPR}}$$

where

KAEPR = f(TOTT) varied as shown in Figure 6.

Table 3 details the results obtained from the flight simulator.

Table 3. Results Obtained From Harris Simulator for 0.2 Change in EPR Command

INITIAL VALUES									STEADY-STATE VALUE FOLLOWING STEP IN EPR_{CMD}					
CASE	ALTITUDE (ft)	CAS (kts)	THCM (deg)	THTRM (deg)	EPRIC	EPRIDL	XSHARG (deg)	DEPRO	THCM (deg)	XSHARG (deg)	EPROUT	s.s.g. $\frac{EPR}{EPR_{CMD}}$	$\frac{d(EPR)}{d(XSA)}$	$\frac{d(EPR)}{d(TH)}$
1	5000	150	21.02	21.02	1.39	1.03	57.8	.365	28.6	65.2	1.59	1.0	.0277	.0249
2	10000	150	22.49	22.49	1.48	1.04	59.2	.444	29.5	66.1	1.69	1.0	.0296	.0266
3	20000	150	27.75	27.75	1.78	1.00	64.3	.711	33.9	70.1	1.97	0.95	.0332	.0299
4	20000	250	20.47	20.47	1.44	0.93	57.3							
5	30000	250	24.37	24.37	1.68	0.97	61.0	.694	31.1	67.7	1.90	1.1	.0334	.03

Refer to Figure 7 for definition of variable names.

It can be seen that the throttle command (THCM) exactly matches the trimmed throttle position (THTRM). For step responses over the range of aerodynamic conditions shown, then the steady-state gain variation was less than ±10%. Figure 8 shows step response (ΔEPR_{CMD} = 0.2) for both the software and hardware simulations of the throttle. An excellent response was obtained using the software simulation, whereas the hardware caused minor oscillation. Attempts have previously been made to provide an exact match between the software and hardware throttle by matching the rate limits and linear response.

Figure 9 shows the result of a ramp input of 0.04 EPR/s. Again a minor oscillation was evident with the hardware, though of reduced magnitude. As the input to the EPR control loop is via an integrator, then for most types of command changes to the system, the input to the EPR loop will take the form of a ramp. In practice, the small oscillation has not caused any noticeable problems. However, should this happen, then reduction of loop gain will improve the response.

Results at 20,000 ft, 150 kn (Case 3) yielded similar performance (fig. 10). Figure 11 shows the performance at 1,500 ft, 120 kn, flaps 40-deg, and gear down for a series of step commands (DEPRO) designed to compare normal spool up, spool down, and spool up after sustained operation with the throttles at idle. Although spool up is considerably slower, EPR shows no overshoot.

6.0 FLARE LAW

6.1 INTRODUCTION

Conventional flare laws in use today control sink rate as a function of altitude above the runway (ref. 2). A simple form of this law consists of summing radar altitude, sink rate, an altitude bias term, a ramp (to provide average trim requirements), and inner loop damping to generate an elevator command (δe_c) during flare. For example,

$$\delta e_C = K_{\dot{h}}\dot{h} + K_h(h + h_B) + Damping + Ramp \tag{30}$$

where

δe_c = *elevator command*

h = *vehicle altitude*

h_B = *bias signal*

$-\dot{h}$ = *sink rate*

K_h, $K_{\dot{h}}$ *and* h_B = *designed gains*

Ignoring the trim and damping requirements, then the elevator is driven to satisfy:

$$K_{\dot{h}}\dot{h} + K_h(h + h_B) = 0 \tag{31}$$

At decreasing altitudes, the control law calls for a proportional reduction in sink rate. The bias term h_B provides the desired sink rate at touchdown.

The solution of Equation (31) is:

$$h(t) = (h_o + h_B)e^{-t/\tau} - h_B \tag{32}$$

where

$$\tau = \frac{K_{\dot{h}}}{K_h}$$

h_o = altitude at flare initiation

t = time from start of flare.

For constant τ and increasing approach groundspeed (i.e., sink rate), the control law calls for a proportional increase in flare initiation height to achieve transient free flare initiation. Hence, in different wind conditions which give rise to different groundspeeds (i.e., different sink rates), the flare is initiated at different altitudes. Also, the time to touchdown from a given altitude is independent of speed. As a result, for varying groundspeeds, landing occurs at different positions along the runway.

This problem has been investigated under the NASA TCV program (ref. 2) and one of the solutions was a "variable tau flare law." In this flare law, the value for τ (see equation 32) is varied as a function of groundspeed, i.e.,

$$\tau = \tau_o \frac{V_{Go}}{V_G} \tag{33}$$

where

τ = *flare response time constant*

τ_o = *nominal time constant*

V_{Go} = *nominal approach groundspeed*

V_G = *actual groundspeed*

Substituting Equation (33) into Equation (31) yields

$$\frac{\tau_o V_{Go}}{V_G}\frac{dh}{dt} + (h + h_B) = 0 \tag{34}$$

$$\frac{dh}{dt} = \frac{dh}{dx}\frac{dx}{dt} = \frac{dh}{dx} V_G \tag{35}$$

Using Equation (35), then Equation (34) becomes

$$\tau_o V_{Go}\frac{dh}{dx} + (h + h_B) = 0 \tag{36}$$

The solution to this equation is:

$$h(x) = (h_o + h_B)e^{\frac{x}{-\tau_{oGo}}} - h_B \tag{37}$$

This solution shows that when Equation (36) is satisfied, then the resulting trajectory is independent of groundspeed, and only a function of distance. Also, flare may be initiated transient free at constant altitude, regardless of thrust speed.

The implementation of a variable tau flare law was successfully test flown on the TCV airplane and satisfied Category II landing requirements. Provided this concept could be implemented easily with the TECS, then it offered a proven solution in which the theory had been validated by flight test.

6.2 VARIABLE TAU IMPLEMENTATION

The equation used for implementation of the variable tau flare law can be derived by considering Equation (31) from above:

$$K_{\dot{h}}\dot{h} + K_h(h + h_B) = 0 \tag{38}$$

τ is defined as $K_{\dot{h}}/K_h$, hence,

$$\tau_{\dot{h}} + (h + h_B) = 0 \tag{39}$$

Groundspeed variation can be compensated for by substituting in Equation (33), i.e.,

$$\tau = \tau_o \frac{V_{Go}}{V_G} \tag{40}$$

Therefore,

$$\tau_o \frac{V_{Go}}{V_G} \dot{h} + (h + h_B) = 0 \tag{41}$$

If the $\dot{h}$ signal is complemented with a height rate signal derived using radar altimeter measurements, then it is not necessary to utilize height directly.

Hence, the control equation can be rewritten:

$$\tau_o \frac{V_{Go}}{V_G} \dot{h} + \frac{1}{s}(\dot{h} + \dot{h}_B) = 0 \; or \; \frac{\dot{h}}{V_G} + \frac{1}{\tau_o V_{G_o}}(\dot{h} + \dot{h}_b)\frac{1}{s} = 0 \tag{42}$$

However, since the flare time is inversely proportional to groundspeed, $\dot{h}_b$ must be made proportional to groundspeed to assure equivalence of Equations (41) and (42). Implementation of this control law fits well in with the existing TEC architecture (see fig. 12). The justification for using $\hat{h}$ (derived from h_R and h_I) and not h_I feedback is discussed in the following paragraph.

To ensure a smooth, low-g maneuver, flare initiation should start at an altitude of approximately 40 ft. A necessary feature of flare is to ensure a transient free switch over to flare from glideslope mode. For the nominal approach speed of 117 kn, height rate is approximately –10 ft/s. To achieve transient free switch to flare, the gain ratio between the $\dot{h}$-path and the integrated $\dot{h}$-path (h-path), shown in Figure 12, should be 4. It should also be recognized that this gain ratio is the flare time constant (τ_0) shown in Equation (42).

The gain $K_{FL} = 1/\tau_0 V_{Go}$ in Figure 12, incorporates this gain factor τ_0. Compensation for groundspeed is achieved in the h-path as part of the basic TECS architecture. The bias term in the (h_{BIAS}) path ensures the desired sink rate at touchdown. In addition to ensuring that the throttles retard during flare, a negative $\dot{V}_{CMD}$ signal also is switched in at flare. The $\dot{V}_{CMD}$ signal provides an additional elevator command that aids the rotation of the airplane during flare.

The system as described above makes use of an $\hat{\dot{h}}$ signal feedback. This derived signal is used in place of simply h_I to enable the airplane to flare successfully on runways that are not horizontal. To cope with runways that slope, dip, or are humped, it is necessary to utilize radar altimeter measurements complemented with $\dot{h}_I$ signals to derive an $\hat{\dot{h}}$-signal in which the low-frequency components are referenced to the runway (fig. 12).

6.3 RESULTS FOR VARIABLE TAU FLARE LAW

The performance of the variable tau flare law was assessed using the flight simulator. It should be noted that $\dot{h}_b$ was implemented as a constant. Figure 13 shows the flare law for nominal weight and normal approach velocity in zero wind. The control law has not been fully optimized to cope with all situations but for the present gain values shown in Figure 12, sink rate was 3.2 ft/s at touchdown, and touchdown displacement from runway threshold was

1,200 ft. In addition, the system was tested at minimum and maximum weight configurations using the appropriate approach speed for the weight (figs. 14 and 15). Sink rate at touchdown was 3 ft/s for maximum and minimum weight.

These figures show that the flare dynamics are satisfactory for the various test cases, summarized in Table 4. The flares are somewhat short for heavy weight and long for light weight. This will improve by use of the correct $\dot{h}_b$ (proportional to groundspeed). The system has not been examined in headwinds or tailwinds with this configuration.

Table 4. Summary of Results for Variable Tau Flare Law

RUN NO.	GROSS WEIGHT (lb)	V_{CAS} (kn)	HDOT AT TOUCHDOWN (ft/s)	TOUCHDOWN ALONG RUNWAY SX (ft)	TIME TO FLARE (s)
1	85,000	117	-3.2	1,200	6
2	115,000	139	-3.	1,150	4.25
3	70,000	106	-3.	1,275	7.25

6.4 GAMMA-VDOT FLARE LAW

Implementation of the variable tau flare law concept to the integrated autopilot/autothrottle system highlighted the basic requirements for flare:

1) To rotate the FPA through an appropriate angle such that the sink rate is reduced to the touchdown requirement. This rotation should be independent of velocity (groundspeed).

2) The throttles should be returned to idle during flare and rollout.

The integrated autopilot/autothrottle system has been designed around a fixed inner loop configuration. All autopilot modes generate an FPA command (γ_{CMD}) and an acceleration command ($\dot{V}_{CMD}$). It was considered that this inherent feature of the system could provide a means of obtaining flare. The inner loop configuration could remain intact and flare achieved by commanding a γ signal to achieve the necessary rotation of the velocity vector of the airplane and obtain the desired sink rate at touchdown. In addition, the $\dot{V}$ command signal is used to retard the throttle and aid rotation of the airplane velocity vector. To arrive at a flare law in which the flare touchdown performance is independent of groundspeed, it was necessary to introduce this flare flightpath angle command through a lag. Since the FPA response must be quicker at higher groundspeeds to maintain the same flare trajectory, the lag time constant of γ_{CMD} must be scaled inversely proportional to groundspeed. The magnitude of the γ_{CMD} signal is computed to give the required $\dot{h}$ at touchdown knowing V_G. Also, the $\dot{V}_{CMD}$ signal is scheduled proportional to V_G to help minimize touchdown dispersion.

As with the variable tau flare law, complementary filtering of $\dot{h}_I$ and $\dot{h}_R$ (radio altimeter measurements) was employed to provide for sloping runways. Figure 16 shows the implementation of the gamma-Vdot flare law.

6.5 RESULTS FOR GAMMA-VDOT FLARE LAW

To test the gamma-Vdot flare concept, an ACSL simulation was developed using the TCV B737 linearized aerodynamics for approach (nominal 120-kn EAS, flaps 40-deg). This simulation does not consider the effect of airplane geometry on touchdown distance (i.e., the vertical separation between center of gravity and the landing gear has been ignored). In addition, ground effects of the airplane have not been modeled.

The gamma command time constant (τ_F) was set to 0.75 sec and $\bullet h_{TD}$ to -2.5 ft/s (fig. 16). This time constant (τ_F) is combined with the basic γ-response time constant ($\sim$2.5 sec) to provide the desired flare response time constant ($\sim$4 sec) for the overall system. However, no attempt is made to force the system to accurately follow a specified trajectory. The results for no wind, 15-, and 30-kn tailwinds are shown in Figures 17 through 20. Figure 17 shows height and height rate plotted against X, displacement along runway from the glideslope interception point. This point is 800 ft past runway threshold. Flare initiation occurred at an altitude of 40 ft. Figure 18 is an enlargement of the touchdown area highlighting the dispersion in displacement (90 ft) and touchdown sink rate (0.2 ft/s). Figure 19 shows the lagged γ response to γ_{CMD} and also shows the variation in groundspeed during flare. Figure 20 illustrates the throttle position during flare and also shows effect of flare on α and θ. These responses are all satisfactory.

The sensitivity of the flare law to turbulence was investigated by adding longitudinal turbulence (5-ft/s rms). These results are summarized in Table 5. It can be seen that the standard deviation of the displacement for γ-$\bullet$V flare was 5% lower than the existing TCV airplane (standard deviation for H is 25% lower).

Table 5. Effect of Horizontal Turbulence (U_g = 5-ft/s rms) for γ–$\dot{V}$ Flare Law

	γ–$\dot{V}$ FLARE LAW		EXISTING TCV AIRPLANE	
	X G/S ft	$\dot{H}$ ft/s	X G/S ft	$\dot{H}$ ft/s
mean	547.7	-3.0		
s.d.	199.9	0.66	211.2	0.89

- Results obtained from ensemble average of 15 runs (using ACSL simulation)

- Corresponding TCV airplane results calculated from D6-37006; Lambregts and Hansen (ref. 2)

6.6 RESULTS OBTAINED USING THE FLIGHT SIMULATOR

The γ-$\dot{V}$ was also evaluated on the flight simulator. The results shown in Figures 21 and 22 illustrate the performance for no wind and 32-kn headwind. Sink rate varied from $\sim$3 ft/s for the no wind case to 2.4 ft/s for headwinds of 32 kn. The zero wind flare lasted 6.5 sec compared with 10 sec in a 32-kn headwind. A comparison of the γ_{CMD} and γ traces shows the effect of groundspeed on the flare time constant.

6.7 GO-AROUND MODE

The inner loop configuration of the TECS, which controls FPA and speed, allows for the implementation of a simple but effective go-around mode. This implementation is shown in Figure 23. The go-around is achieved by switching out the glideslope mode signal and switching in the desired positive FPA command. Simulation experience and results from pilot evaluation showed that a FPA of $\sim$10 deg was satisfactory. This FPA provides a takeoff thrust go-around for weights greater than $\sim$85,000 lb and reduced thrust go-around for lower airplane weights. For passenger comfort, normal acceleration levels may be reduced by lagging the FPA command with a filter of time constant τ_{GA}. During go-around the system will continue to control speed to the selected command, without significant control coupling errors.

The performance of go-around is shown in Figures 24 and 25 for two values of τ_{GA}. The airplane is on final approach down the glideslope and go-around is engaged at an altitude of 100 ft. In Figure 24, τ_{GA} is small (0.2 sec), and g levels during go-around reach 0.5g. However, the height loss after engagement was only 24 ft.

For large values of τ_{GA} (3.0 sec), maximum acceleration (AZCG) was lower at 0.3g, but height loss increased to 36 ft. The final value of τ_{GA} will be decided following further pilot evaluation of the system.

In the simulation results, it can be seen that the system can just achieve the 10-deg FPA at the aerodynamic condition and weight below 1,000 ft. At about 1,000 ft, the throttle is at the forward limit and performance limitations are reached. Speed control has priority, hence the system maintains speed but the maximum attainable FPA (GAMMAD) drops below 10 deg.

7.0 VELOCITY VECTOR CONTROL COLUMN STEERING

7.1 INTRODUCTION

Velocity vector control column steering (vel-CCS) is a semiautomatic mode giving the pilot direct control over the inertial FPA angle γ_I through a column input. Column inputs are used in a rate command/hold system change the FPA reference command for the vel-CCS control laws and shape the system response to provide natural airplane control handling characteristics.

The objective of the pitch vel-CCS mode is to reduce pilot workload when flying a desired flightpath. For example, in following an approach profile with defined FPAs but varying speeds, aircraft configuration, and winds, then a substantial reduction in pilot workload will result if the pilot can simply set up the desired inertial FPA path using column inputs and the automatic control system can track this command in spite of the disturbances.

7.2 VELOCITY CCS CONTROL AND DISPLAY SYSTEM REQUIREMENTS

Earlier work on developing vel-CCS for the NASA TCV airplane (ref. 3) led to the formulation of general control and display requirements for the vel-CCS:

1) The response between the pilot's input and the response of the display variable through which the pilot closes the inner control loop should be critically damped and exhibit a small enough lag to avoid pilot-induced oscillations.

2) The γ-response should be smooth, well dampened, and overshoot free. For steady state column deflection, the γ-response should quickly establish the desired steady-state rate of change of FPA (fig. 26).

3) Pitch attitude overshoot should not be excessive. Reference 3 established a lower limit of 1 sec for the γ-response lag to meet this requirement.

7.3 DESIGN OF VEL-CCS SYSTEM

The basic control concept of the TECS is to control FPA (γ) and speed using control commands to the elevator and thrust. The vel-CCS develops a γ_{CMD} proportional to the integral of column deflection (fig. 27). The display uses both γ_{CMD} and γ. Use of γ_{CMD} to close the profile control loop bypasses the lag between command and response. The γ_{CMD} signal is used to drive the basic TECS algorithm without modification.

One desirable feature was to maintain the same a_z levels for the same column deflection as with the existing airplane.

The TCV B737 airplane has a δ_e/g value of 15.89. This gives a column displacement $(\delta_{col})/g$ of 4.83 in at 120 kn, 40-deg flaps.

Hence,

$$\delta_{col}/\ddot{h} = 0.15\ in/ft/s^2 \tag{43}$$

Since

$$\dot{\gamma} = \frac{\ddot{h}57.3}{V_g} \; deg/s \tag{44}$$

then

$$\frac{\dot{\gamma}}{\delta_{col}} = \frac{57.3}{0.15(202.2)} = 1.88 \; \frac{deg/s}{in} \tag{45}$$

This ratio $\dot{\gamma}/\delta_{col}$ established the gain GAINV. In addition, a deadzone is incorporated in the output from the column. This was to ensure zero column signal to the control law when the column is in the neutral position. The results for this system are shown in Figures 28 and 29. Run 1 shows the basic response to the ramping gamma command. With the standard TECS gains, the γ response lag is approximately 4 sec. Root locus analysis showed that the integrator gains in the thrust and elevator processing loops (KTI and KEI) could be doubled decreasing the response lag to approximately 2 sec. However, the resulting overshoot of the final γ value is undesirable. Furthermore, gain changes in the basic TECS algorithm for a specific mode are undesirable and will not reduce the γ response lag to the desired level of 1 sec. Reducing the lag requires faster elevator response to rotate the airplane to the required FPA and tighter control of throttle to achieve a parallel γ to γ_{CMD} response with a lag of ~ 1 sec.

This was accomplished by feeding a proportional and derivative $\dot{\gamma}_{CMD}$ signal directly to the elevator and a proportional γ_{CMD} signal directly to the throttle command.

Designing the gains for this configuration requires consideration of the physics of the problem. For a response lag (τ) of 1 sec and γ_c of 1-deg/s, the steady-state FPA error (γ_ϵ) will be 1-deg (fig. 26). The command signals to the elevator and throttle can be calculated to achieve this steady-state error during column inputs, from which the system gains can be calculated.

Considering the change in throttle position required to maintain 1-deg/s rate of change of FPA with zero longitudinal acceleration, then

$$\Delta\text{Thrust} = \Delta\dot{\gamma}W \qquad \text{where W = weight, } \dot{\gamma} \text{ in radians/sec} \tag{46}$$

and

$$\frac{\Delta\text{Thrust}}{\Delta T} = 450 \; lb/deg \qquad (\Delta T = \text{incremental throttle position})$$

Hence,

$$\Delta T = \frac{\Delta\dot{\gamma}W}{450} = \frac{1.85000}{(57.3).450} = 3.3 \; deg/s \tag{47}$$

For the existing system, the required γ_ϵ of 1-deg contributes a throttle rate of only

$$\gamma_\epsilon g K_{TI} \; deg/s = \frac{1}{57.3} \; g \; 1.5 = 0.84 \; deg/s$$

Hence, a proportional path of γ_{CMD} to the throttle should be added with a gain

$$\text{KTP2} = \frac{57.3(3.3-0.84)}{g} = 4.37$$

During the steady-state γ rate, the airplane altitude must change at the same rate as γ. Therefore the rate of change of pitch command must equal γ for the existing system. Pitch rate command θ_c is

$$\theta_c = \gamma_{\epsilon\, g} \frac{\text{KEI}}{\text{S}} = g \frac{1}{57.3s} = 0.662\ deg/s$$

Hence, a proportional path of γ_c must provide an additional signal of

$$1 - 0.562 = 0.438$$

and therefore, the gain of this proportional γ_c path (KGCP) should be:

$$\frac{1}{57.3}\,\text{KGCP}\, g = 0.438$$

$$\text{KGCP} = \frac{57.3}{g}\, x\, 0.438 = 0.78$$

However, because of the gamma feedback signal of magnitude 1/57.3 rad/s, a gain component of unity is also required. Therefore, total gain required is

$$\text{KGCP} = 1 + 0.78 = 1.78$$

In addition to the proportional γ_c path to elevator, a proportional γ_c signal path (KCPS) is used to provide a command signal to balance out pitch rate feedback during pitch maneuvers.

From Figure 30:

$$\frac{1}{57.3 \times 1.88} \text{KCP}\, g.\text{K}_\theta.\text{KEP} = 1\ \text{K}q$$

$$\text{KCP} = \frac{\text{K}q\ 57.3 \times 1.88}{g\ \text{K}_\theta\text{KEP}} = \frac{4 \times 57.3 \times 1.88}{32.2 \times 8.1} = 1.673$$

However, these calculations were for steady-state conditions and adjustments were made to improve the transient response. The resulting gains were KTP2 = 3.9, KGCP = 2.75, KCP = 2.0. For this system, a column deflection of 0.5 in. held for 8 sec gives a ramping γ_{CMD}, which reaches a final γ of 6.2-deg (fig. 31). The γ response lag is reduced to 1 sec and the response is parallel to the γ_{CMD}. Overshoot of γ is 3% and maximum error in CAS is 2 kn. Throttle response, velocity error, and attitude are shown in Figure 32.

Figures 33 through 36 show the effect on performance of $\pm 50\%$ variation in the significant gains of the vel-CCS system. As discussed above, the proportional and derivative gains (KGCP and KCP) affect the rate of rotation of the airplane to the γ_{CMD}, the response lag, and to a certain extent overshoot (figs. 33 and 34). The proportional and integral gains to the throttle (KTI and KTP2) affect parallelism and final overshoot (figs. 35 and 36).

The system was tested over a range of aerodynamic conditions from 120-kn EAS 1,500 ft, to 310-kn EAS, 20,000 ft (figs. 37 through 40). The result showed that the gains associated with CCS control could remain fixed without degrading performance significantly. Overshoot increased to 4.8% in the high-speed case compared with 3% for the nominal case. Variation in parallelism was insignificant over the whole flight regime.

7.4 DISPLAY CONCEPTS

Requirements for the display have been met by the use of γ_{CMD} for use by the pilot to close the inner control loop. The actual FPA is also displayed for response monitoring. Display of both γ_{CMD} and γ reduces the likelihood of pilot intervention during command tracking in turbulence.

Previous work with CCS that examined the display requirements described the synthesis of a single display signal combining γ_{CMD} and γ. This approach is feasible when the response lag of γ is constant for all flight conditions and reduces display clutter. However, during periods with the column in detent, only actual γ would be displayed and perturbations in turbulence may draw the pilot unnecessarily into the control loop.

8.0 PERFORMANCE ASSESSMENT

The following paragraphs document the overall performance of the system as implemented on the Boeing Renton Flight Simulator [M-Cab].

8.1 ALTITUDE CONTROL

For large maneuvers, an earlier altitude control mode was unsatisfactory in that it was impossible to maintain low g levels. In addition, $\dot{h}$ was limited restricting the maximum performance of the system. The problem with g levels is shown in Figure 41 with a +2,000-ft altitude change. It can be seen that maximum normal acceleration (AZ) reached -10 ft/s^2 and velocity error reached 5 kn. This problem was solved by the use of nonlinear elements designed to restrict acceleration levels and vary the start of exponential capture as a function of height rate. Figure 42 shows the effect of the nonlinear design in reducing normal acceleration levels.

The performance of the system to a small height change (+300 ft) and a large change (+2,500 ft) is shown in Figures 43 through 46 for low-speed and high-speed flight conditions. The small height change shows the linear performance of the system with 95% of the final value achieved by about 33 sec. Typically for small and large height changes, captures of the commanded height are obtained without overshoot with maximum a_z levels less than 0.1 g and velocity error less than 0.5 kn. At the extremes of the performance envelope (e.g., fig. 46), when commanding a lower height such that the throttles remain at the aft limit for a significant time, the nonlinearities of the engine spool up affect the throttle response giving rise to higher a_z levels than desired ($\sim$0.15g). This peak a_z lasts for only a very short time. This problem will be examined in the future.

8.2 VELOCITY CONTROL

The velocity hold system allows the airplane to control Mach, CAS, or groundspeed. The speed error (e.g., Mach or CAS) is converted to a TAS error which is processed through a gain and limiter to generate a V_{CMD} which drives the inner loops. The major system changes, different from that described in Reference 1, are the redesign of the gain and limiters so that for any combination of command inputs of speed and FPA, the system will satisfy the performance requirements discussed in Section 4.

The performance results for the velocity control system are presented in Figures 47 through 49. It can be seen that typically the height error does not exceed 10 ft. The linear performance (fig. 47) is constant over the performance envelope and the commanded velocity is captured with an exponential capture (τ = 12.5 sec).

The ability to control Mach is shown for a high-speed, high-altitude situation where control of Mach is mostly used (fig. 49). The control dynamics are identical to the CAS mode.

The system is designed to automatically switch between CAS and Mach control during climb and vice versa during descent. This feature is discussed in Reference 1.

8.3 α CONTROL MODE

The primary requirement of the α control mode is to prevent stall by holding the airplane to the safe α reference should the angle of attack reach this reference. This can occur when the pilot commands too low a velocity. The system described in Reference 1 worked successfully during approach at a fixed flap setting, but was not developed to cope with all flap settings and over the full flight regime. This has now been accomplished by varying the α reference as a function of flaps, varying the loop gain as a function of speed, and by linear filtering and the addition of nonlinearities to eliminate adverse throttle reaction. The mode was tested at different velocities, airplane weights, flap settings, and CG positions. Typical results are shown in Figures 50 and 51 for α limiting in response to commanding a low velocity. Figure 50 shows the response with maximum airplane weight, flaps fully extended, and aft CG position (31%). Figure 51 shows the result of minimum weight, 0-deg flaps and forward CG position (5%). Maximum height error recorded was 17 ft (fig. 51).

8.4 FPA CONTROL MODE

The performance of the FPA control mode is demonstrated at low speed (figs. 52 and 53). The linear performance for ± 2.5-deg FPA command (fig. 52) shows overshoot free capture with approximately 2-sec time constant. Velocity error is less than 1 kn and vertical acceleration levels (a_z) were less than 0.1 g.

For large FPA commands, a_z levels are limited by the addition of a rate limit in the FPA error (γ_ϵ) path. This can clearly be seen in Figure 53 where the effect of the limit is shown in a_z.

In the case of large FPA changes, it is necessary to modify the control law configuration when throttle limiting occurs. This problem has been discussed in detail in Reference 1. However, briefly restating the problem: When the throttle limits, only the elevator remains available for control, and therefore only one variable can continue to be controlled and the preferred one is speed. The approach maintains the decoupled control concept whereby control command for one variable does not cause significant errors for the other controlled variable. This speed priority also avoids the danger of stalling and overspeeding. To this effect, the FPA error crossfeed to the elevator integrator is temporarily disconnected until the FPA command is reduced or the target altitude is captured. The response to large γ_{CMD} with throttle limiting is shown in Figure 53. In each case, the FPA settles at the maximum value commensurate with maintaining velocity.

8.5 GLIDESLOPE CONTROL MODE

The basic control law to capture the ILS glideslope has been discussed in Reference 1. This system has not been changed significantly. Performance is illustrated in Figures 54 and 55. In Figure 54, the engagement starts in altitude hold mode at 2,000-ft altitude approximately "2 dots" under the glideslope. This corresponds to an initial glideslope error of 0.66 deg. The glideslope is captured in a overshoot free manner with neglible speed transient with the airplane following the glideslope to an altitude of 40 ft, at which point flare is initiated. In the noise free simulation run shown, the glideslope error is negligible.

A flaps-up glideslope capture with incremental flap extension is presented in Figure 55. Again, the glideslope is captured overshoot free due to the fully adaptive FPA transition feature. This was achieved as a result of the concept of normalizing the glideslope error into the FPA command. This design approach also eliminates glideslope track errors due to decel-

eration. At the start of the run, a low velocity is commanded and the airplane flies at α_{ref} (flaps 0-deg). Angle of attack (ALW) can be seen to approach α_{ref}. As flaps are extended, velocity decreases and the angle of attack follows the new α_{ref} at each new flap position. The glideslope error is negligible throughout this procedure.

8.6 VERTICAL PATH MODE

Vertical path mode allows the airplane to follow preprogrammed straight vertical paths in space. Switchover between vertical paths is arranged to occur in a transient free manner and the airplane captures each new vertical path in an exponential manner, with no overshoot. An example of this control mode is shown in Figure 56. The airplane has been preprogrammed to capture 5,000 ft, fly straight and level until it is over a waypoint, then climb at an FPA of 0.1 rad to intercept a second waypoint at 7,500 ft. After a period of straight and level flight and a speed increase, the airplane passes over a third waypoint and descends at an FPA of 0.05 rad to reach the fourth waypoint at 5,000 ft. The flightpath and speed command executions are virtually perfect.

8.7 CONSTANT ENERGY MANEUVERS

The TECS has been designed on energy considerations. An airplane flying at constant height and velocity has an energy level consisting of the sum of the kinetic energy (KE) and potential energy (PE), where KE is associated with speed and PE with altitude. Certain maneuvers require a net energy change (e.g., an increase in velocity or height). This requires mainly control of thrust. In gusty conditions or when executing a double maneuver (i.e., decrease in height coupled with increase in velocity), the net energy change may be small but the system requires a redistribution of energy. The elevator is controlled to provide the means of redistribution of KE and PE.

This type of double maneuver in which the change in PE is equal to the change in KE is shown in Figure 57. The figure shows the command to decrease altitude by approximately 600 ft is matched (in terms of energy) by the command to increase velocity 20 kn. As no net energy change is required, throttle motion is negligible and the elevator provides the primary means of redistributing energy.

8.8 CLIMB AND ACCELERATE MANEUVERS

A double maneuver requiring simultaneous climb and speed increase is illustrated in Figure 58. The airplane climbs from 10,000 to 20,000 ft during which the speed changes from 250- to 300-kn CAS. It can be seen that the airplane pulls maximum normal acceleration (a_z) of 0.1 g until the steady-state climb rate at maximum thrust is reached. Height rate peaks at 80 ft/s, then decreases slightly as altitude increases. On input of the commanded change in velocity, height rate decreases as a consequence of 50% of the available energy rate being used to increase velocity. Priority is given to velocity control and it is a simple matter to adjust the amount of energy rate used to execute the speed change (50% in this case). Once the required velocity is reached, then all available energy rate is converted to climb rate to reach the commanded altitude. The altitude is captured exponentially without overshoot. Throughout the maneuver, acceleration levels do not exceed 0.1 g.

8.9 DESCENT AND DECELERATION MANEUVERS

The opposite maneuver to climb and acceleration is descent and deceleration. This is shown in Figure 59 for a 4,000-ft descent from 15,000 ft coupled with a 50-kn decrease in speed from 300-kn CAS. In this case, the throttles retard to the aft limit, and the established sink rate depends on the drag configuration of the aircraft with the elevator continuing to control speed. When the command to decelerate is dialed in, velocity control has priority, height rate decreases to zero, and 100% of available energy is directed to capturing speed. The use of 100% of available energy to capture speed was agreed on during pilot evaluation. However, this percentage can be varied easily with TECS to suit agreed flying procedures. In this situation, deceleration is constrained to prevent the airplane increasing altitude while velocity is being captured. Once the required velocity is reached, then sink rate increases again until the new altitude is captured.

8.10 TURBULENCE AND WINDSHEAR

The velocity control loop employs a complementary filter to provide a derived $\dot{V}$ feedback signal. The time constant of this filter largely dictates the final windshear and turbulence performance for the current system. The high-frequency component of $\dot{V}$ consists of the derived $\dot{V}$ signal obtained from

$$\frac{\Delta\text{Thrust}}{\text{Mass}} - \gamma\, g \text{ (see fig. 60).} \tag{48}$$

The first term represents longitudinal acceleration due to thrust and the second term is the component of gravity along the flightpath.

The low frequency component of $\dot{V}$ consists of rate of change of airspeed. This derived $\dot{V}$ signal was developed to eliminate adverse pitch response to sudden gusts and undesired throttle responses due to flap and gear lowering. Variation of the filter break frequency ($1/\tau$) dictates the tradeoff between windshear and turbulence performance. A low frequency breakpoint severely attenuates the air mass desired $\dot{V}$ signal, thereby filtering turbulence and resulting in low throttle activity. However, as the high-frequency components have been attenuated, the response of the system to a windshear has been lagged, and as a consequence, the velocity error due to windshear is higher. Obviously, with a high-frequency breakpoint, the situation is reversed.

Simulation runs were made with either windshear (1-kn/s headwind) or turbulence modeled using the Dryden wind spectrum. Moderate levels of turbulence were used (i.e., 5-ft/s rms longitudinal or horizontal turbulence, and 2.5-ft/s rms vertical turbulence). The two selected aerodynamic conditions were: 1) low speed (125-kn CAS, 500 ft, flaps 40 deg, gear down), and 2) high speed (325-kn CAS, 25,000 ft, flaps 0 deg, gear up).

Figures 61 through 64 show standard deviation (SD) of velocity, height, throttle, and elevator against complementary filter time constant ($\tau_{\dot{V}}$) for longitudinal turbulence. Except for velocity, the variables show a marked increase for increase in filter breakpoint (i.e., reduction in $\tau_{\dot{V}}$). Throttle shows high sensitivity at high speed, whereas the elevator shows increased activity at low speed. In the case of the throttle within the engine control loop, the gain between throttle and thrust increases with increase in altitude. Therefore, the throttle shows increased sensitivity to variation in $\tau_{\dot{V}}$ at high speed. The opposite situation exists for the elevator, where the gain between altitude command and elevator decreases with increase in speed.

In windshear (without turbulence) the maximum velocity error increased with increasing $\tau_{\dot{V}}$ (lowering breakpoint), whereas height error decreased (figs. 65 and 66). Thus, improved speed control is possible at the expense of path tracking.

Plotting the standard deviation of throttle position in turbulence against maximum velocity error due to windshear (fig. 67) shows clearly that a tradeoff can be made between the throttle activity and velocity error. At low speed, good windshear performance is essential to prevent stall and high throttle activity is the penalty. At the high-speed cruise condition, greater emphasis is placed on low throttle activity and windshear performance can be sacrificed.

To achieve this aim, $\tau_{\dot{V}}$ was varied as a function of altitude. For the high-speed case, it was decided to set $\tau_{\dot{V}}$ at 20. For larger values of $\tau_{\dot{V}}$, throttle activity does not decrease significantly whereas velocity error due to windshear increases rapidly.

For the low-speed situation, $\tau_{\dot{V}}$ was set to 10 sec. Although it would have been desirable to have decreased $\tau_{\dot{V}}$ still further to reduce velocity error in windshear, it was determined in simulations of landing approach that high elevator activity and rate limiting of the elevator made the performance unacceptable. Figure 68 illustrates this sensitivity of elevator to variation of $\tau_{\dot{V}}$.

Variation of complementary filter time constant $\tau_{\dot{V}}$ has little effect on rms control activity in the presence of vertical turbulence. The effect of vertical turbulence was examined at low and high speed, the results of which are summarized in Table 6.

Table 6. Effect of Vertical Turbulence (W_g = 2.5-ft/s rms)

	LOW SPEED (HO=500 ft, CAS=125 kn)			HIGH SPEED (HO=25,000 ft, Mach=0.74)		
	Filter breakpoint ($\tau_{\dot{V}}$)			Filter breakpoint ($\tau_{\dot{V}}$)		
	5	10	20	5	10	20
Elevator (deg)	0.33	0.31	0.33	0.08	0.07	0.07
Throttle Position (deg)	1.61	1.55	1.68	1.14	1.11	1.05
Vel error (kn)	0.48	0.59	0.88	0.10	0.14	0.14
H error (ft)	4.02	3.63	3.96	3.14	2.88	2.67

9.0 CONCLUSIONS

The integrated longitudinal autopilot/autothrottle based on the total energy control system (TECS) concept has been developed and evaluated in detail. The feasibility of the TECS design has been demonstrated by meeting all design objectives with a system that is significantly simpler than existing conventional designs. In addition, the system design features numerous system advantages and performance improvements over conventional designs:

1) Use of a single generalized flightpath and speed control algorithm for all modes and flight conditions allows elimination of most autothrottle and flight management computer control laws for the longitudinal axis.

2) The number of computer interfaces is reduced substantially compared to conventional designs.

3) Except for the elevator and throttle innerloop control, the design is completely general and transferable to other airplanes without further development or adjustment.

4) The system operation and performance is consistant for all modes and flight conditions, reducing implementation checkout and certification flight testing requirements.

5) Speed and flightpath control are decoupled for all modes and flight conditions, such that speed errors due to flightpath maneuvers are less than 1 kn and path deviations due to speed maneuvers are less than 20 ft.

6) Energy exchange maneuvers are executed through the elevator, without significant throttle response.

7) Vertical maneuvers are g-limited, except for the go-around mode.

8) Flightpath intercept maneuvers are fully adaptive to the flight condition, resulting in overshoot free captures at all times.

9) No significant flightpath deviations are incurred due to longitudinal accelerations/ decelerations.

10) No significant speed deviations are incurred during climb or descent.

11) During maneuvers in which the thrust limits, elevator priority is given to speed control over flightpath control, preventing overspeed or underspeed.

12) A flare mode using the total energy control concept was developed. This mode commands an incremental FPA proportional to altitude change. A simultaneous deceleration command is used to aid the pitch rotation and retard the throttles.

13) A vel-CCS mode was incorporated in the TEC system concept, using gains tailored for fly-by-wire implementation. Performance equivalent to that achieved on the NASA TCV B-737 aircraft was shown.

14) Performance in windshear and turbulence has been optimized.

10.0 REFERENCES

1. A. A. Lambregts, "Vertical Flight Path and Speed Control Autopilot Design Using Total Energy Principles," AIAA Paper 83-2239CP, August 1983.

2. A. A. Lambregts and J. F. Creedon, "Development and Flight Evaluation of Automatic Flare Laws With Improved Touchdown Dispersion," AIAA Guidance and Control Conference, Paper No. AIAA-80-1757, August 1980.

3. "ACSL Advanced Continuous Simulation Language User Guide and Reference Manual," Mitchel and Gautier Associates, 2nd edition, 1975.

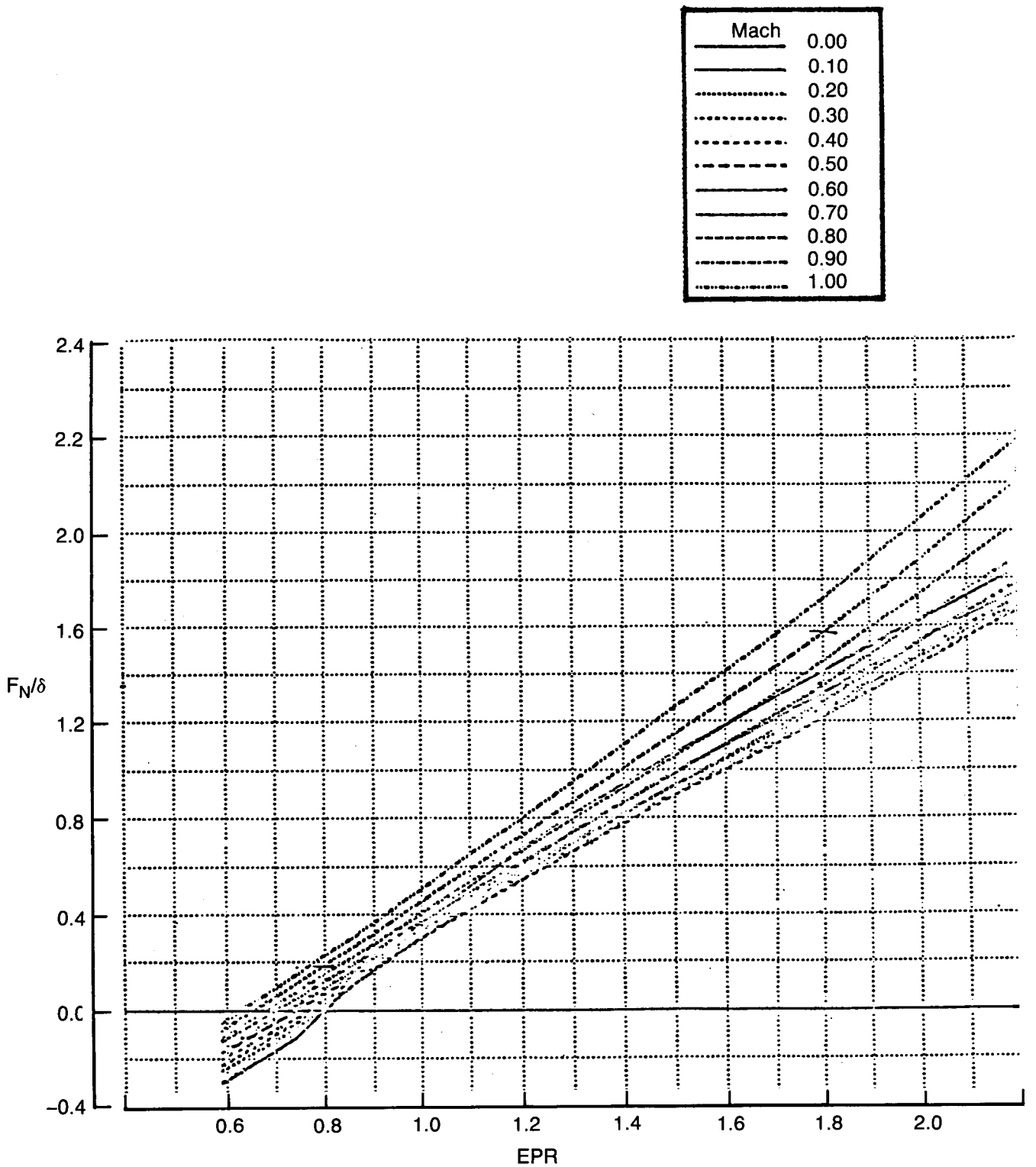

Figure 1. F_N/δ Versus EPR

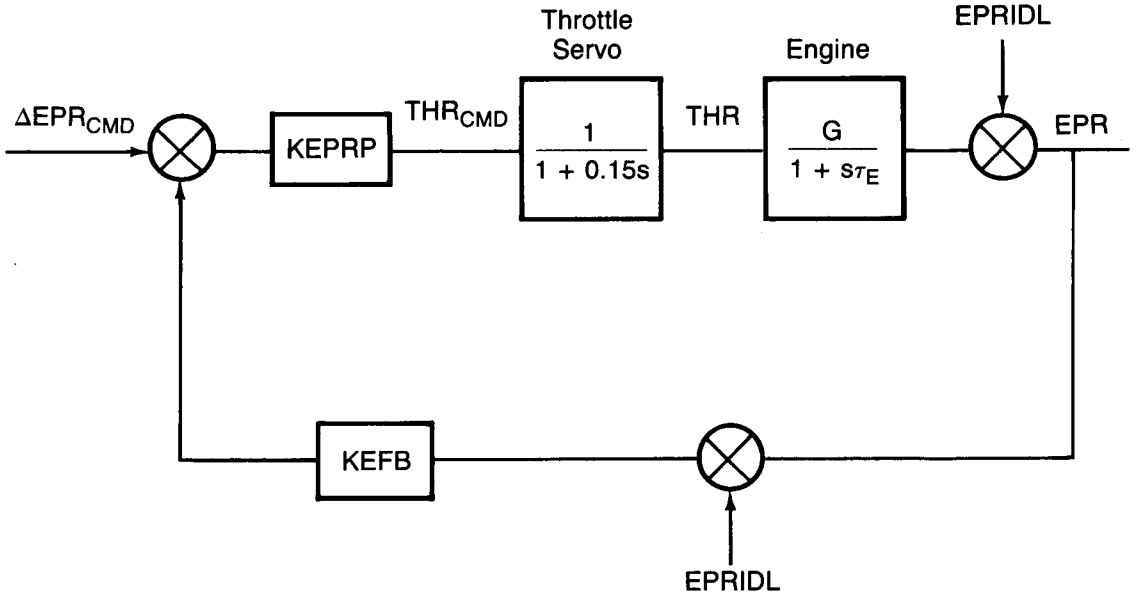

Figure 2. Simplified EPR Control Loop

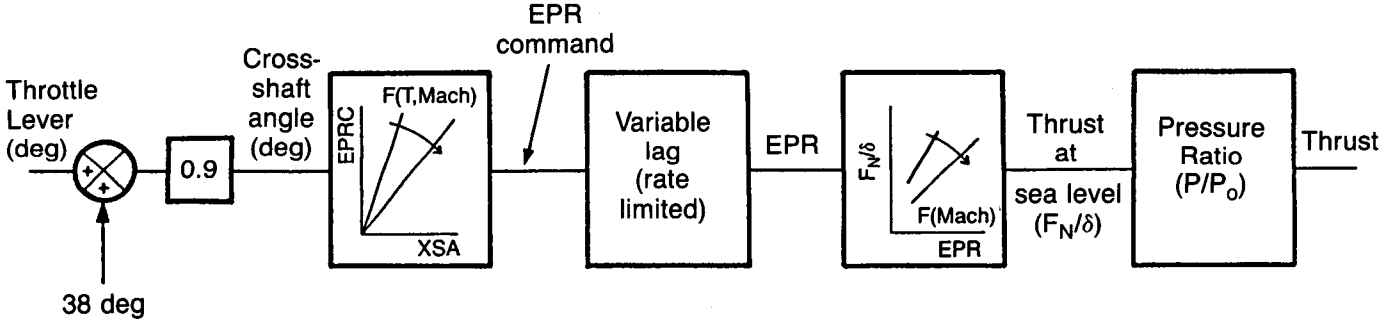

Figure 3. Simplified JT8D-9 Engine Model

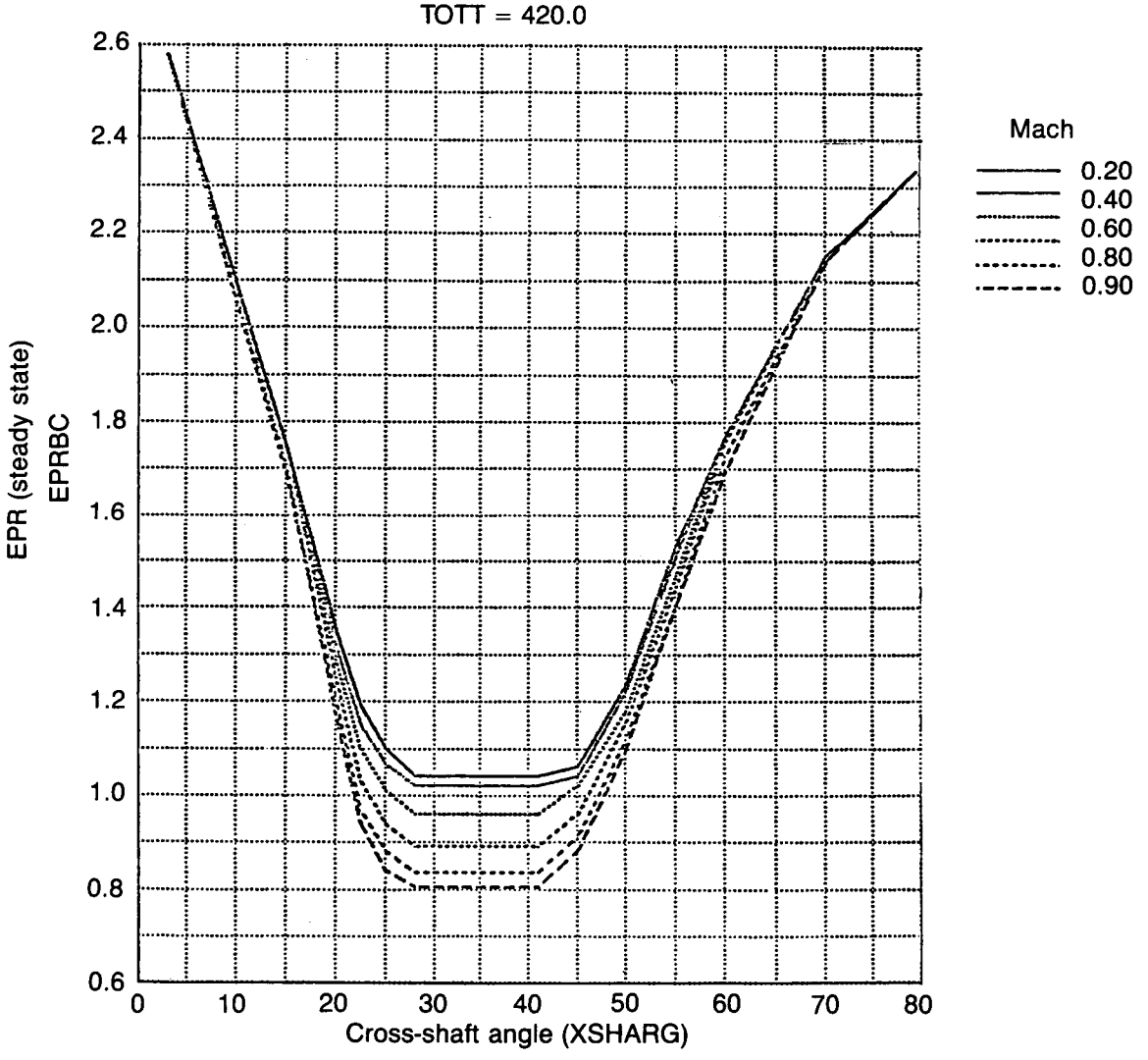

Figure 4. EPR Versus Cross-Shaft Angle (Bleed Valve Closed)

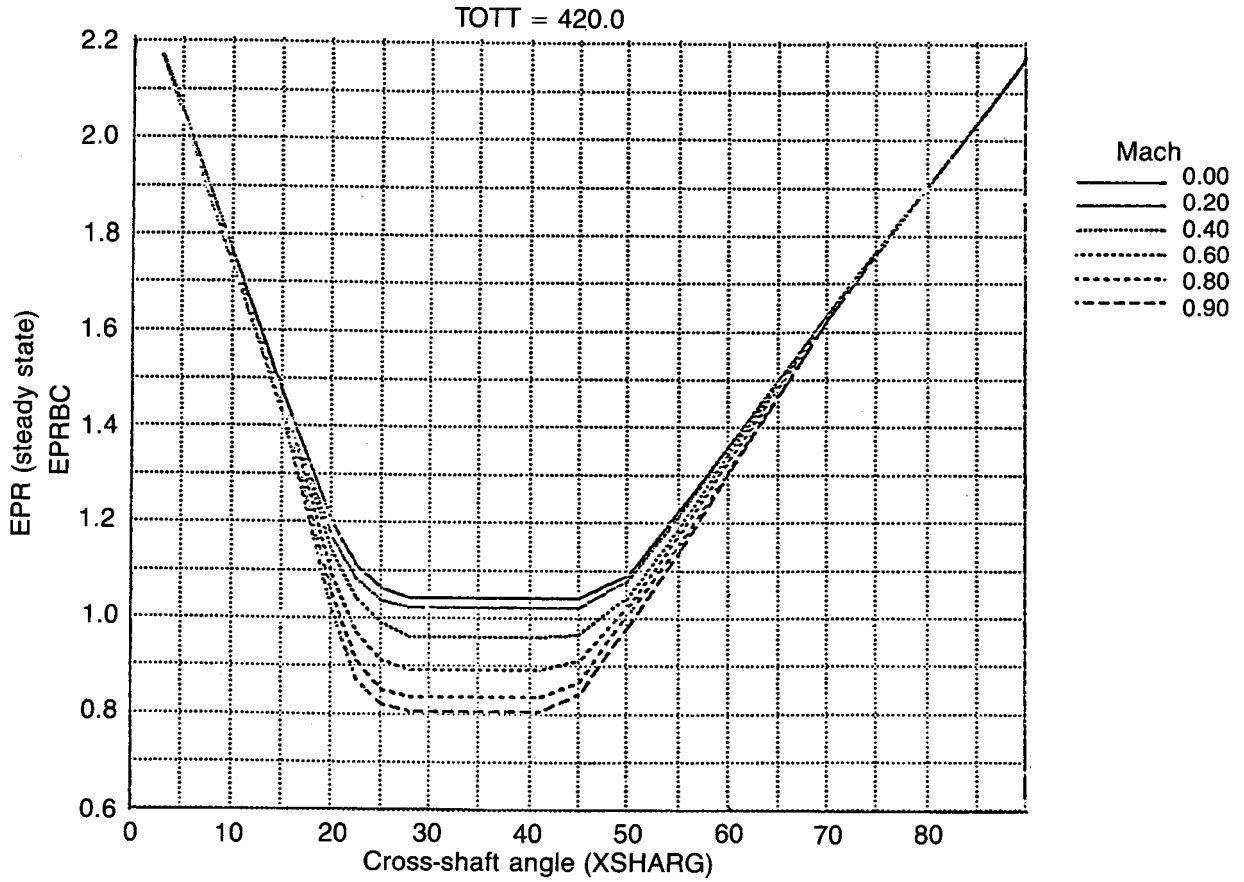

Figure 4. EPR Versus Cross-Shaft Angle (Bleed Valve Open) (Continued)

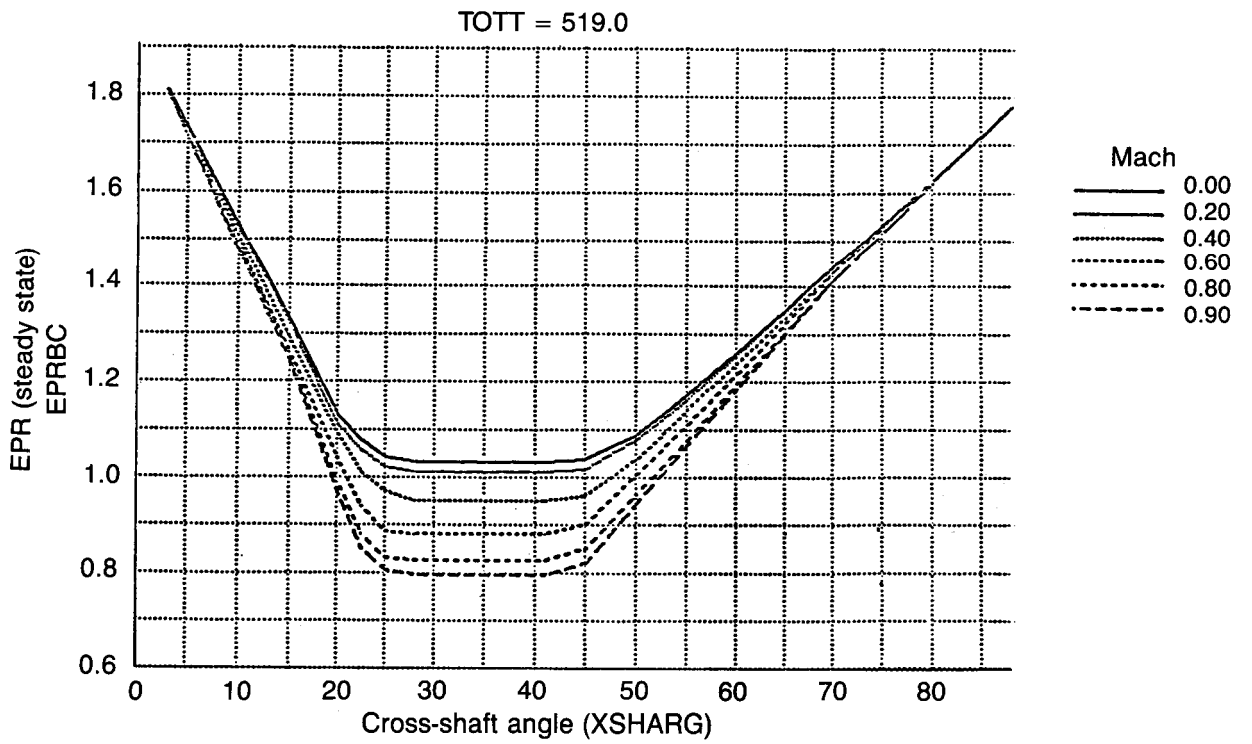

Figure 4. EPR Versus Cross-Shaft Angle (Bleed Valve Closed) (Continued)

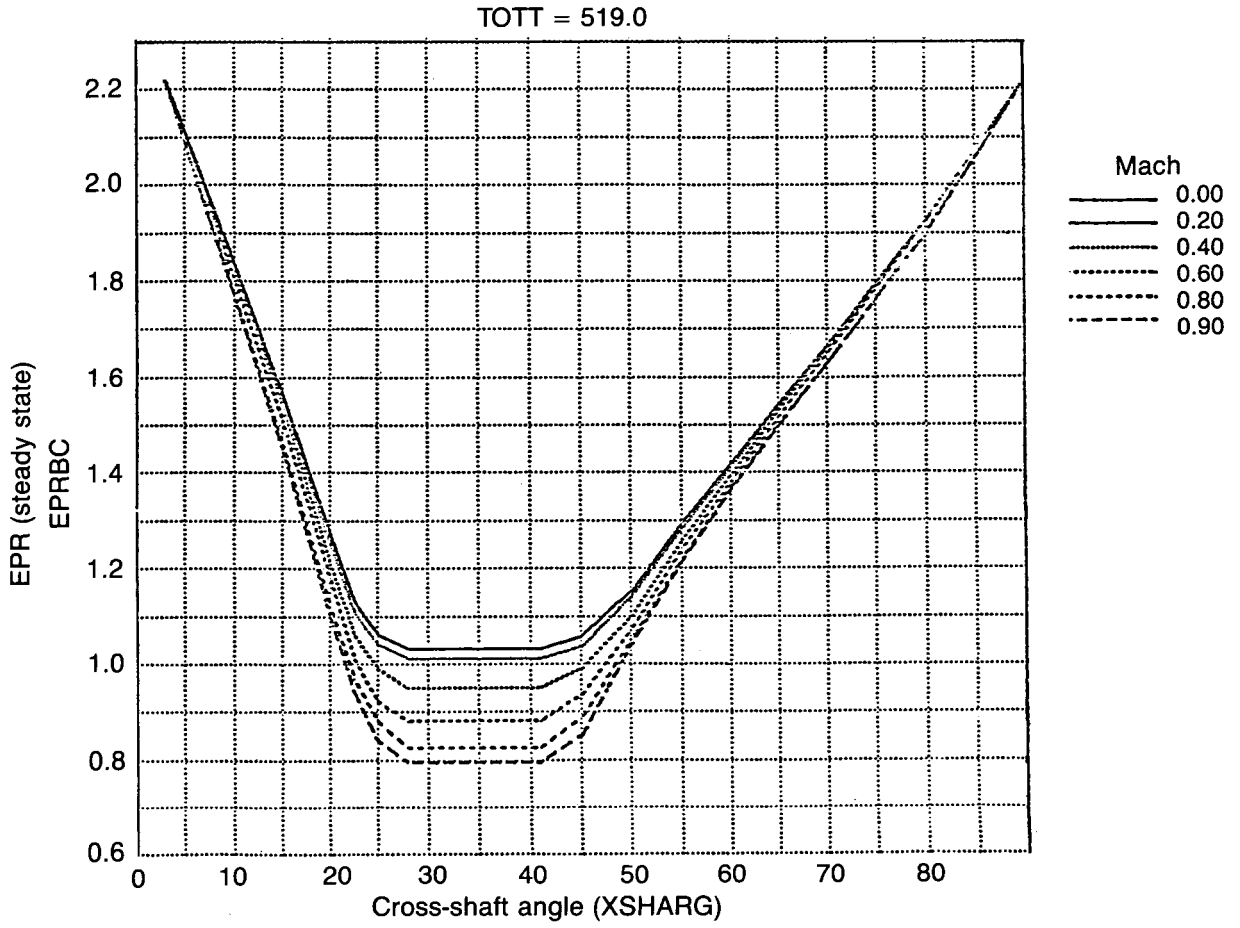

Figure 4. EPR Versus Cross-Shaft Angle (Bleed Valve Open) (Continued)

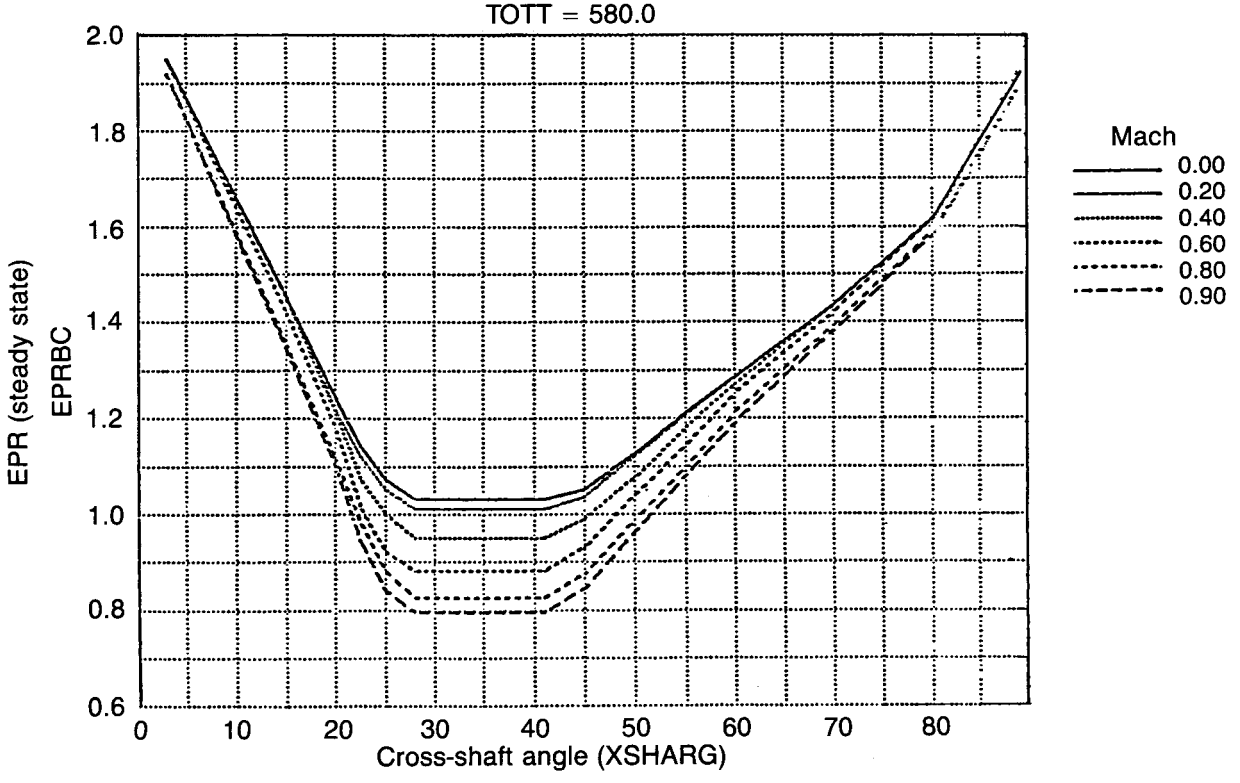

Figure 4. EPR Versus Cross-Shaft Angle (Bleed Valve Closed) (Continued)

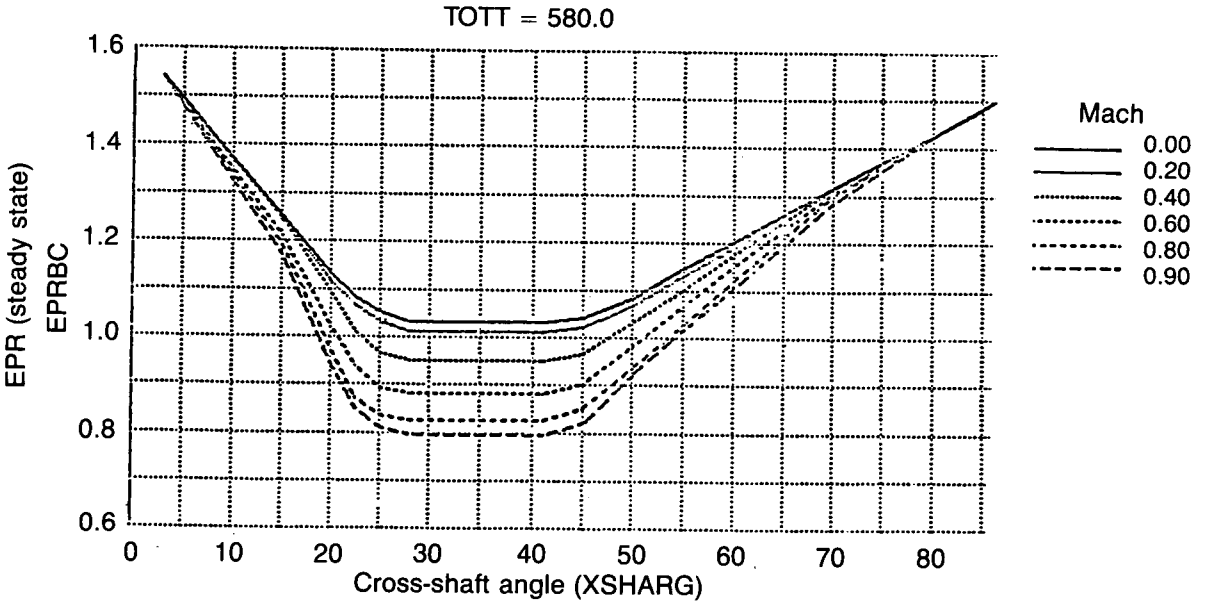

Figure 4. EPR Versus Cross-Shaft Angle (Bleed Valve Open) (Concluded)

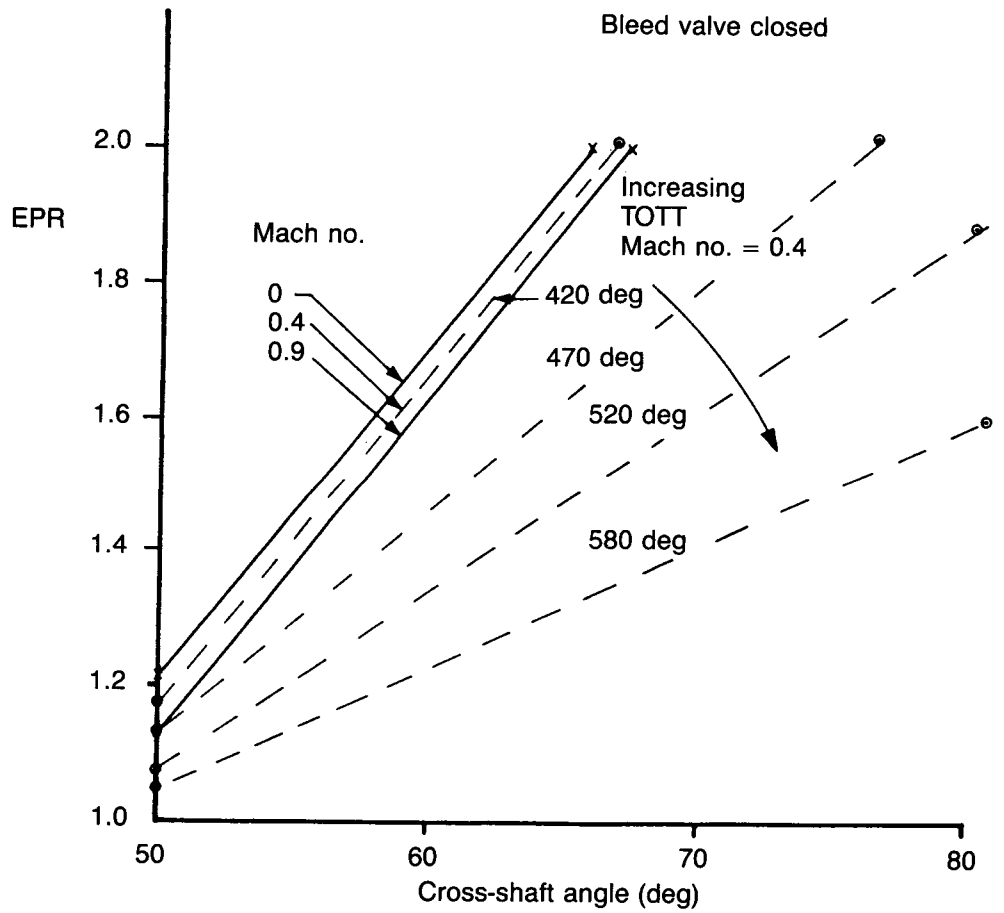

Figure 5. EPR Versus Cross-Shaft Angle Showing Variation With Mach and Total Air Temperature (TOTT)

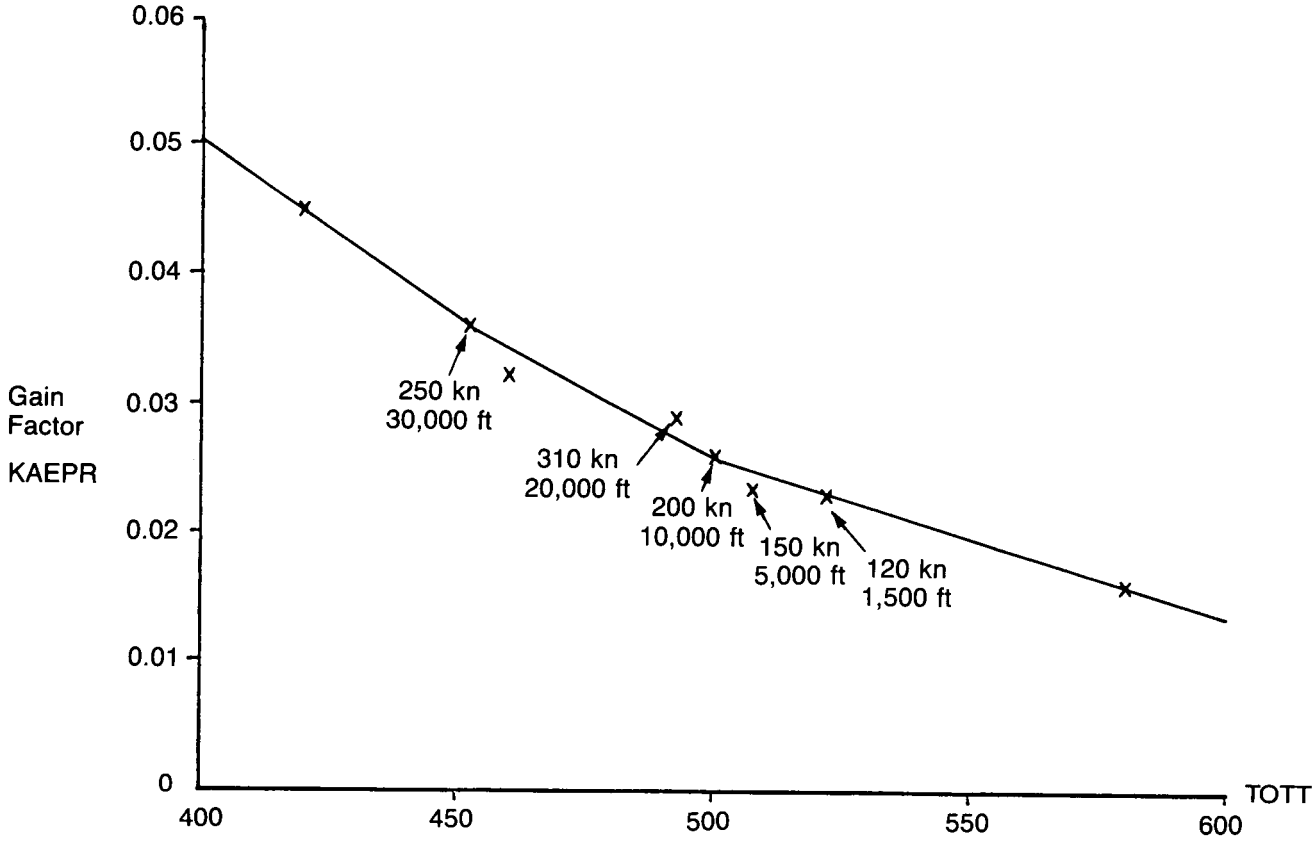

Figure 6. KAEPR Against Total Air Temperature (TOTT)

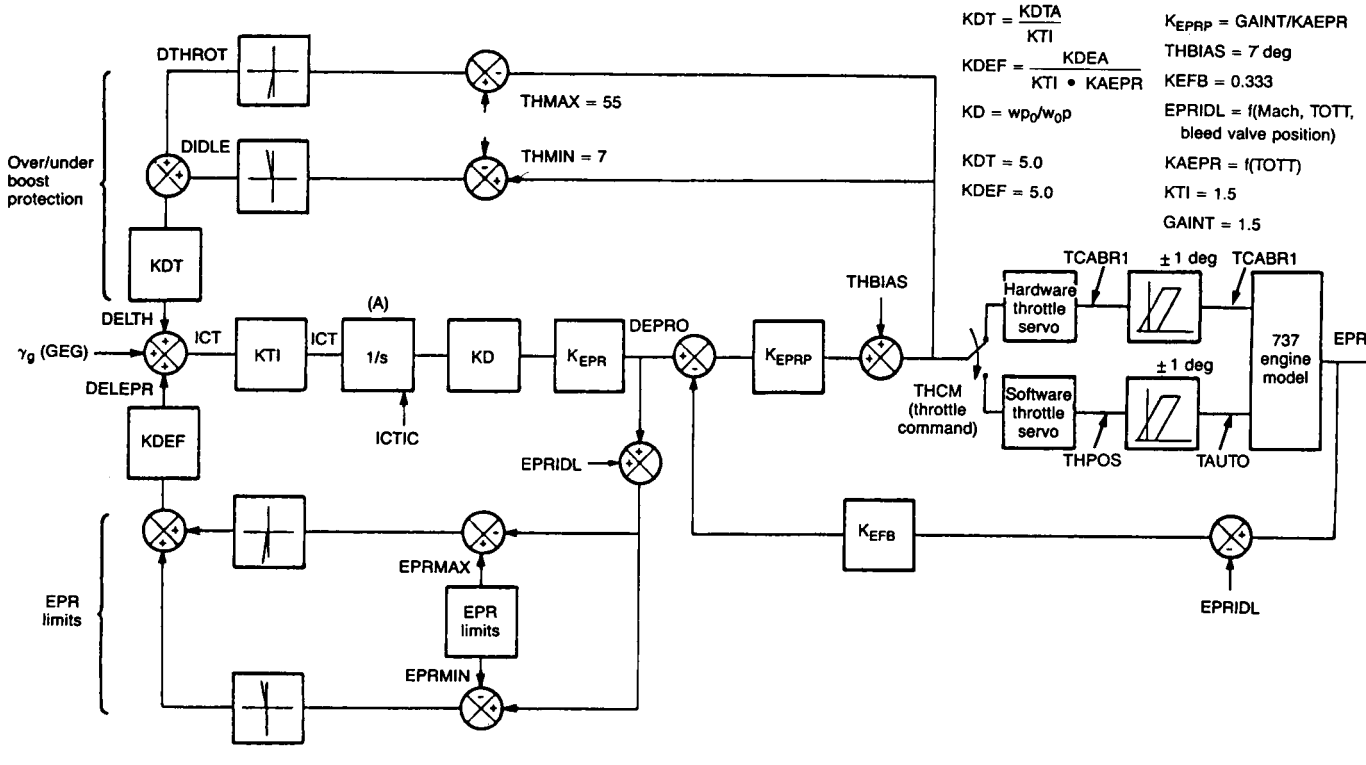

Figure 7. EPR Control Loop

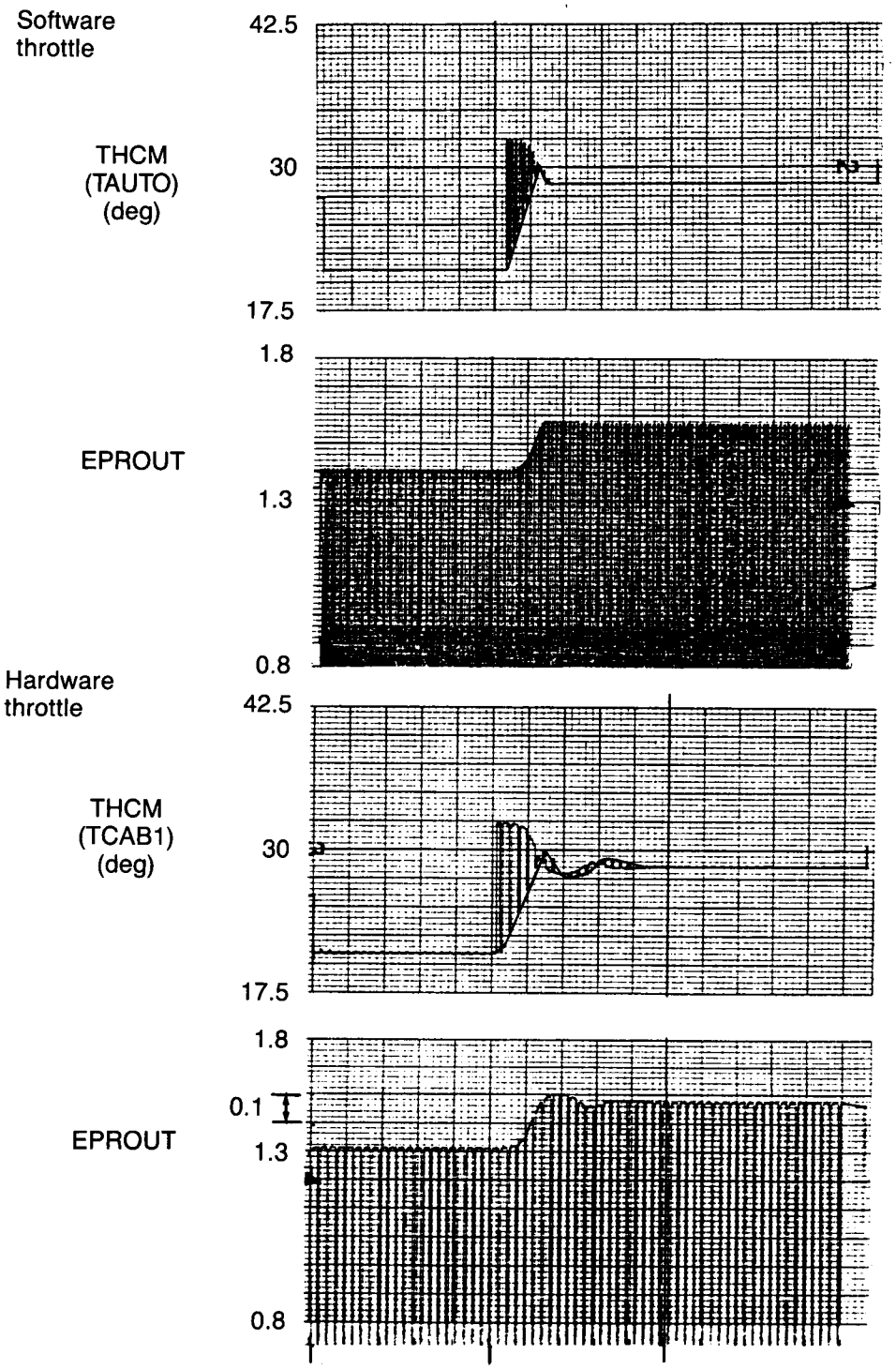

Figure 8. Case 1: Step Response to 0.2 Change in EPR Command

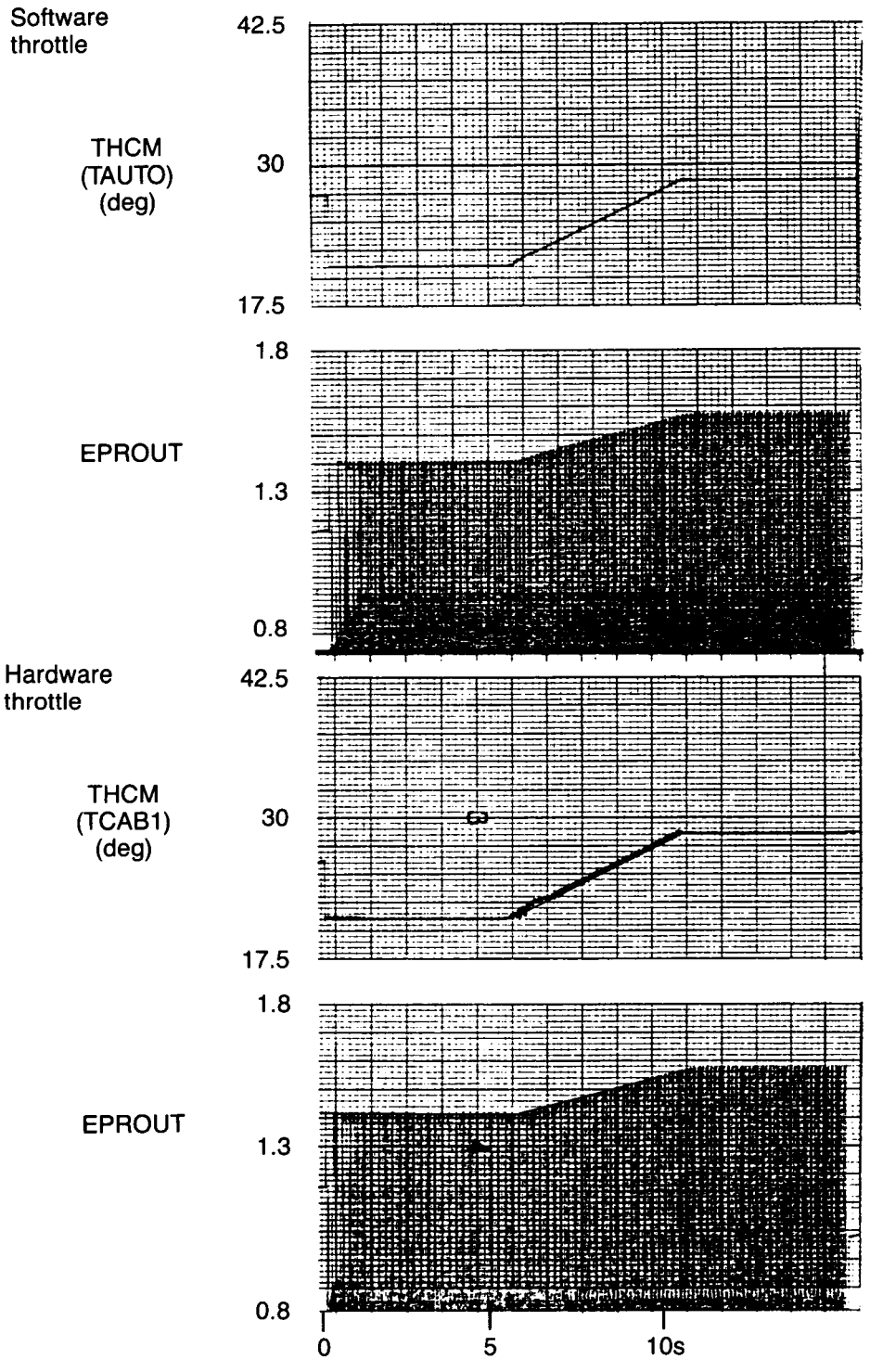

Figure 9. Case 2: Ramp Response to 0.04/s Change in EPR Command

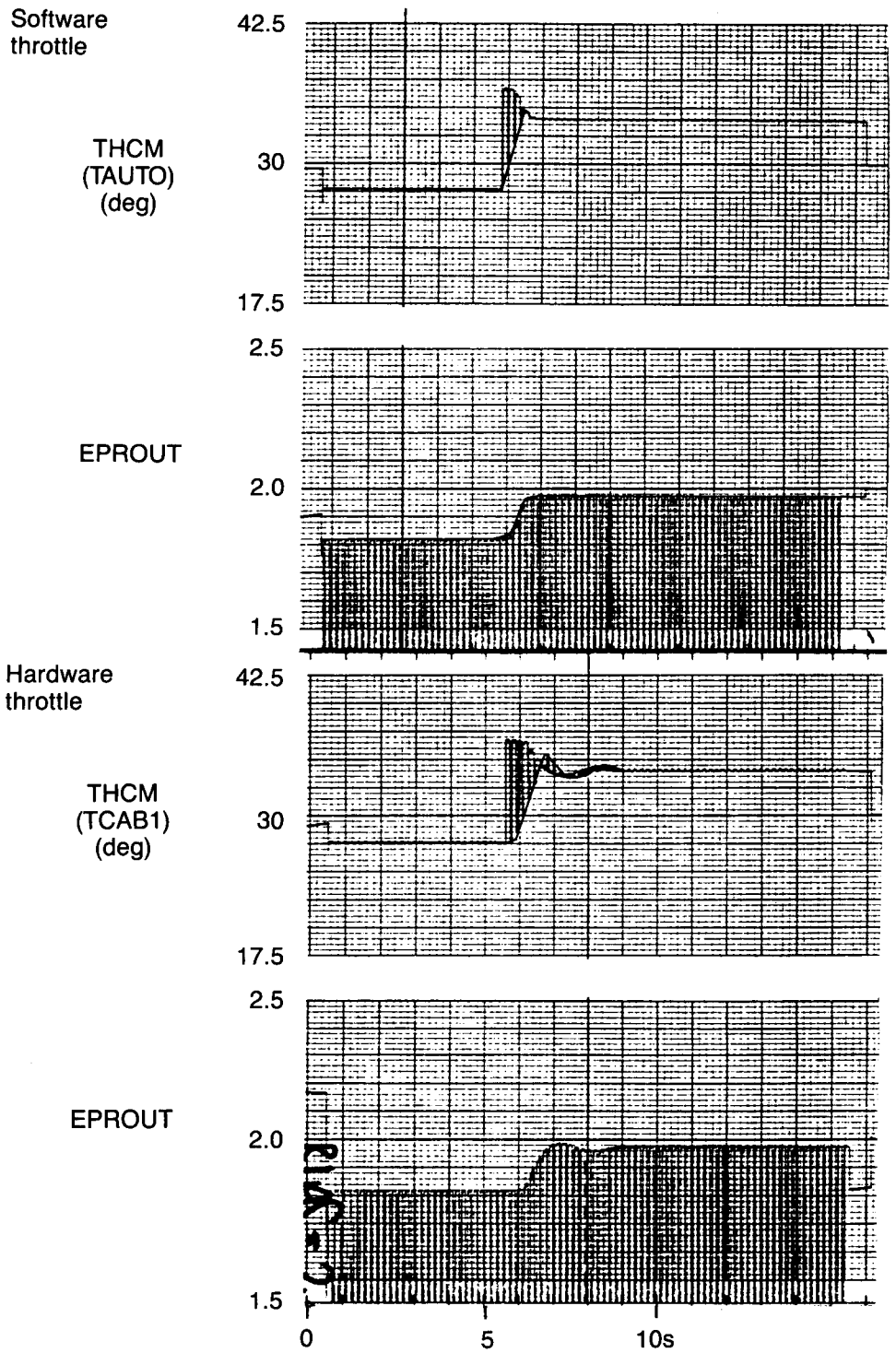

Figure 10. Case 3: Step Response to 0.2 Change in EPR Command

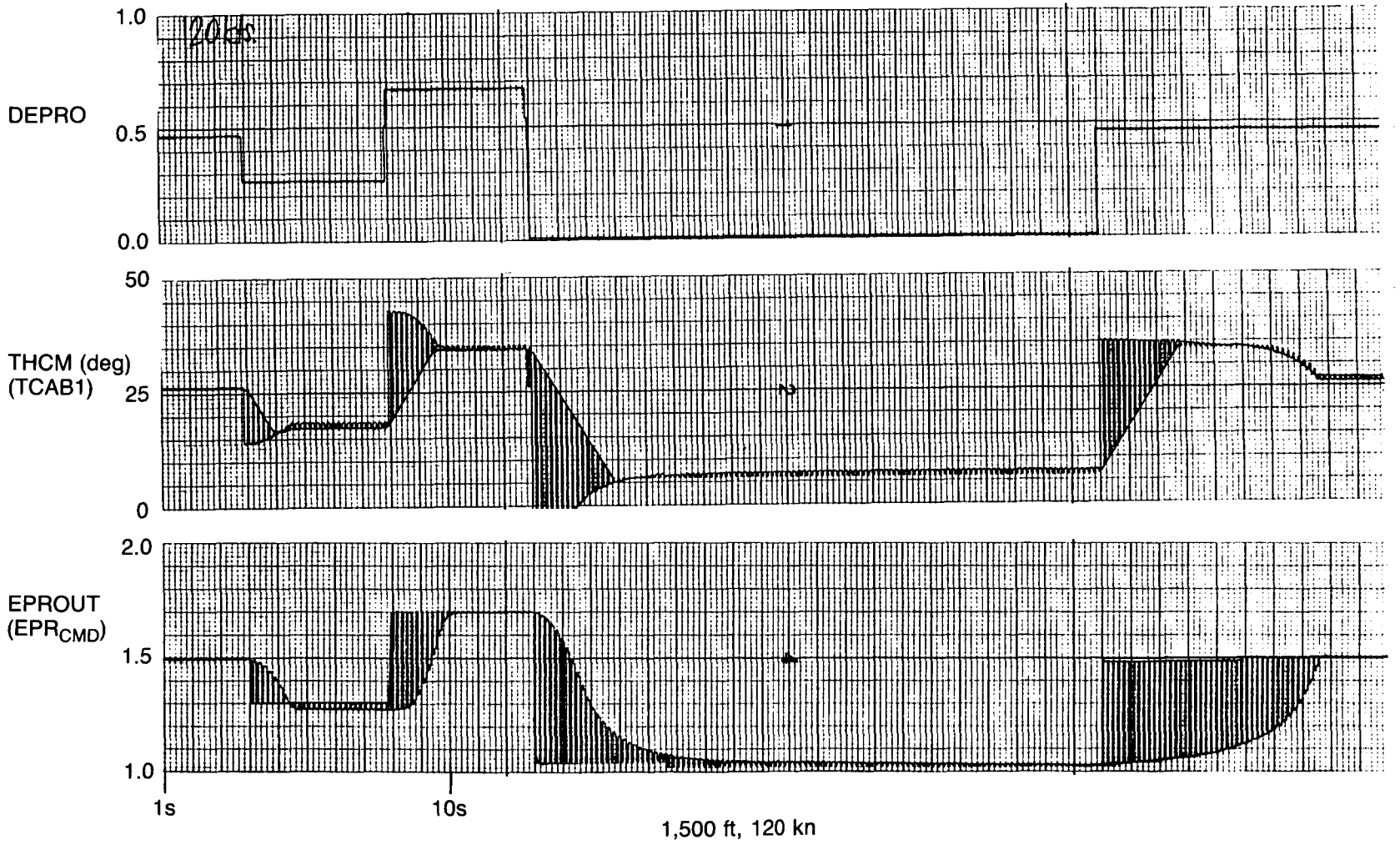

Figure 11. Spool Up and Spool Down Characteristics

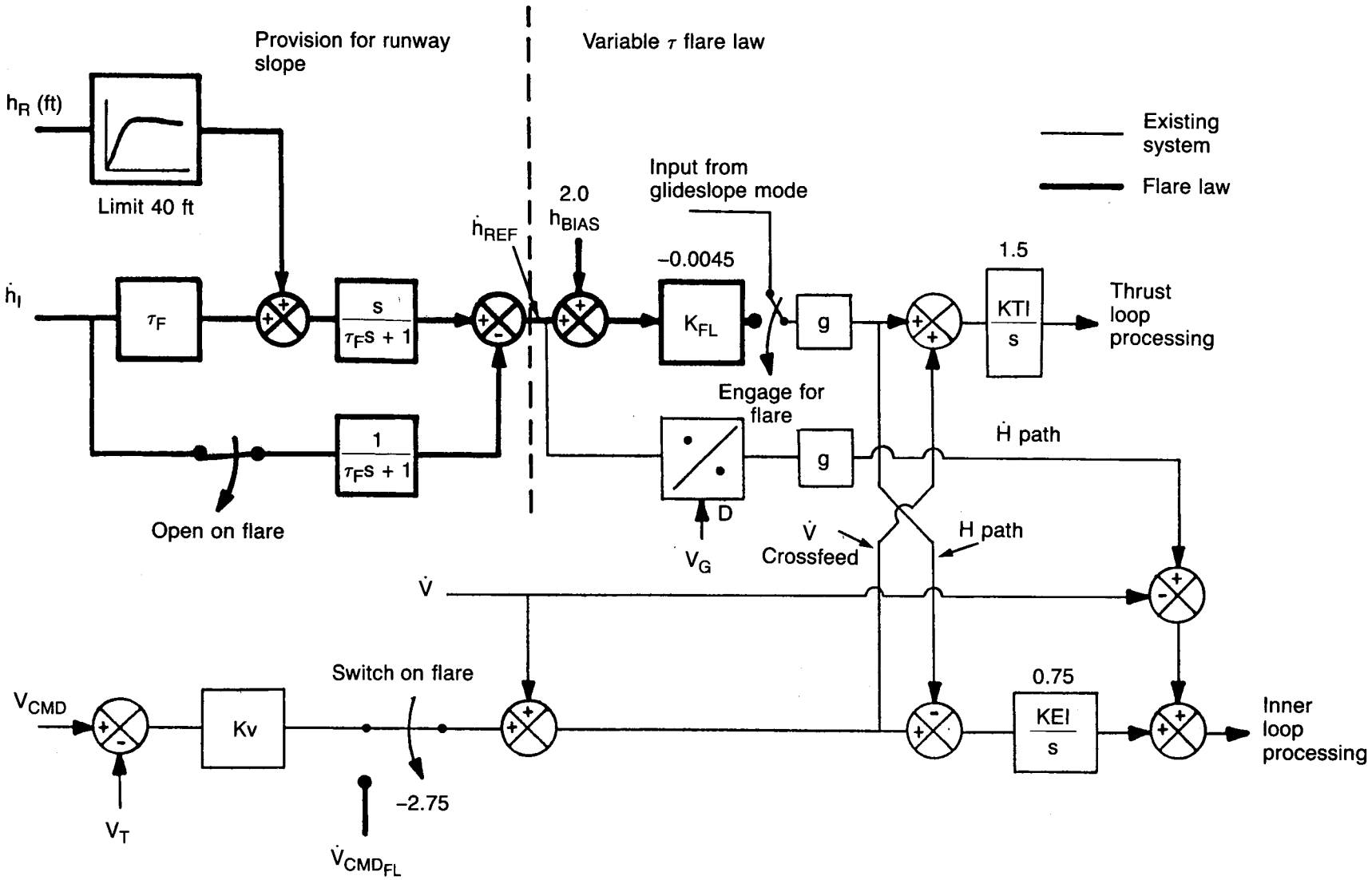

Figure 12. Variable τ Implementation

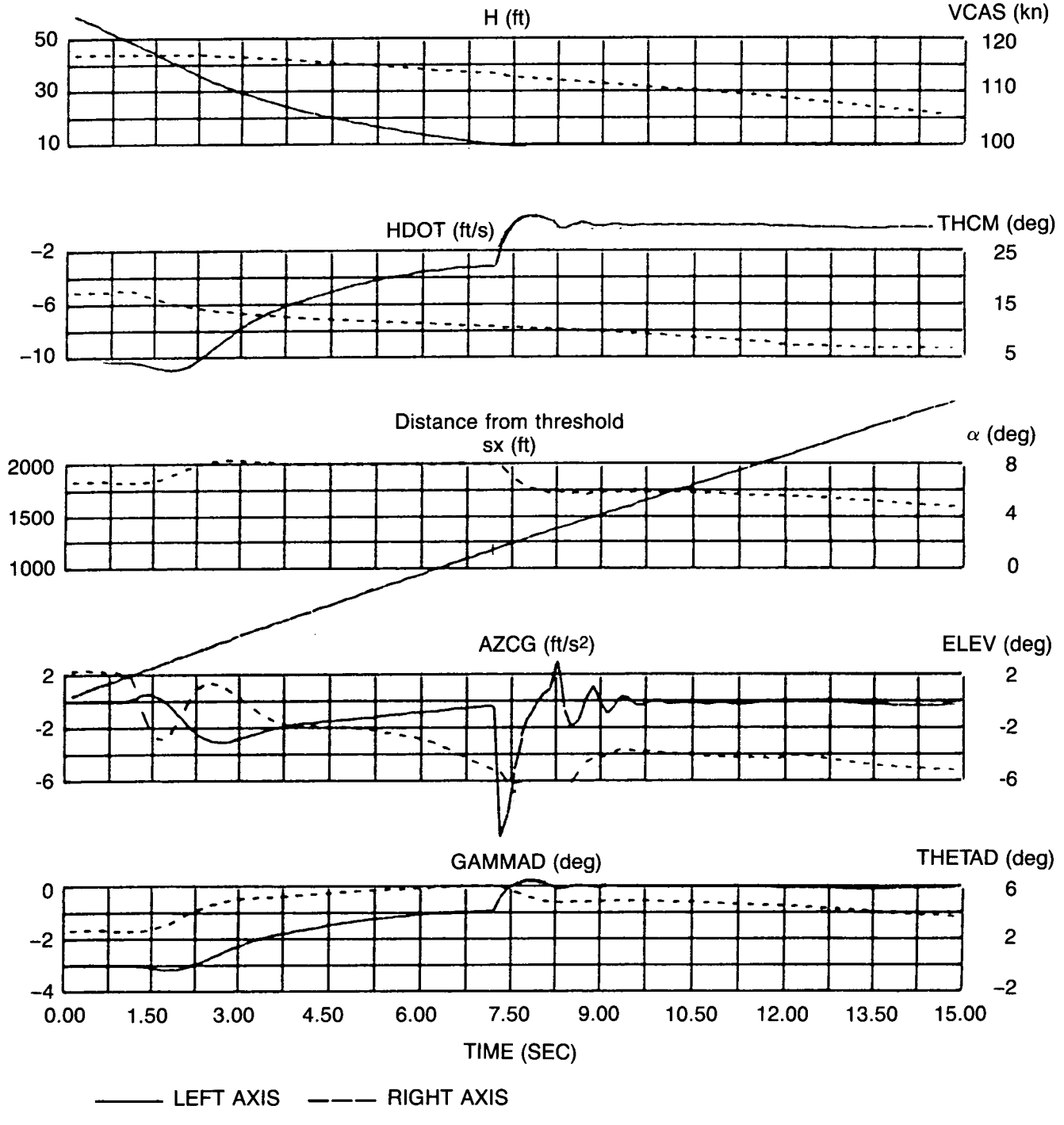

Figure 13. Variable τFlare Law: 85,000 lb, V_{CAS} = 117 kn, CG = 0.20

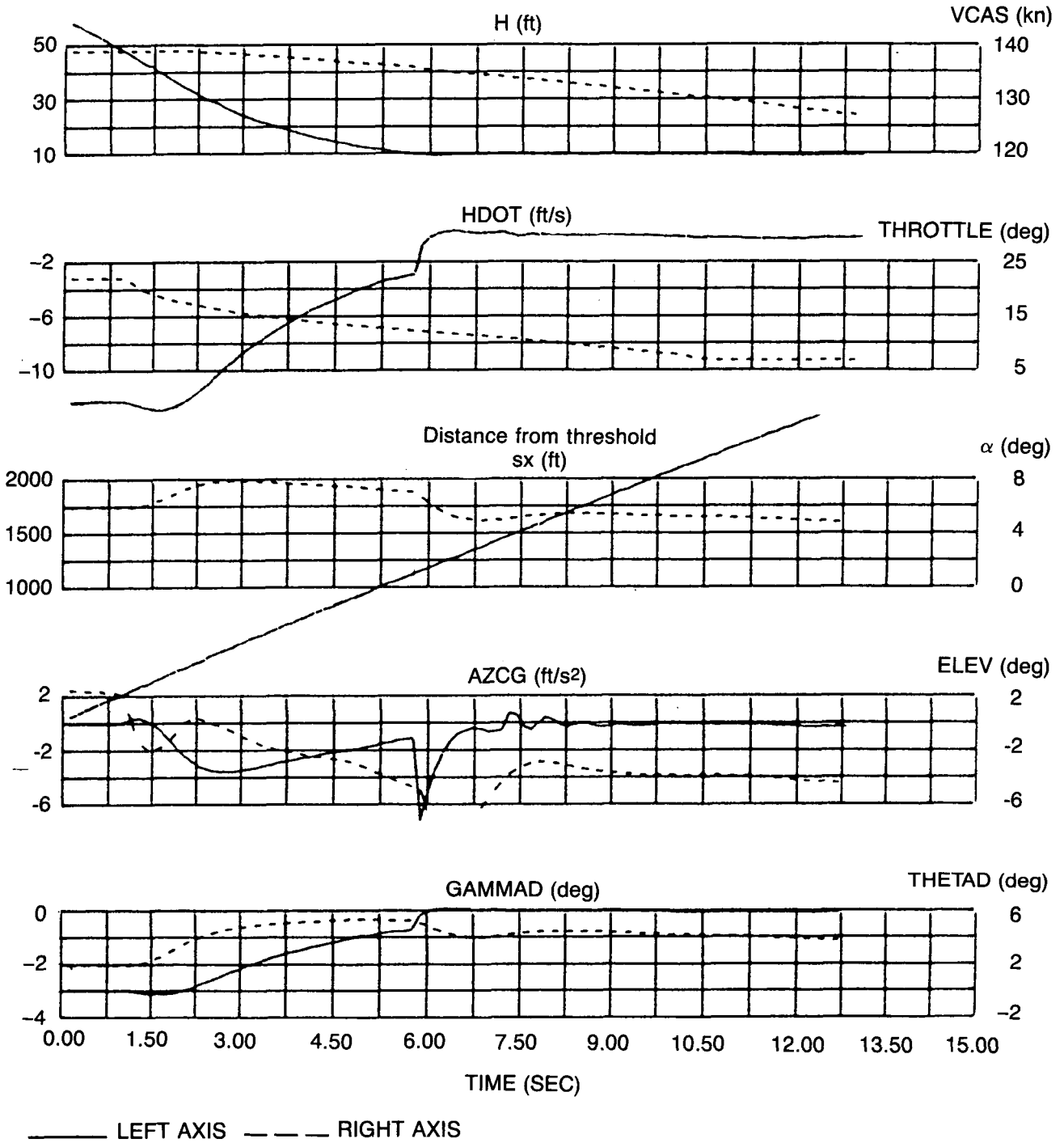

Figure 14. Variable τFlare Law: 115,000 lb, V_{CAS} = 119 kn, CG = 0.2

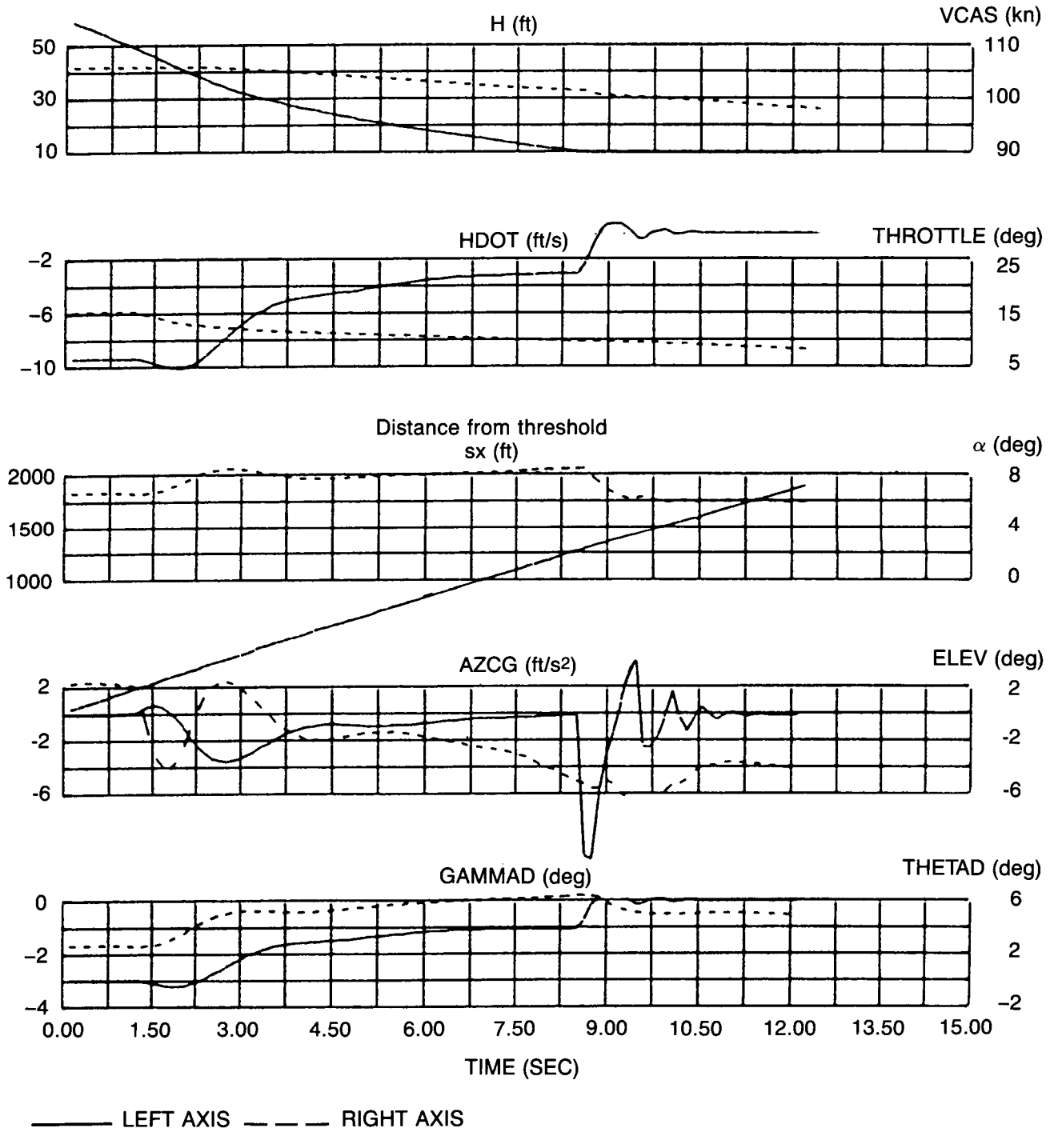

Figure 15. Variable τFlare Law: 70,000 lb, V_{CAS} = 106 kn, CG = 0.20

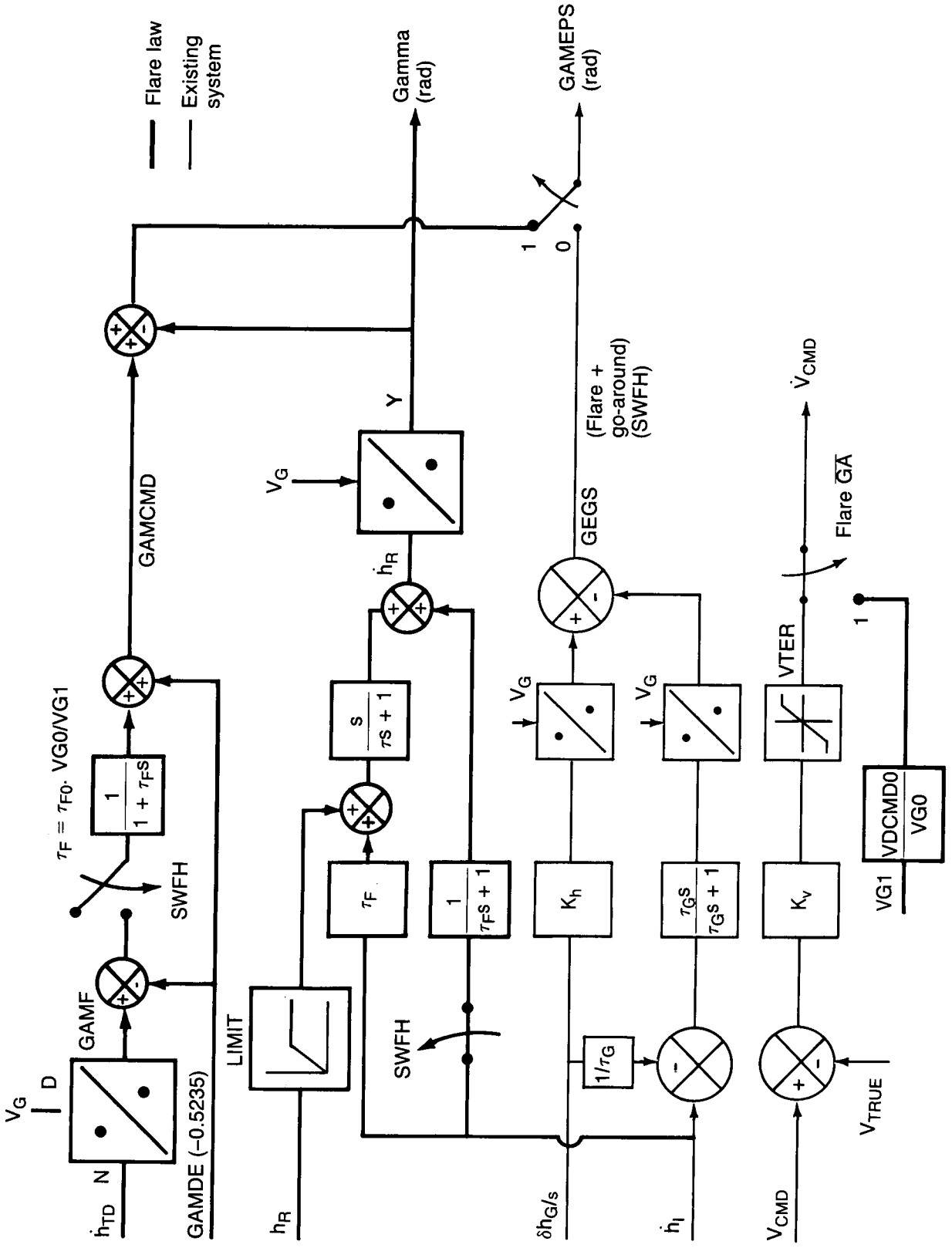

Figure 16. Implementation of Gamma-VDOT Flare Law

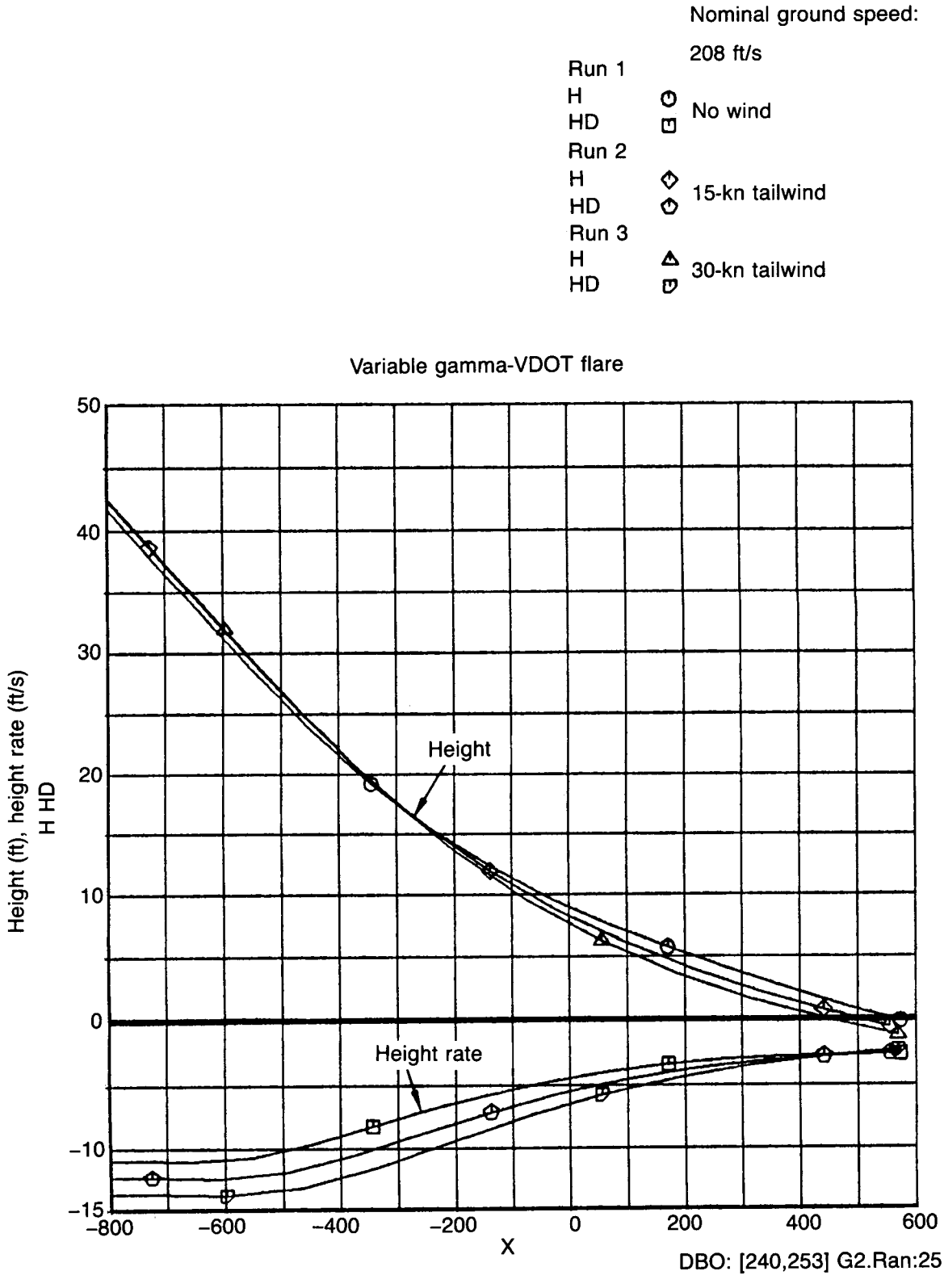

Figure 17. Height and Height Rate Versus Distance Along Runway

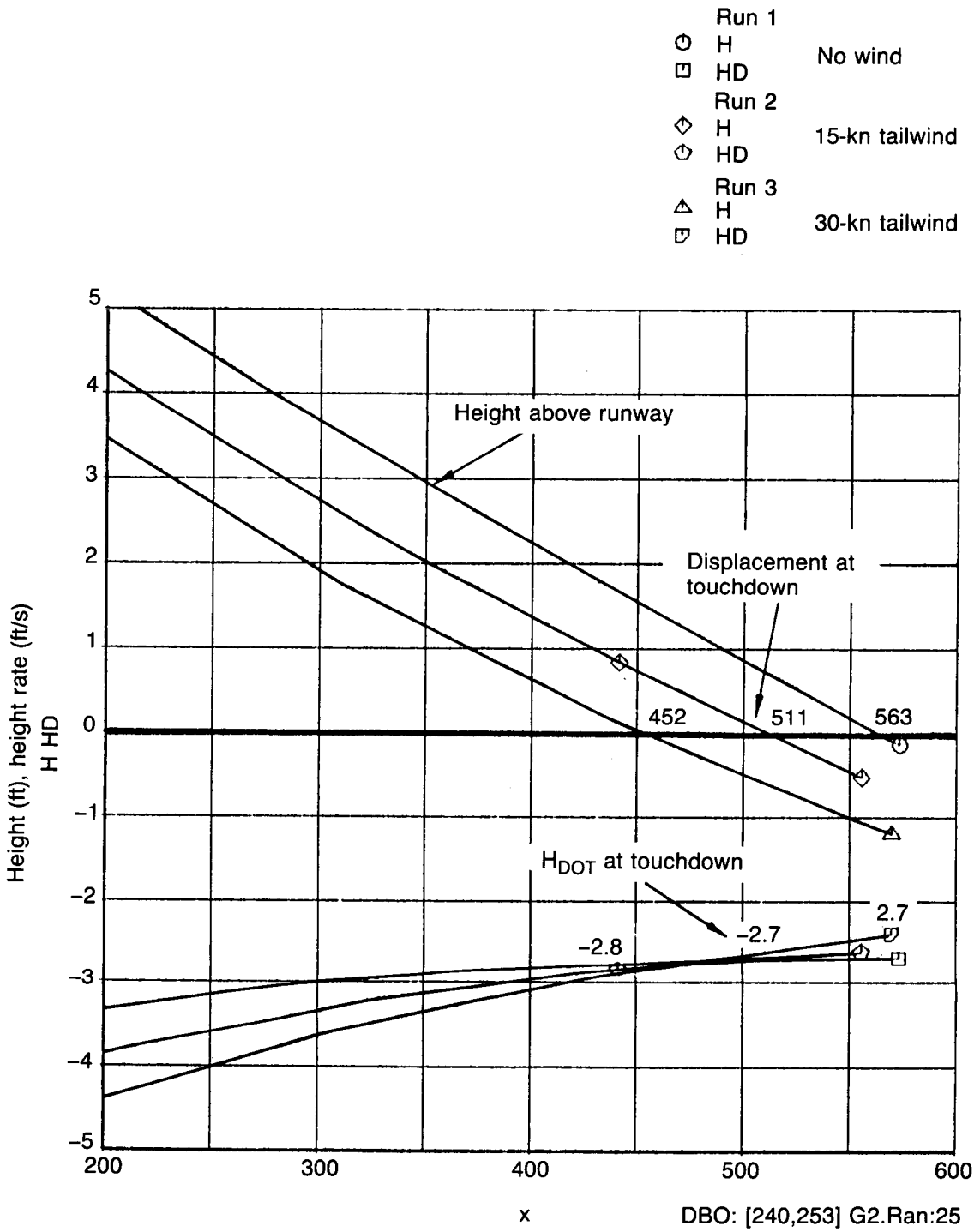

Figure 18. Height, Height Rate Versus Displacement (Enlargement of Touchdown Area)

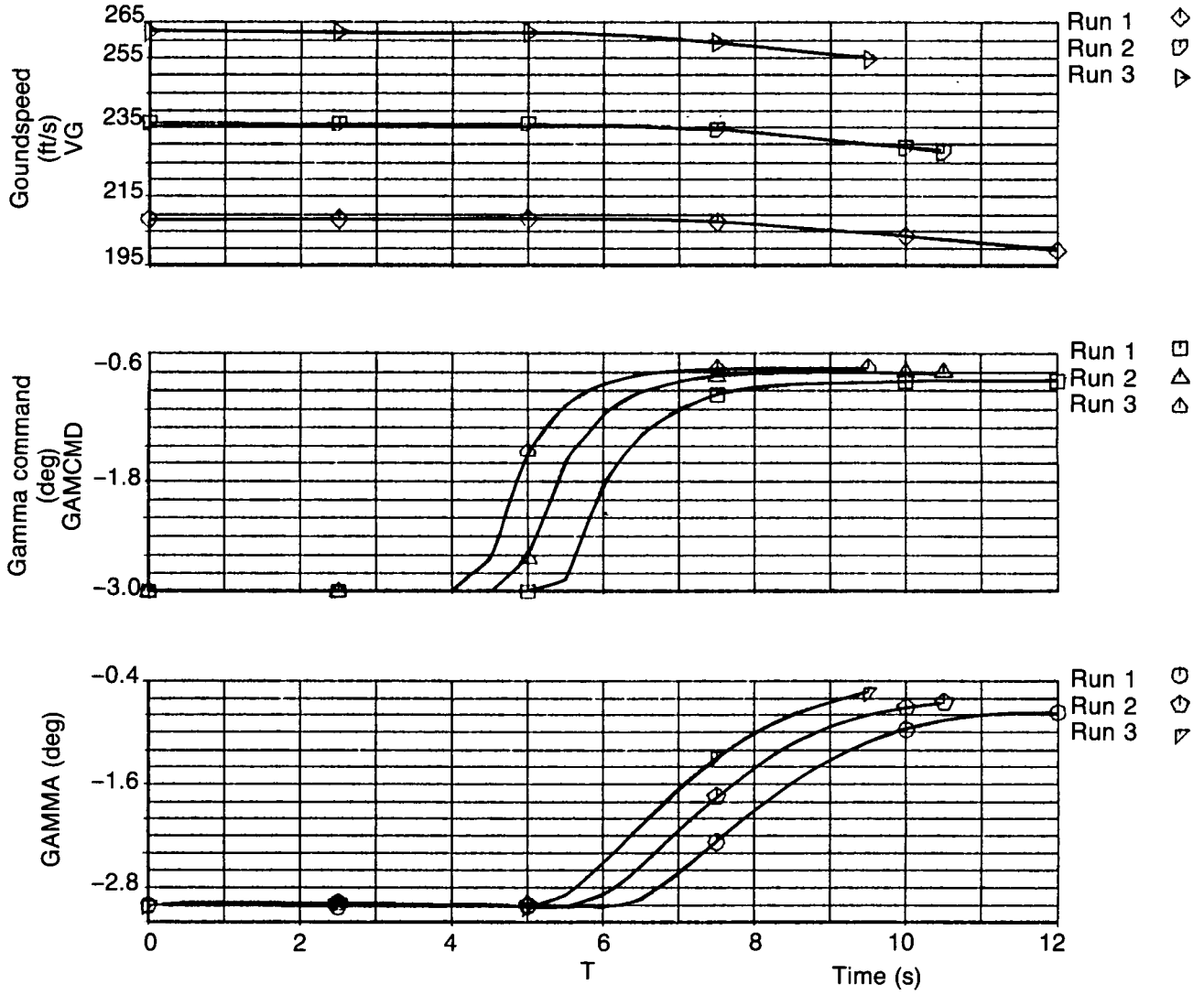

Figure 19. Gamma, Gamma Command, and Groundspeed Against Time

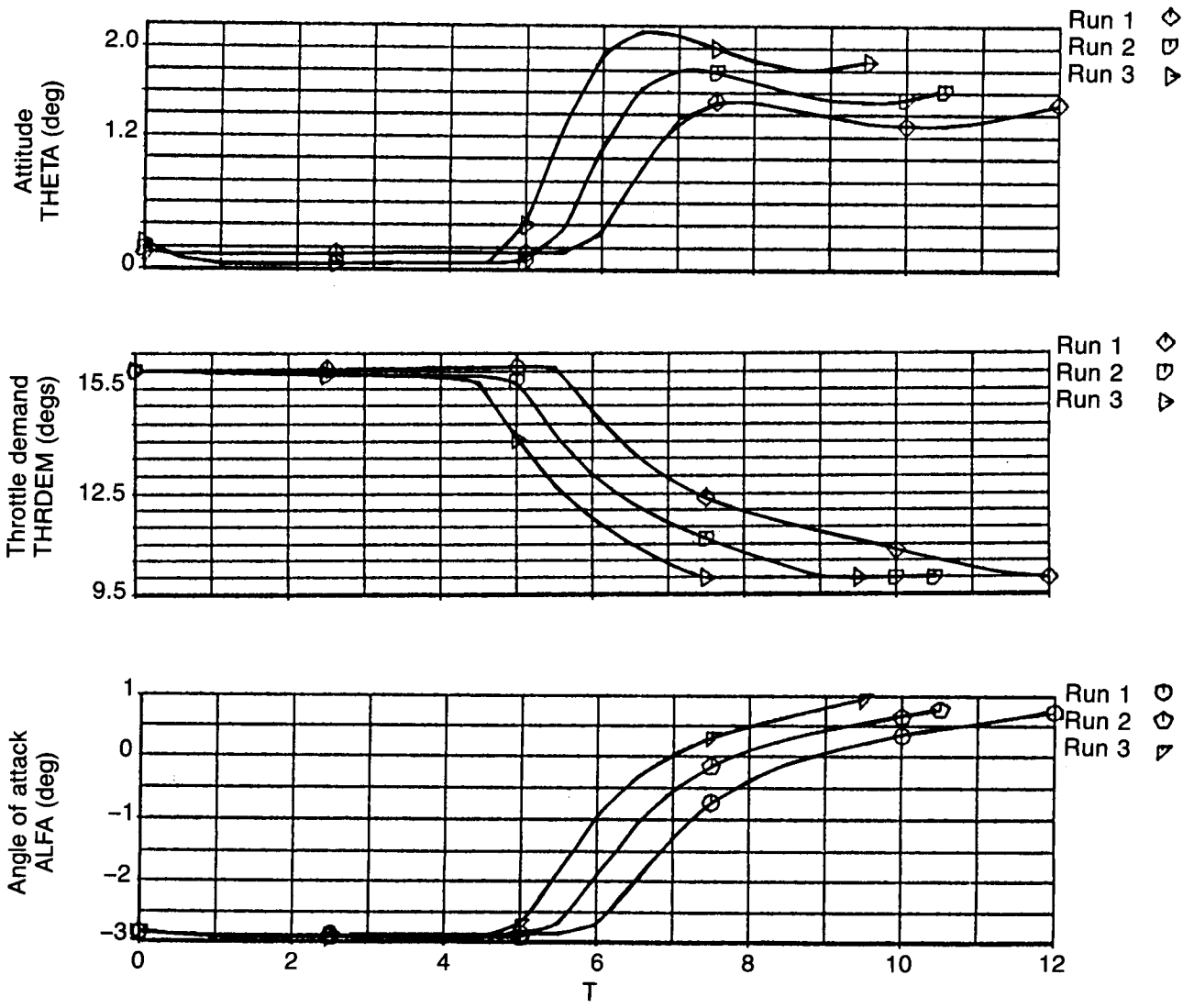

Figure 20. Theta, Throttle Demand, and Alpha Against Time

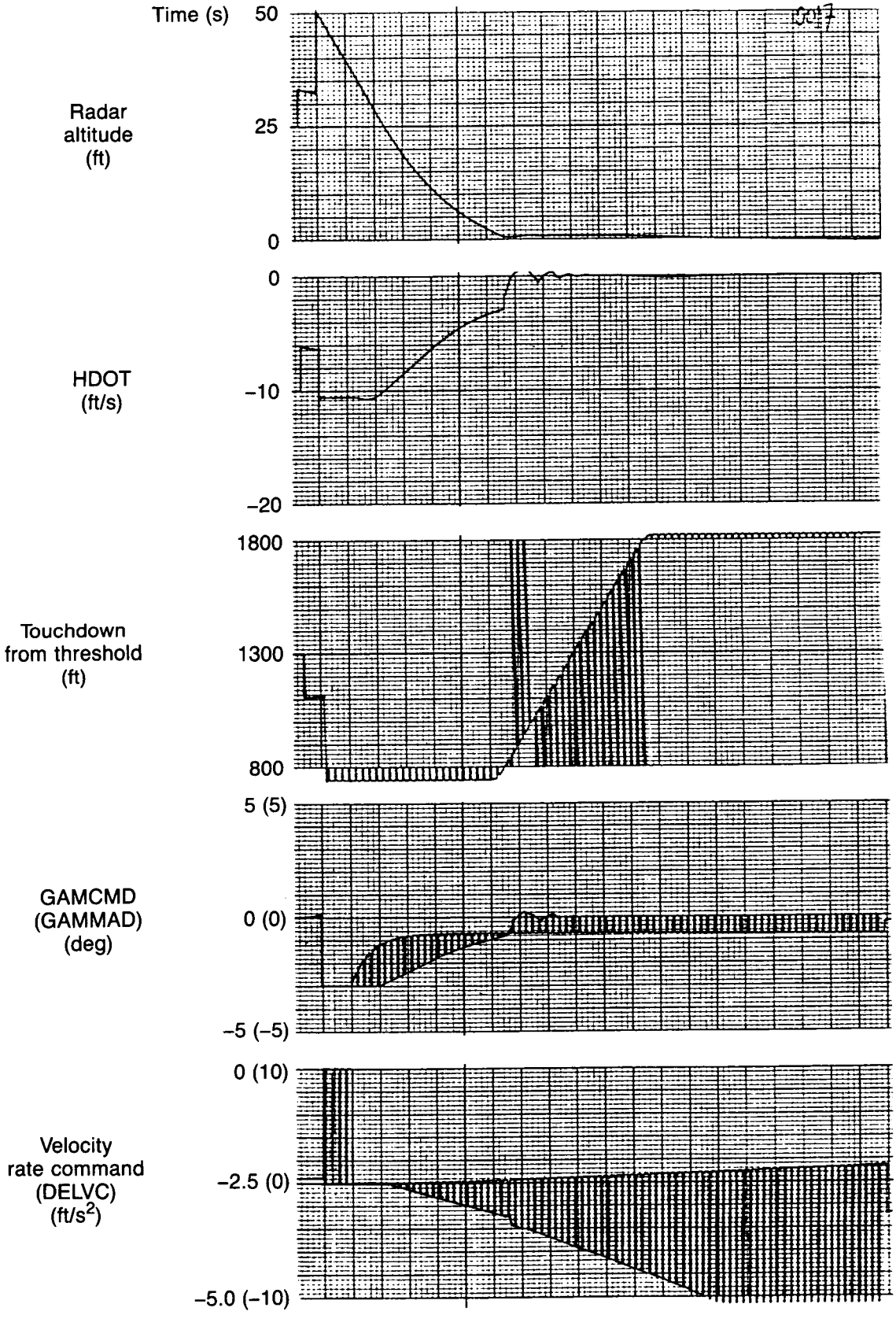

Figure 21. Flare Results: Noise Free

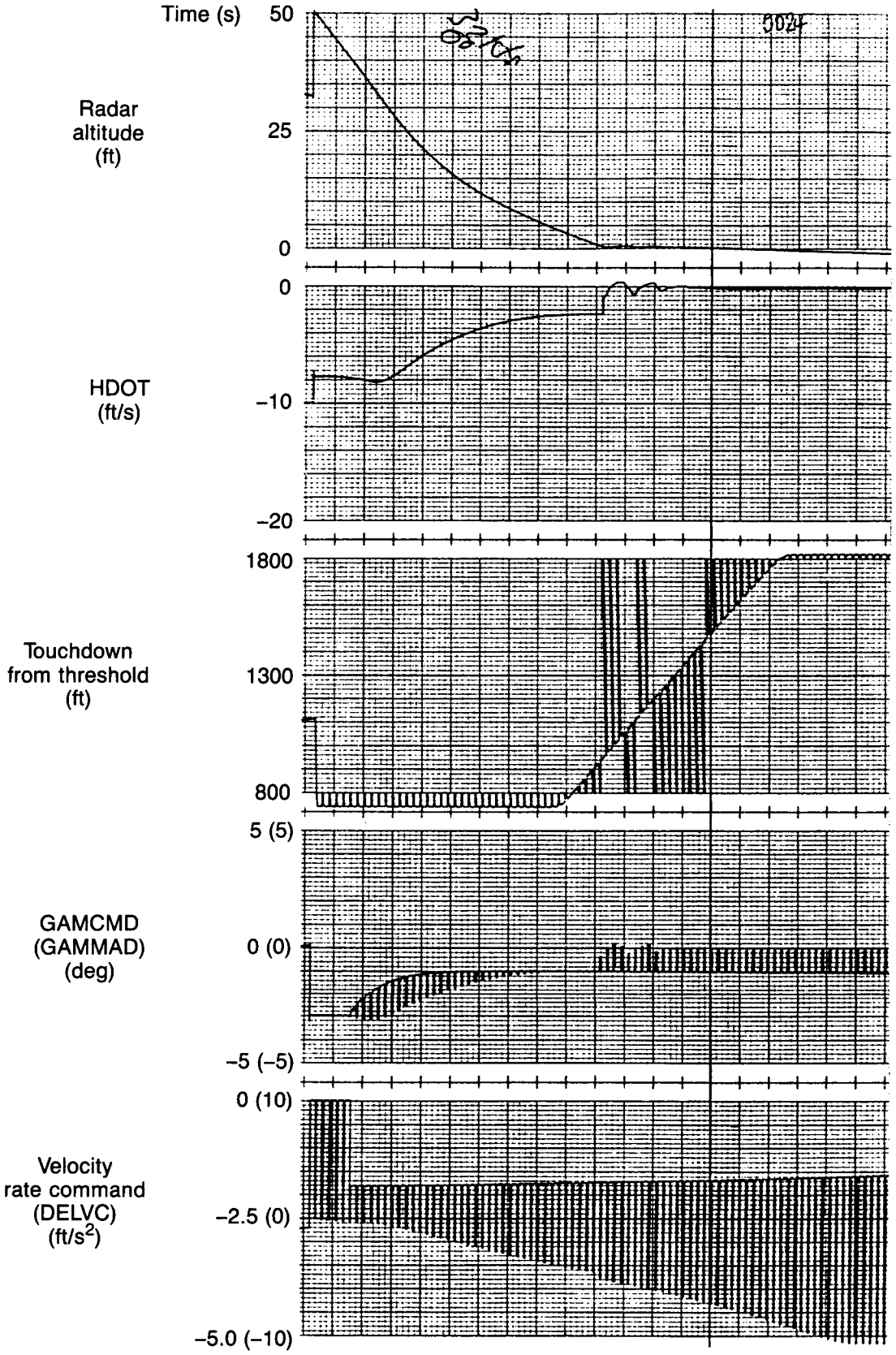

Figure 22. Flare Results: 32-kn Headwind

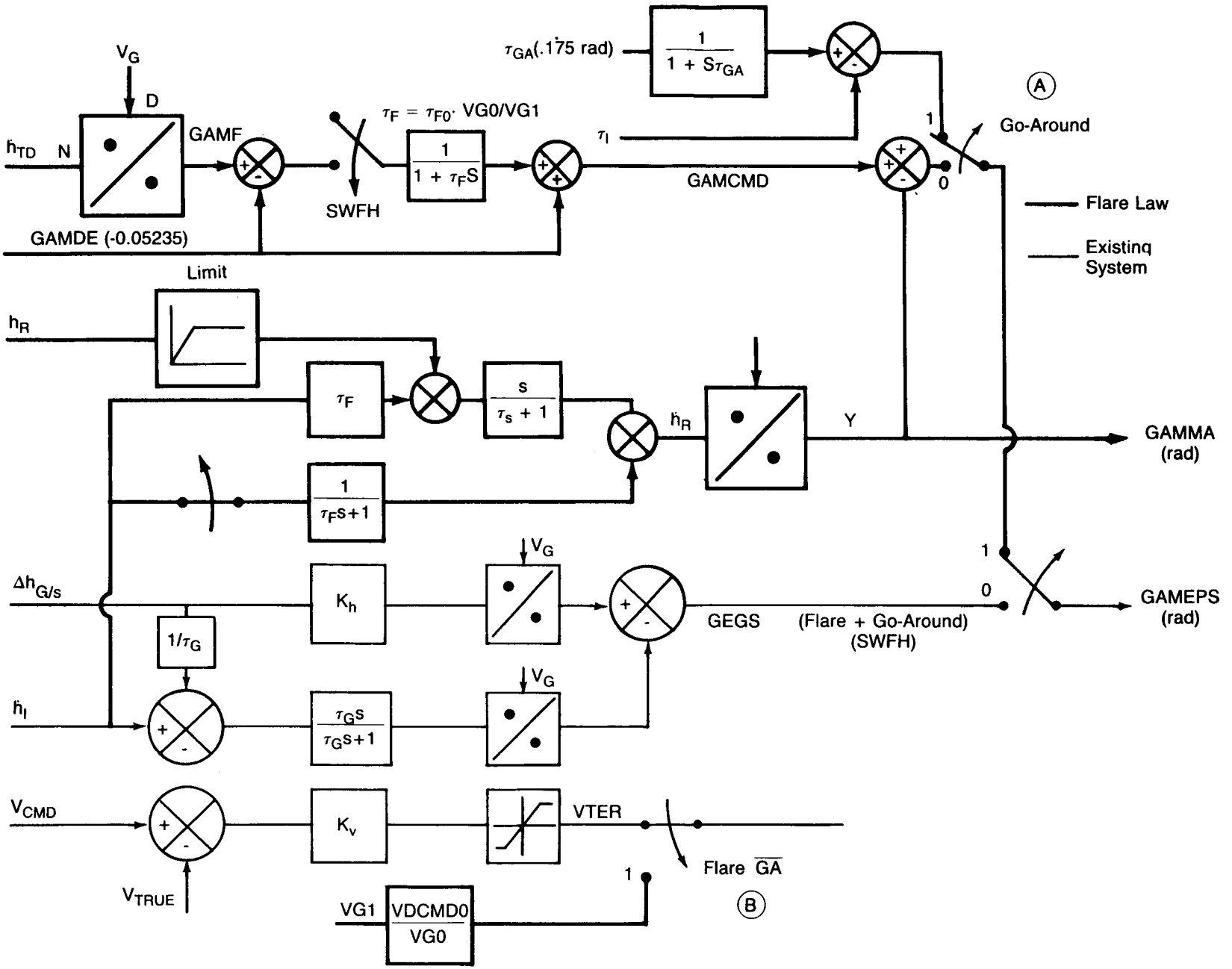

Figure 23. Gamma-VDOT Flare Law With Go-Around Mode

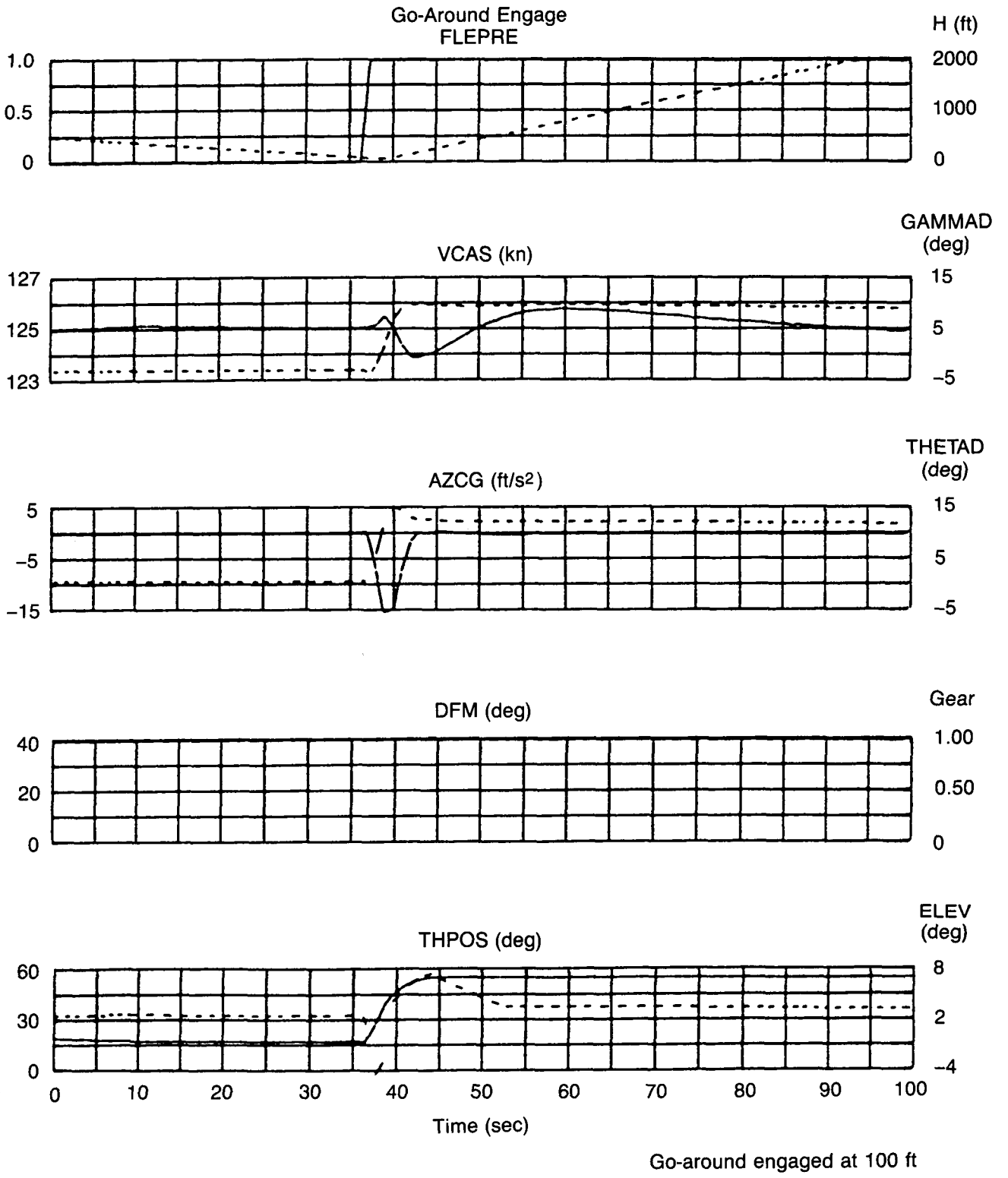

Figure 24. Go-Around (τ_{GA} = 0.2s)

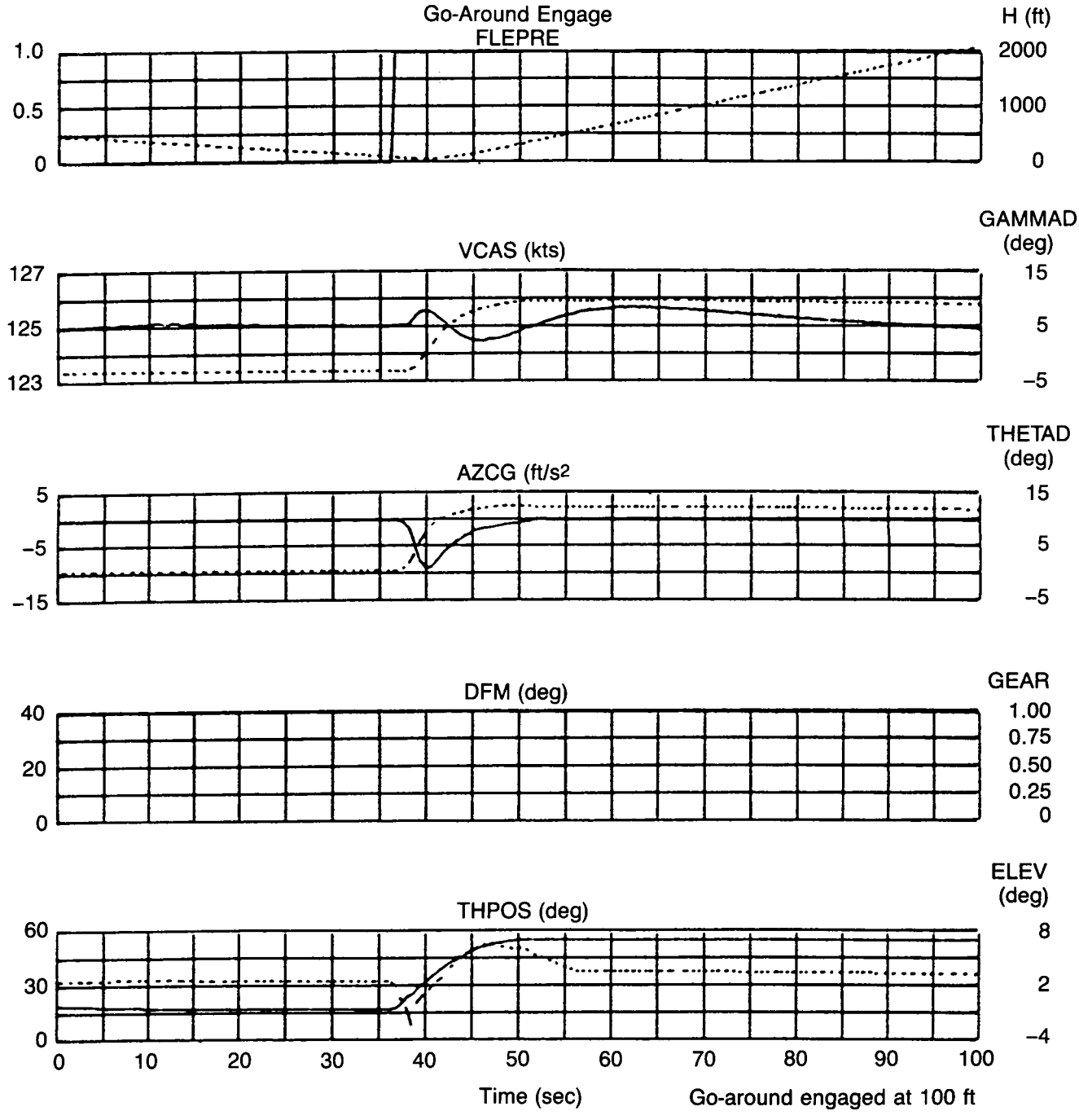

Figure 25. Go-Around (τ_{GA} = 3s)

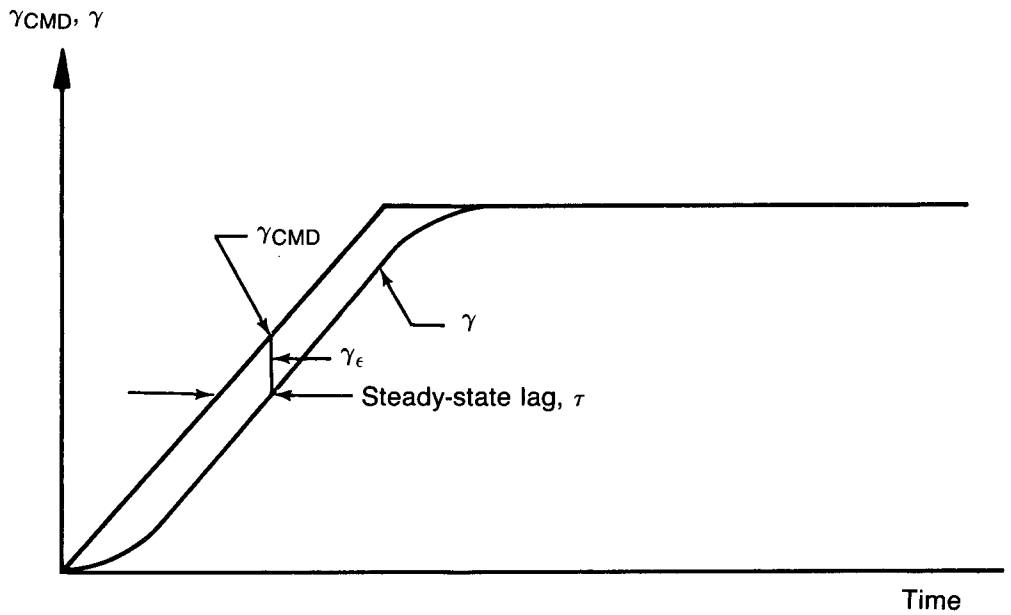

Figure 26. Ideal Vel-CCS Response

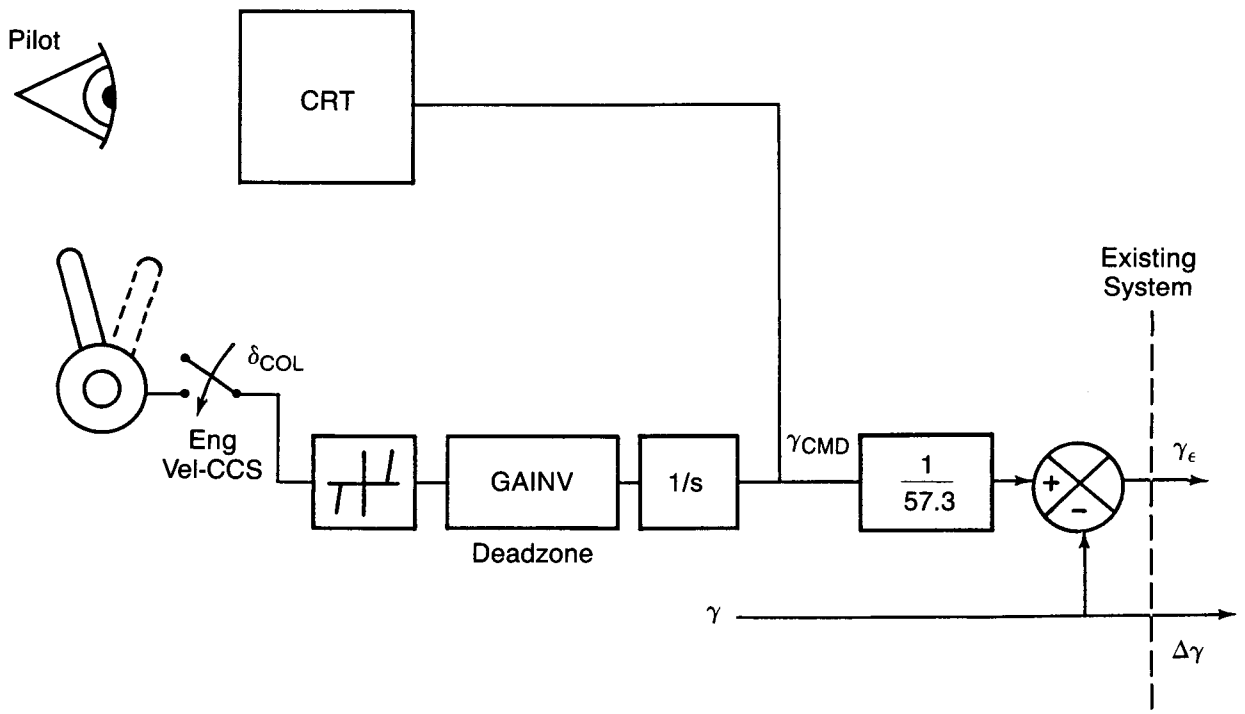

Figure 27. Simplified Block Diagram of Vel-CCS

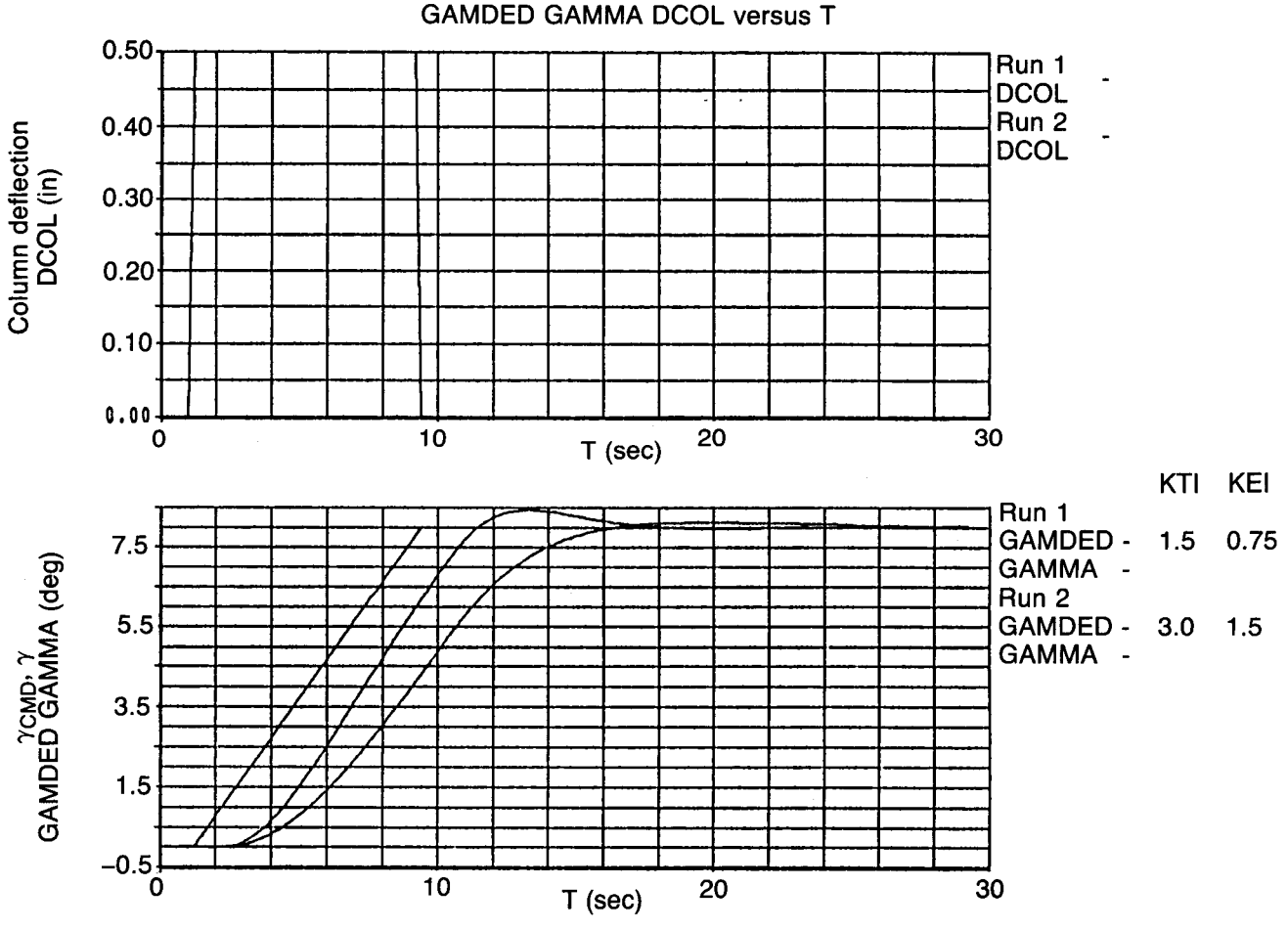

Figure 28. γ_{CMD}, γ for 0.5-in Column Deflection

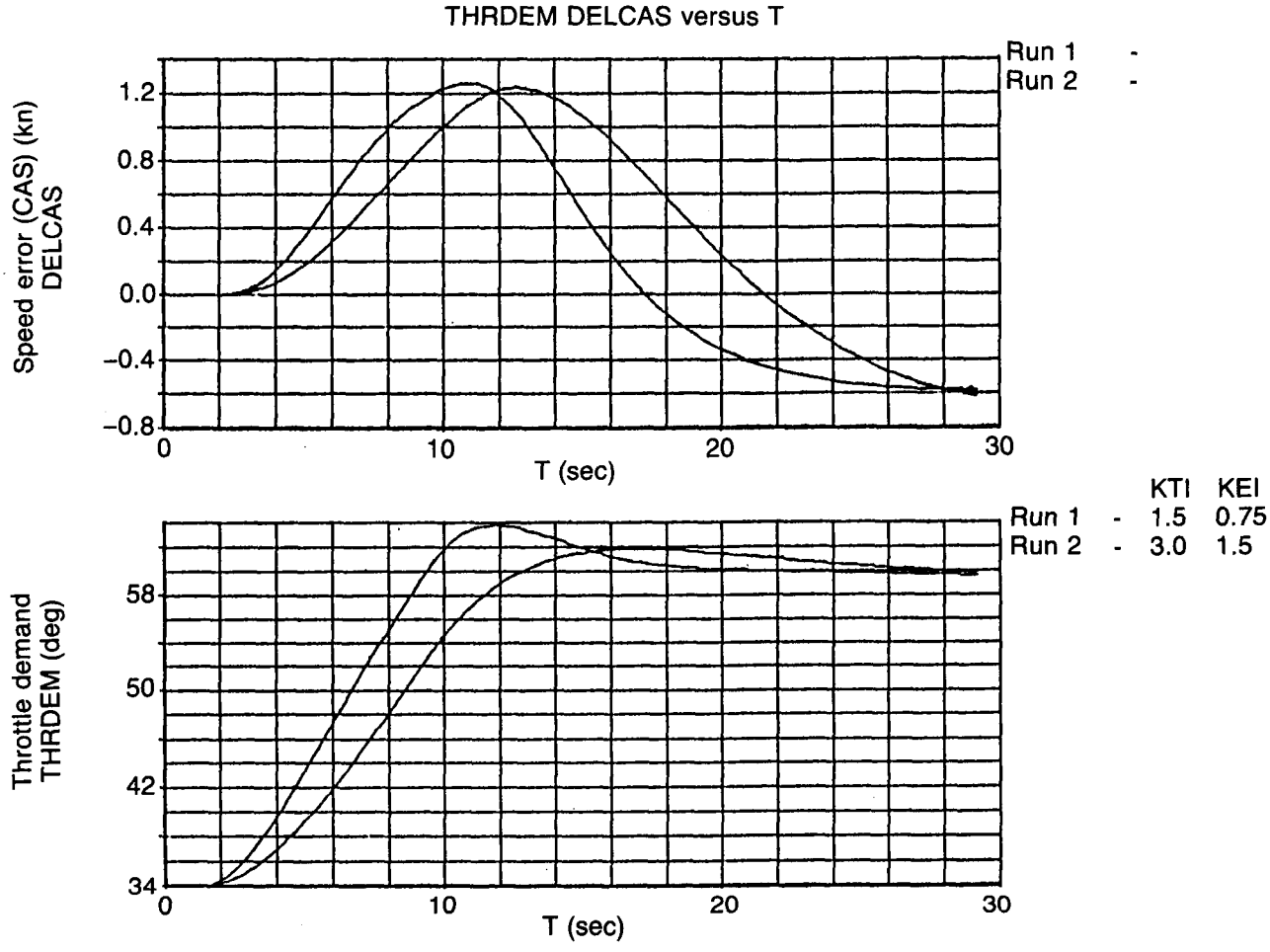

Figure 29. Speed Error, Throttle Demand for 0.5-in Column Deflection

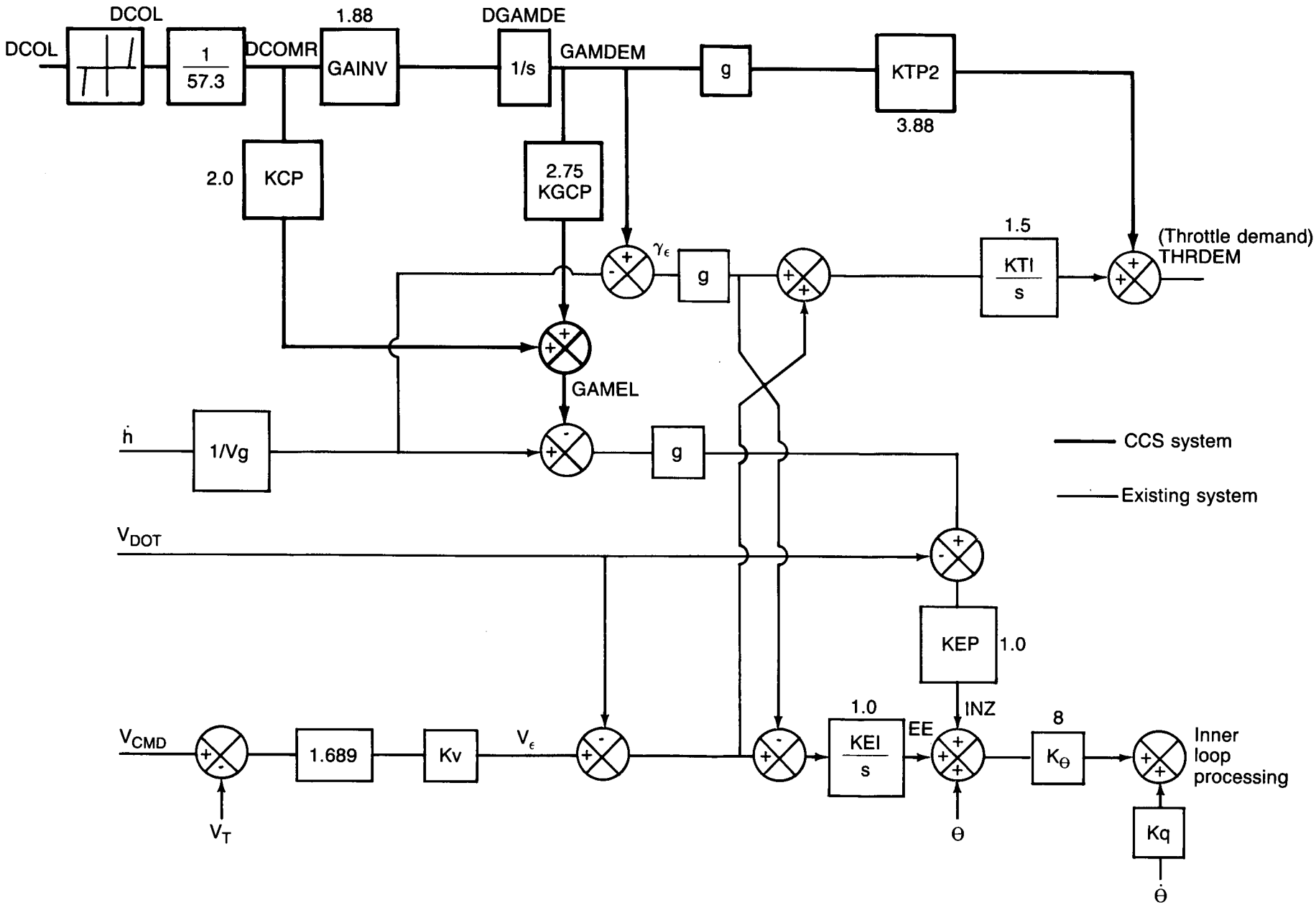

Figure 30. Velocity Vector-Control Column Steering System

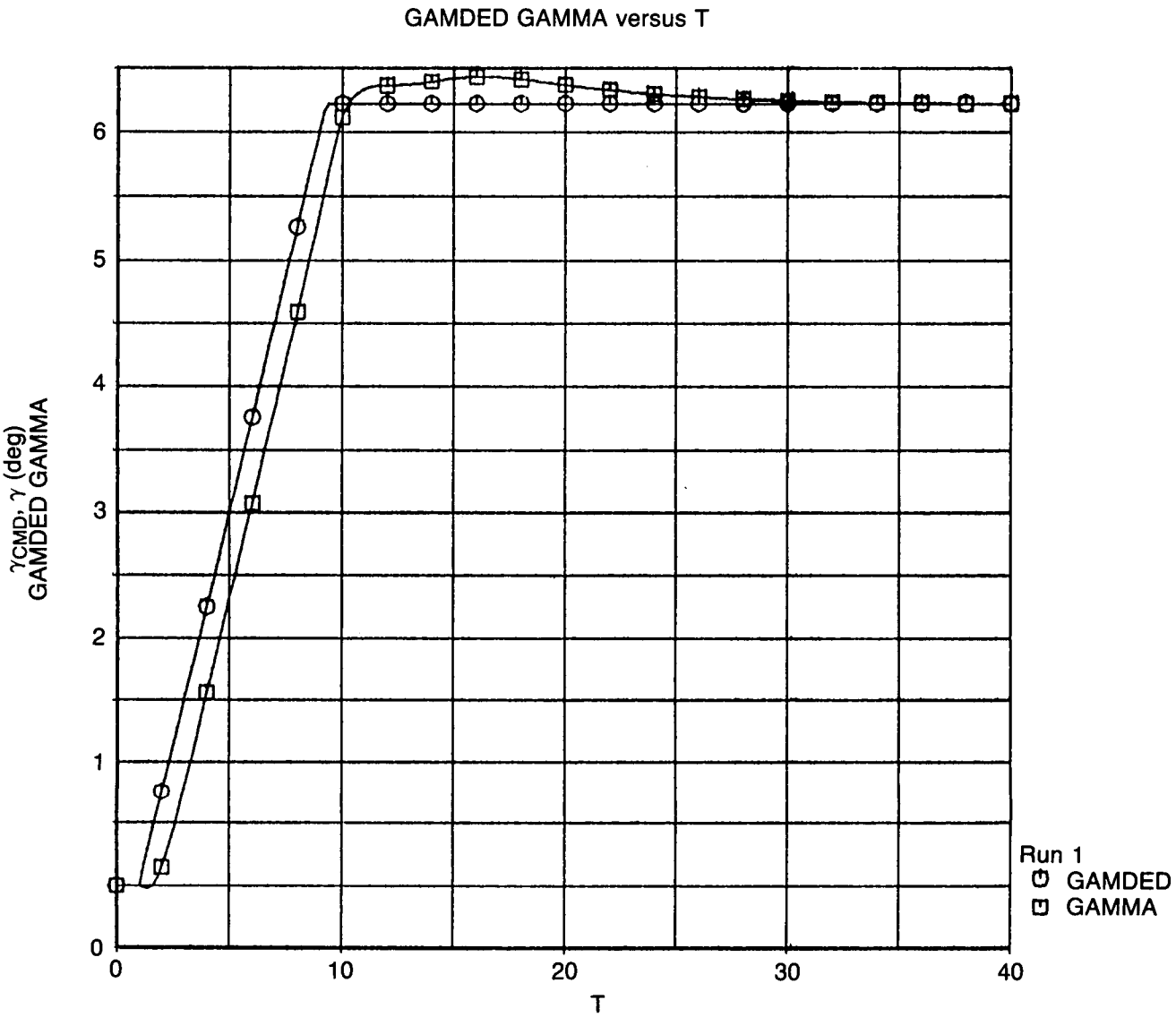

Figure 31. γ_{CMD}, γ for 0.5-in Column Deflection

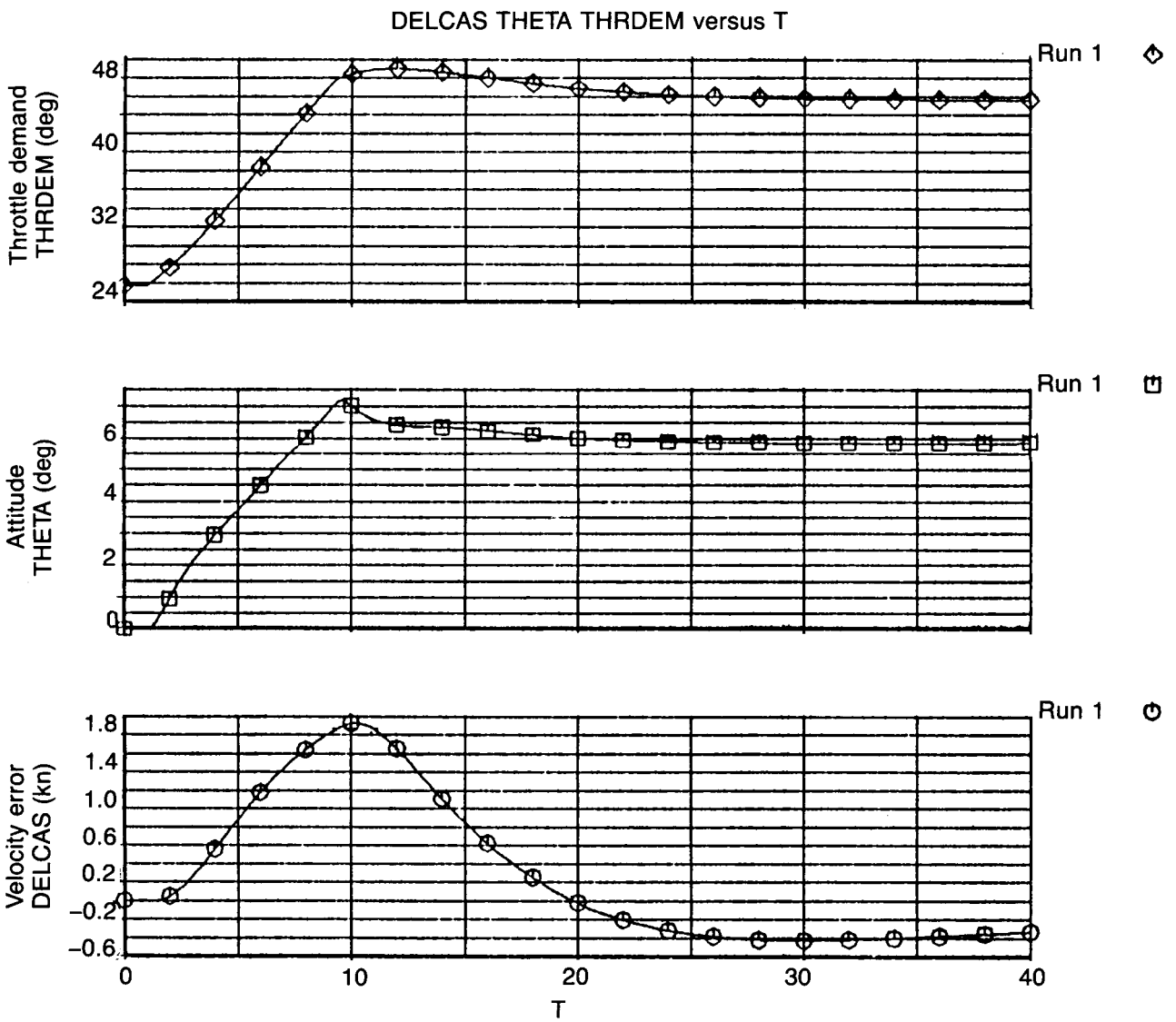

Figure 32. Throttle, Attitude, and Velocity for 0.5-in Column Deflection

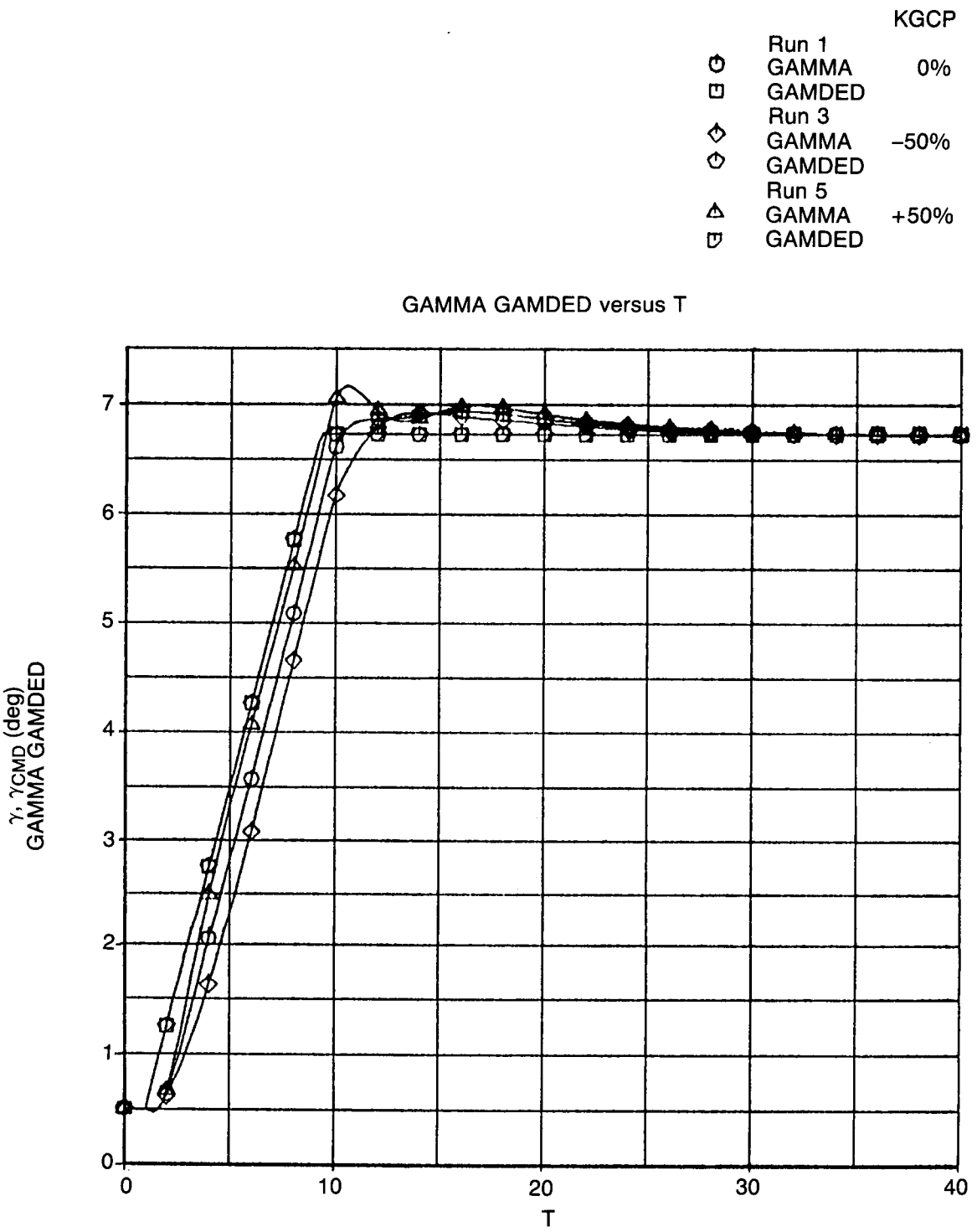

Figure 33. Variation of Gain KGCP

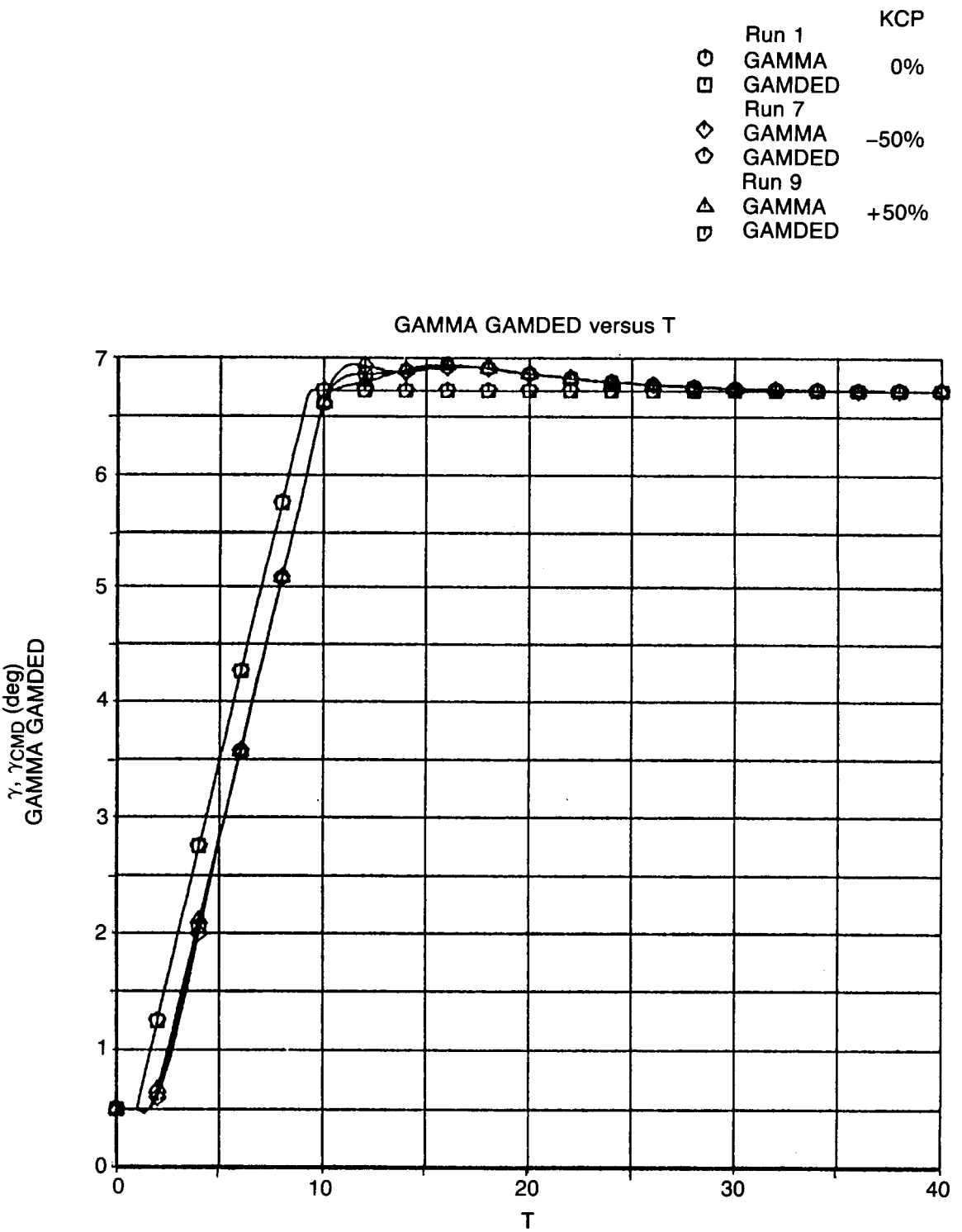

Figure 34. Variation of Gain KCP

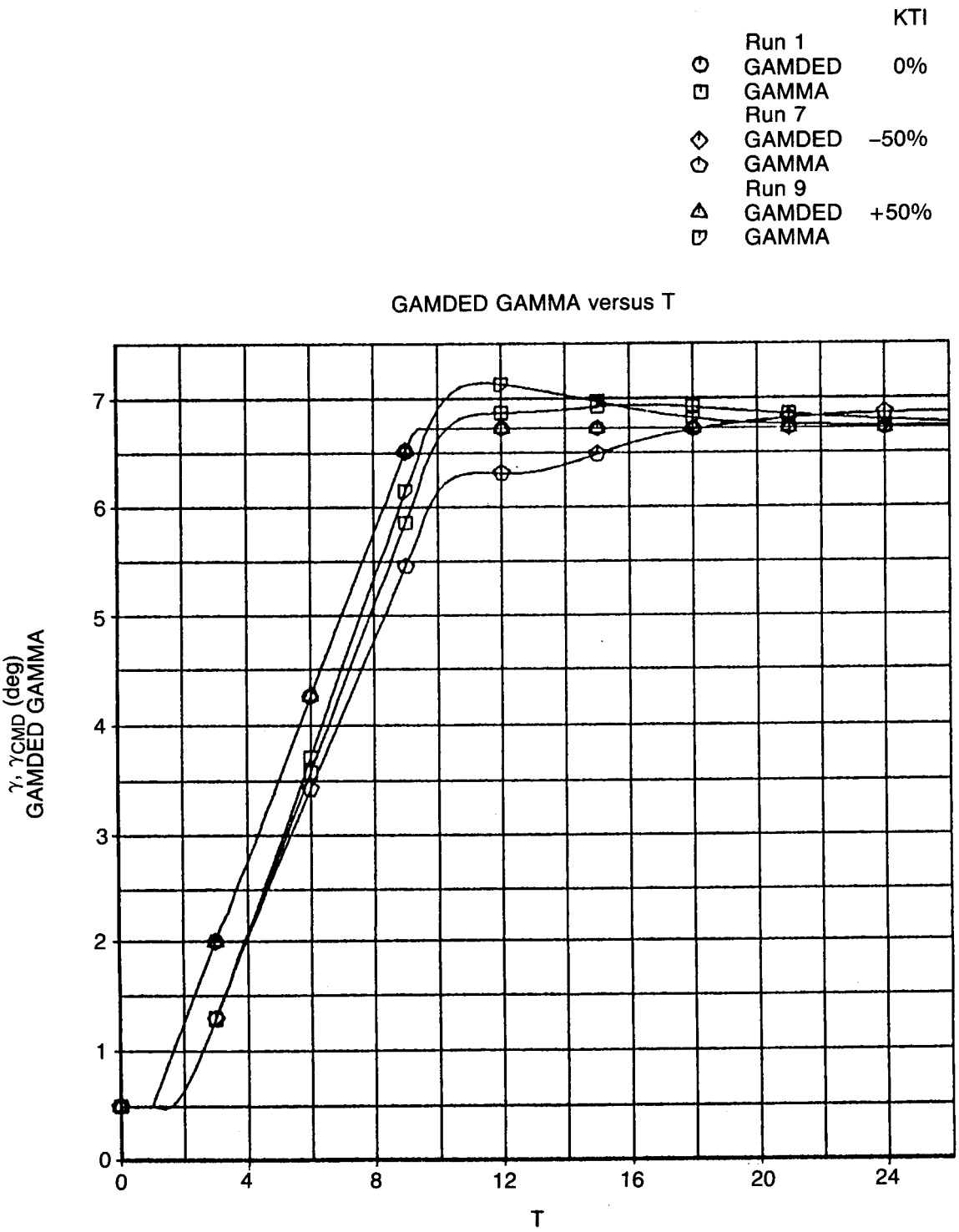

Figure 35. Variation of KTI

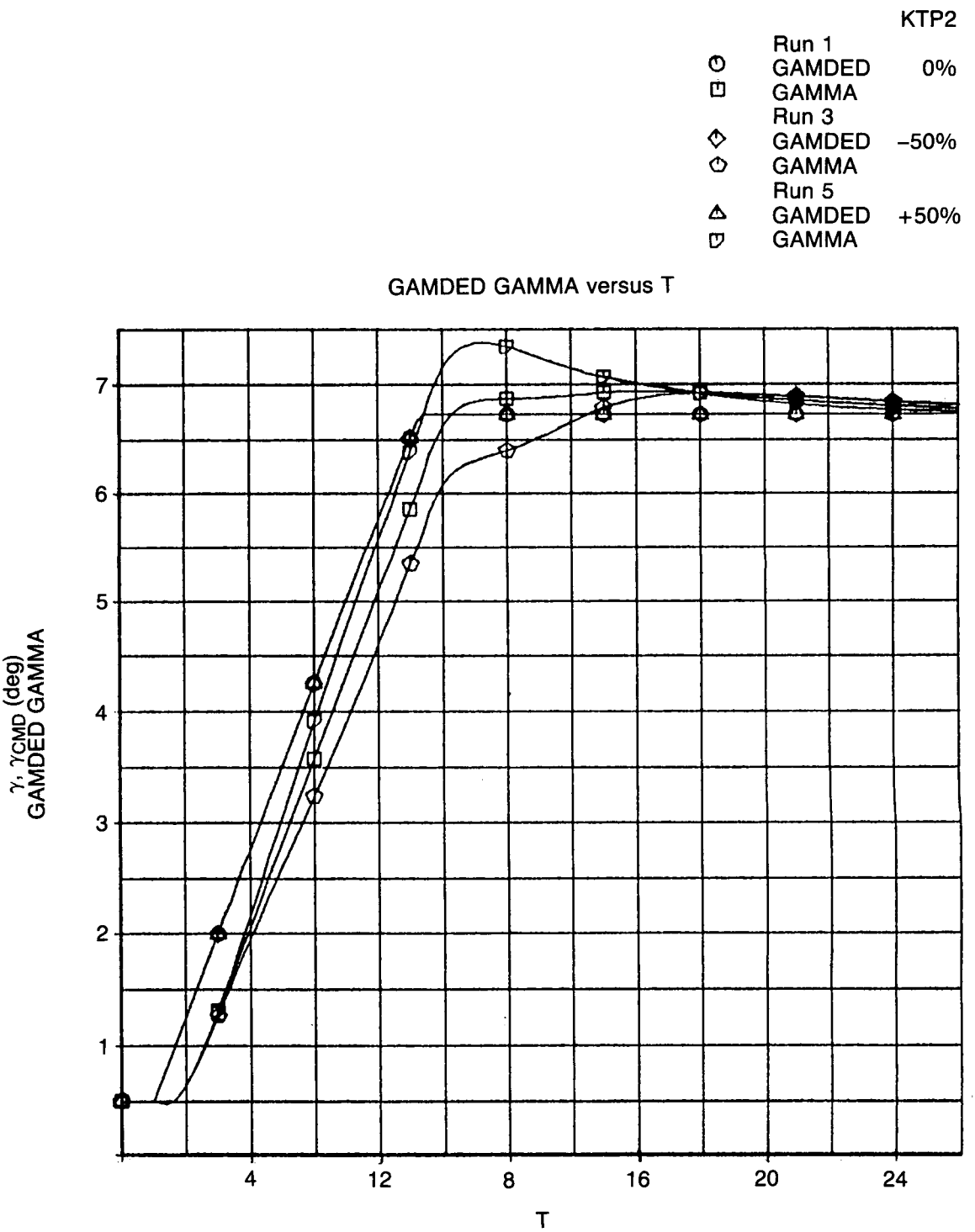

Figure 36. Variation of KTP2

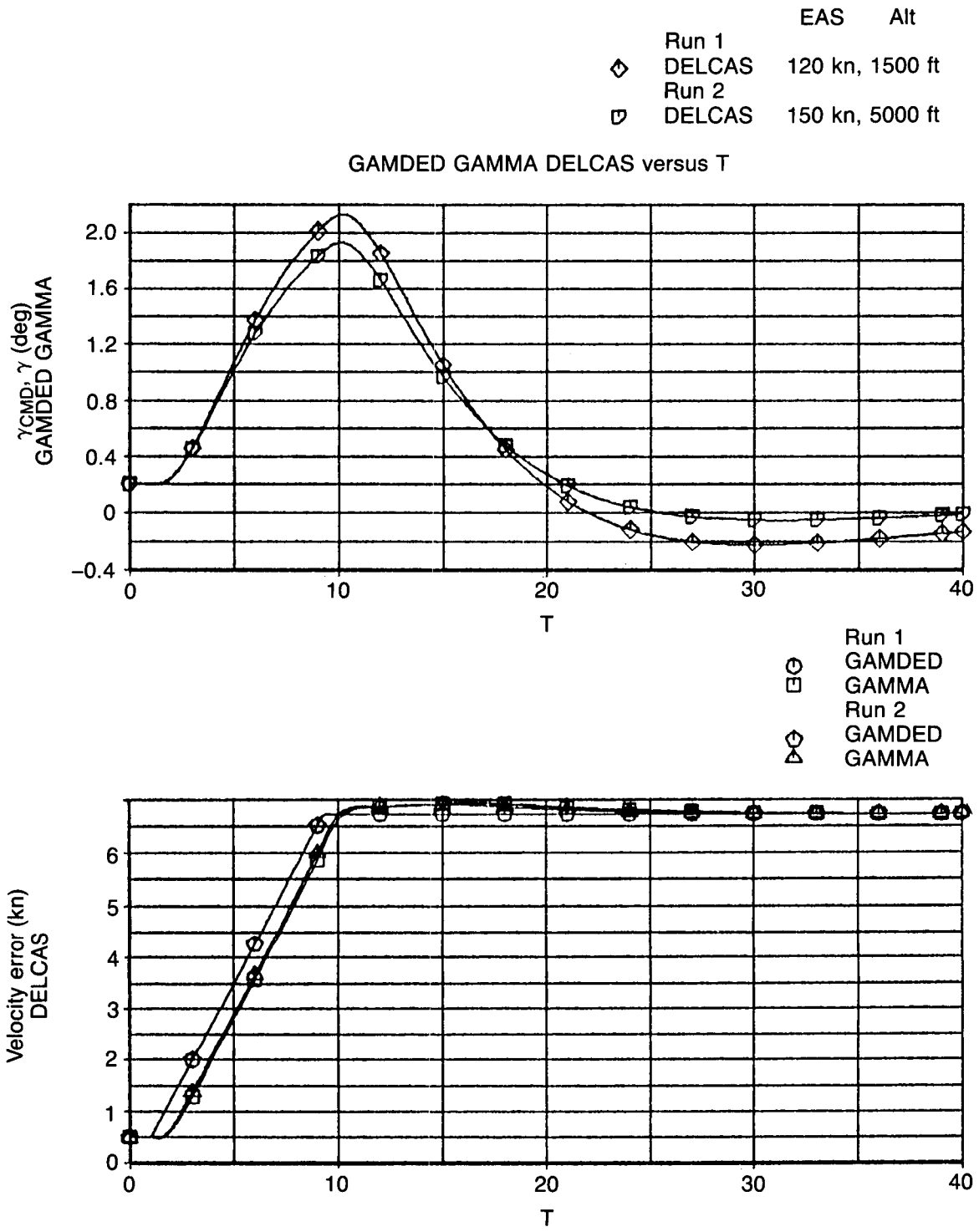

Figure 37. Effect of Aerodynamic Variation (120 kn, 150 kn)

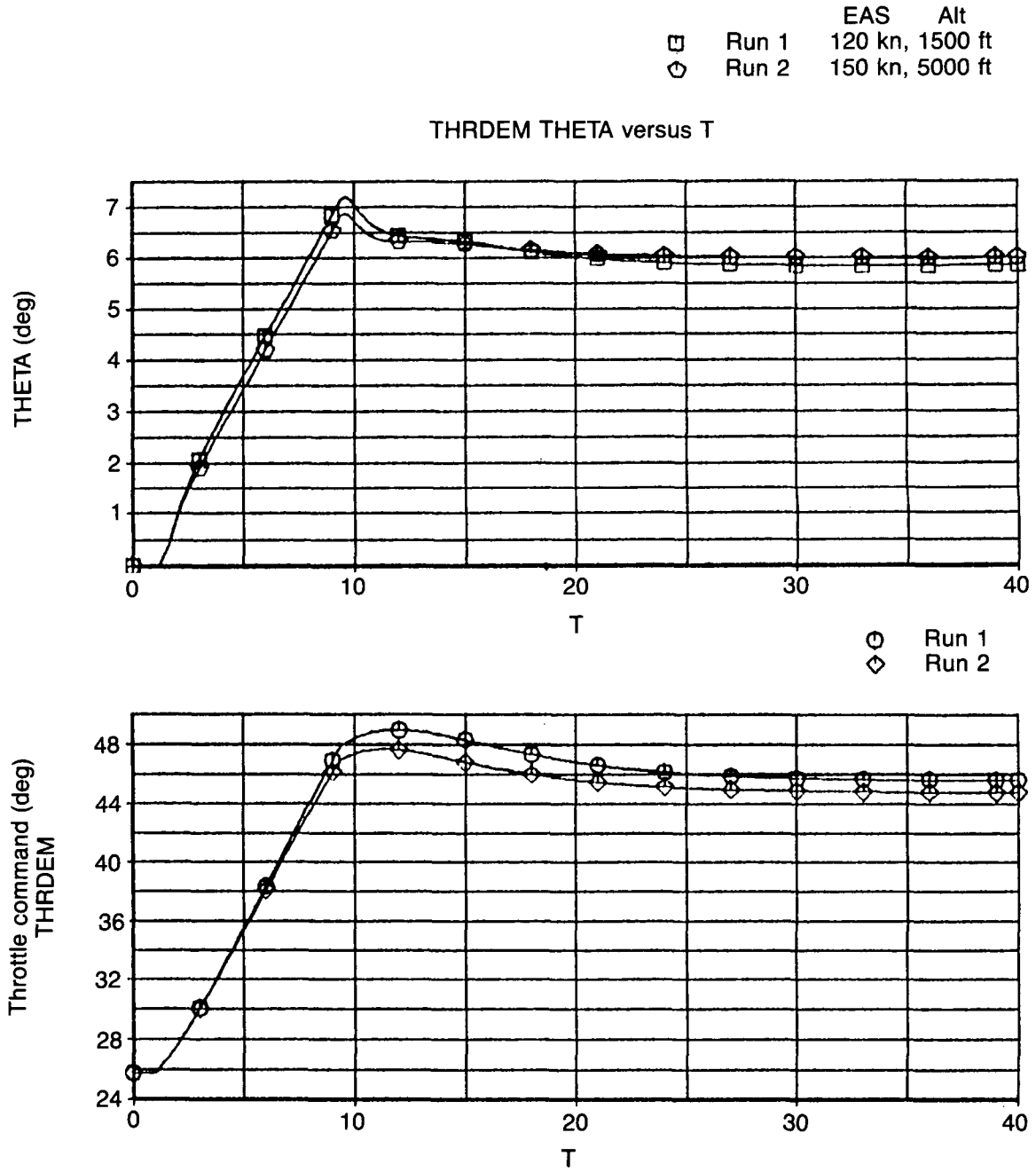

Figure 38. Effect of Aerodynamic Variation (120 kn, 150 kn)

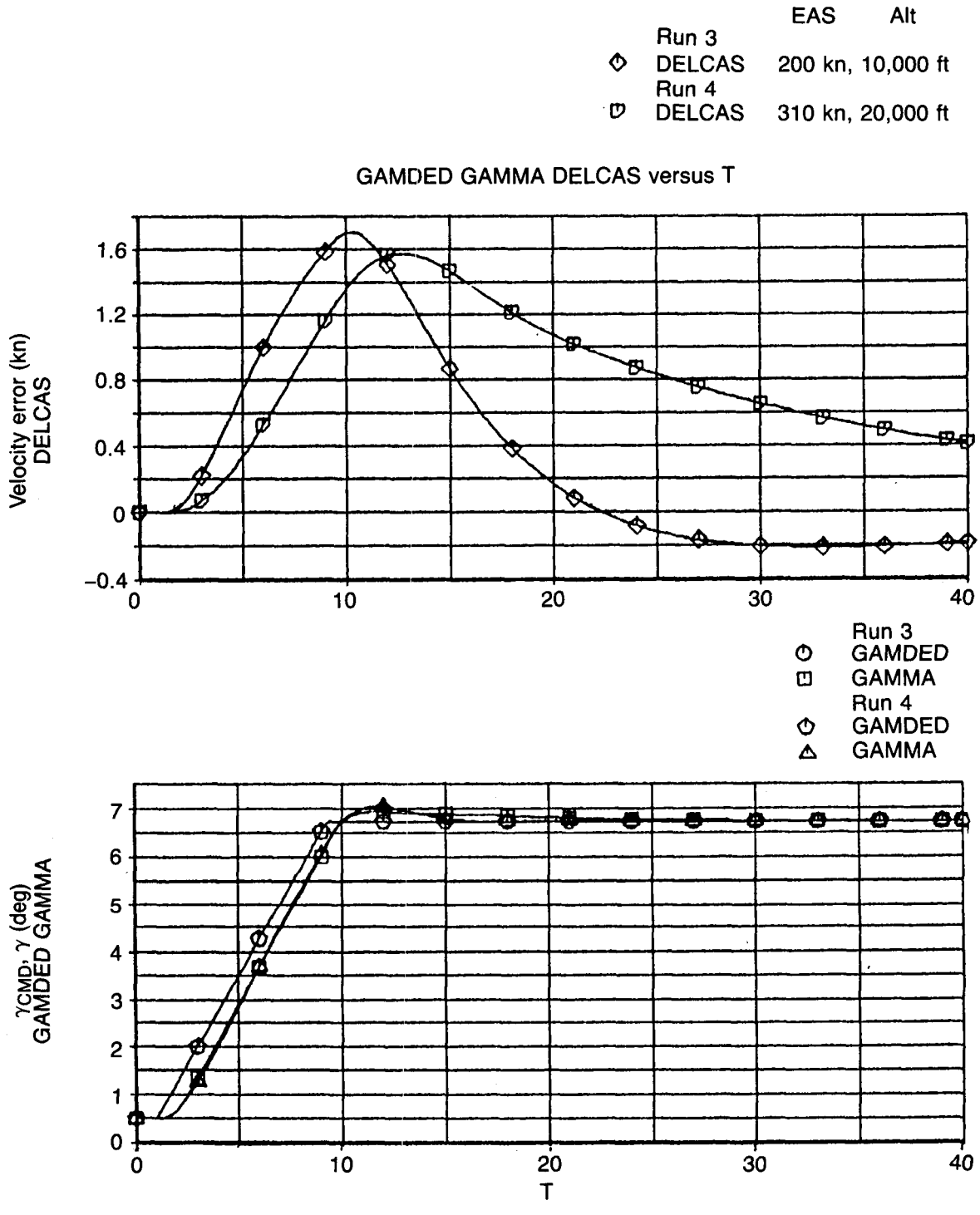

Figure 39. Effect of Aerodynamic Variation (200 kn, 310 kn)

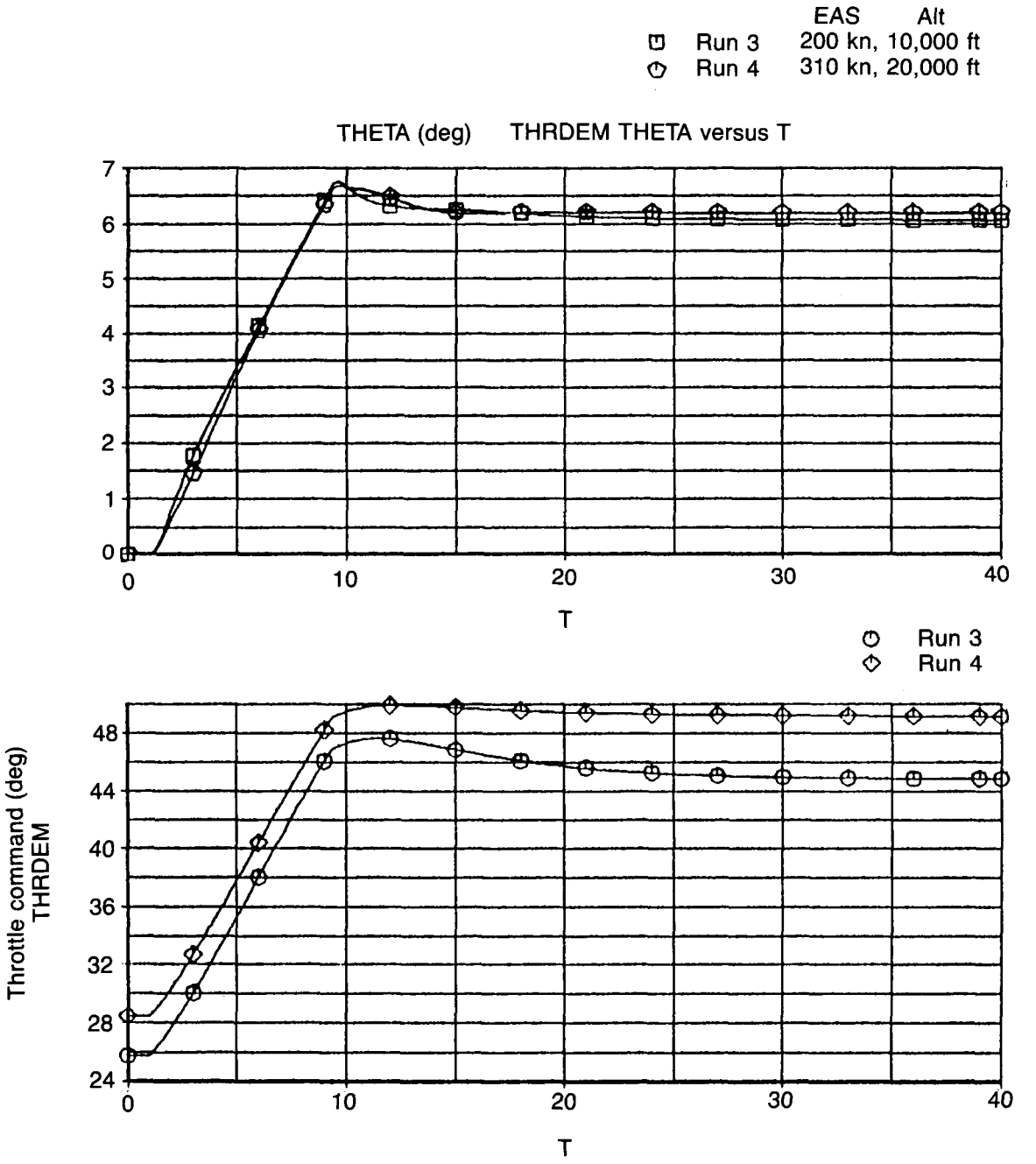

Figure 40. Effect of Aerodynamic Variation (200 kn, 310 kn)

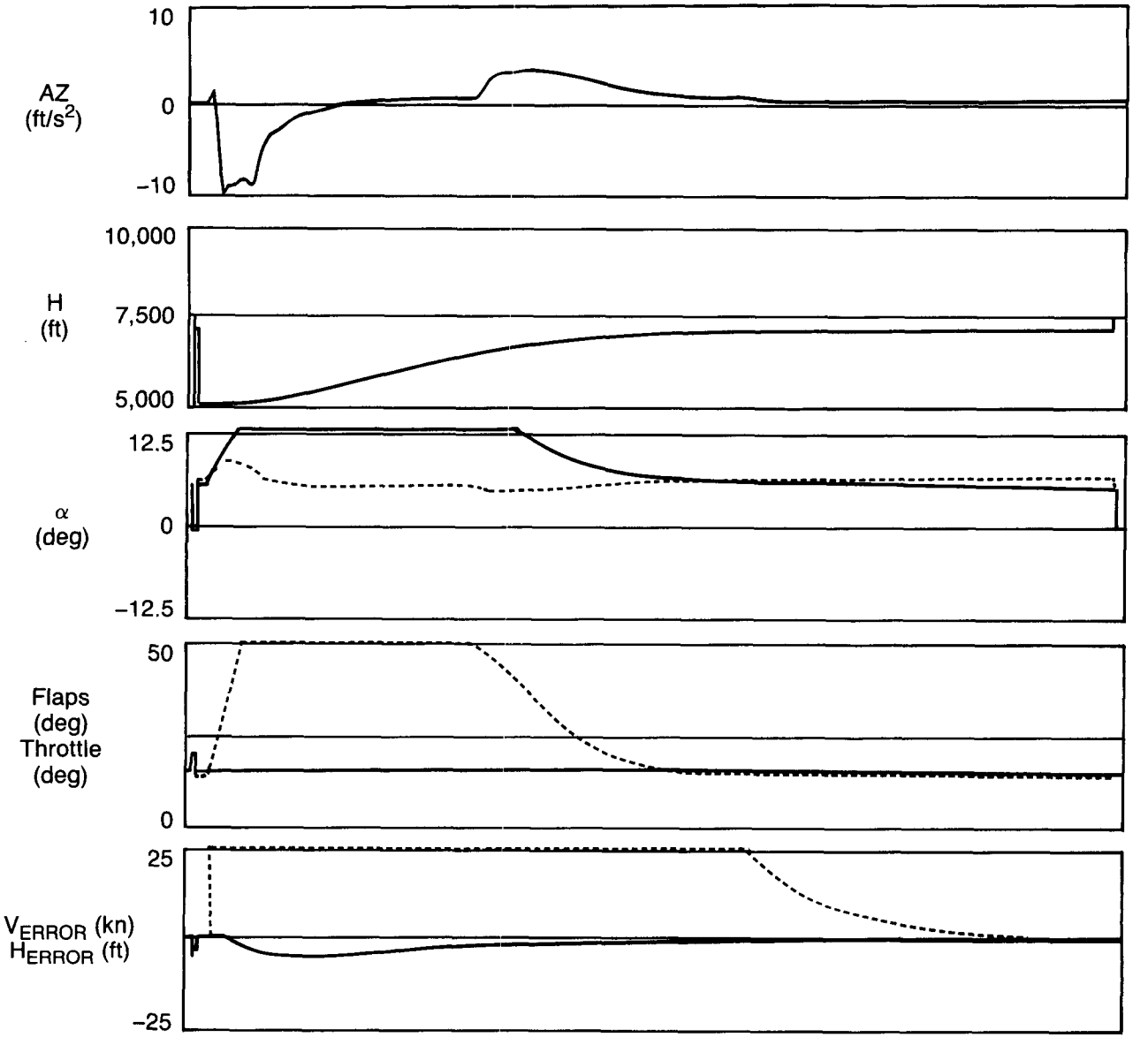

Figure 41. +2,000-ft Height Change (No Limiters)

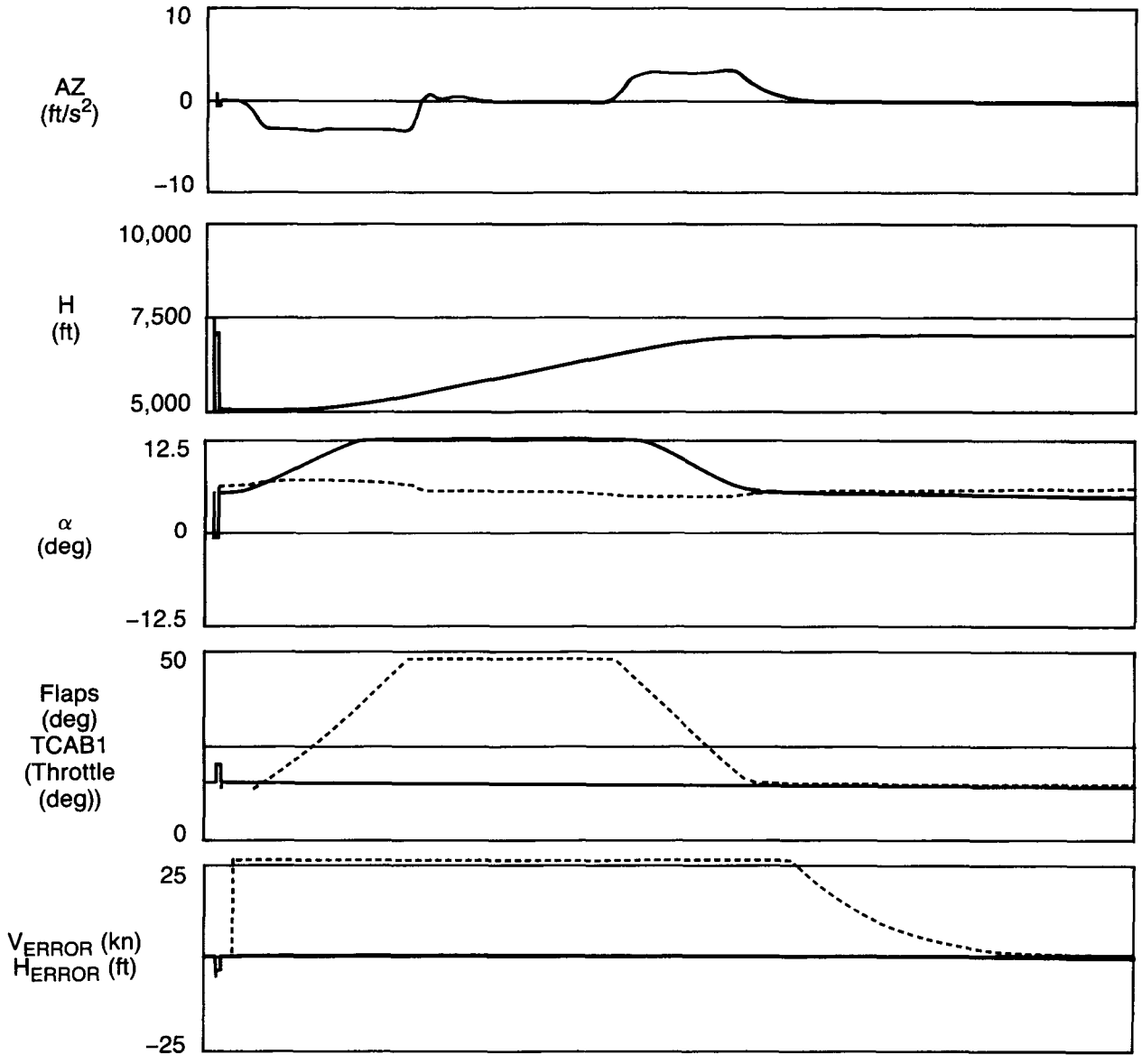

Figure 42. +2,000-ft Height Change (With Nonlinearities)

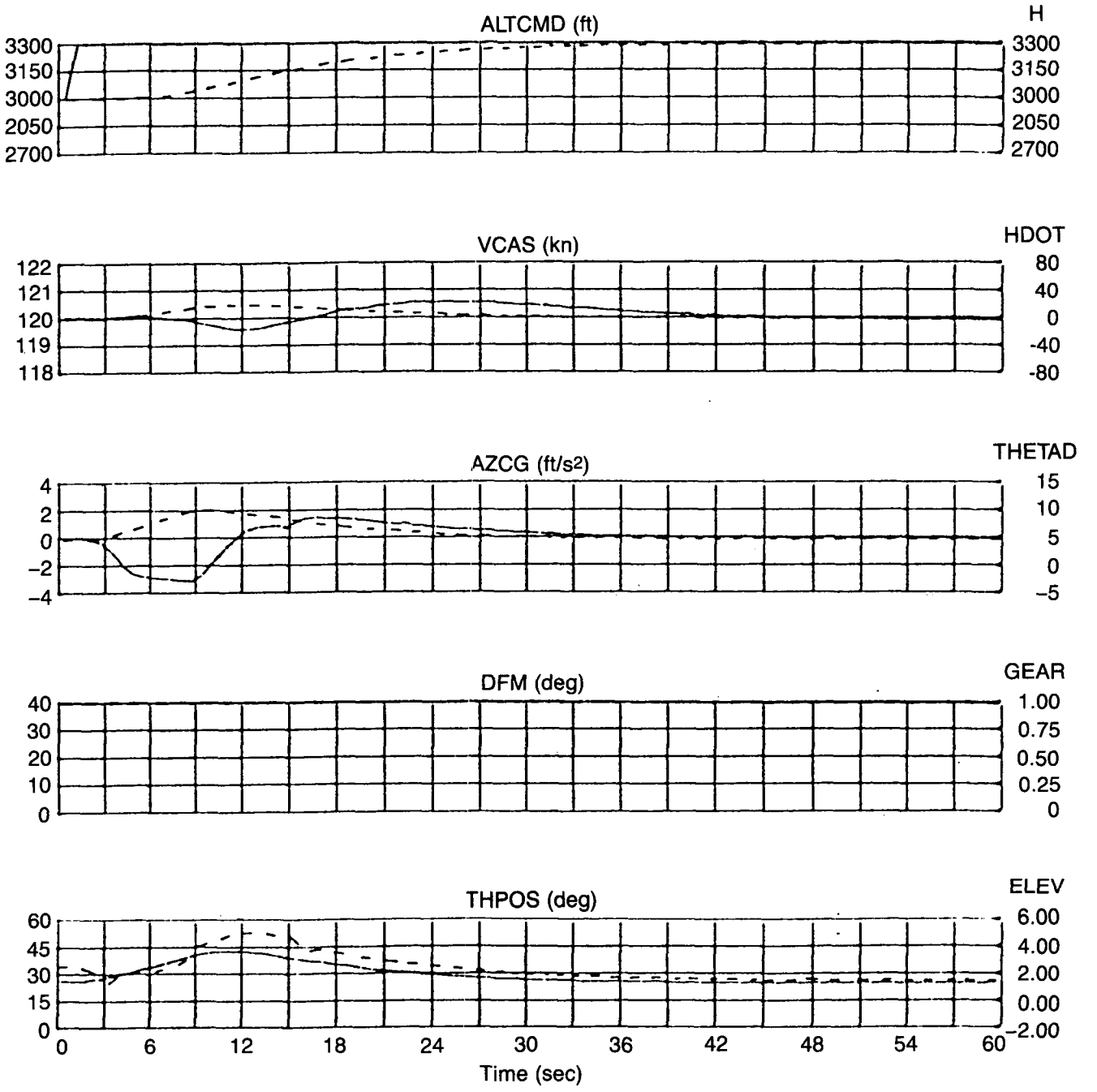

Figure 43. Altitude Control Mode: 120 kn, 3,000 ft, $\Delta h = +300$

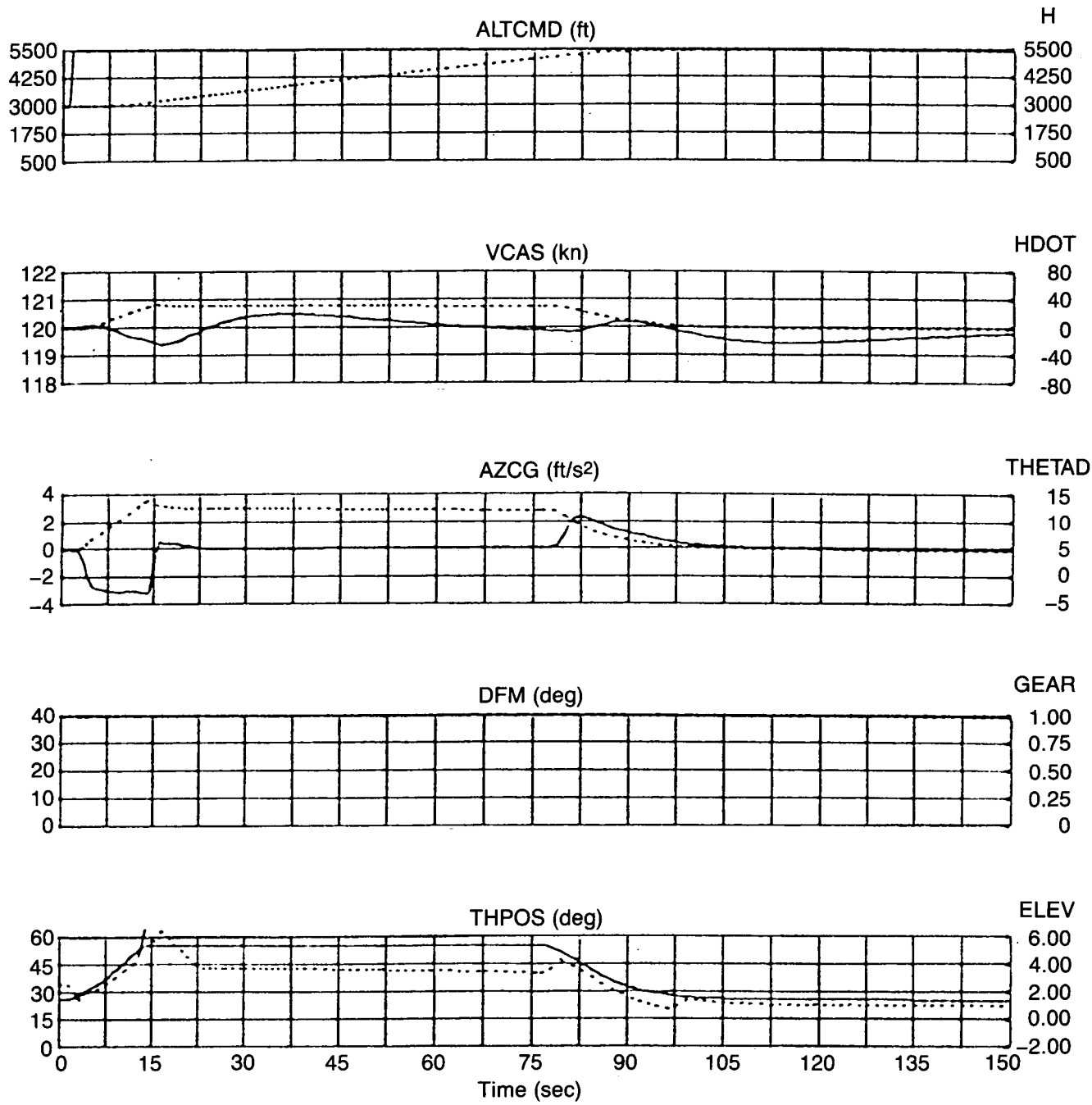

Figure 44. Altitude Control Mode: 120 kn, 3,000 ft, $\Delta h = +2{,}500$

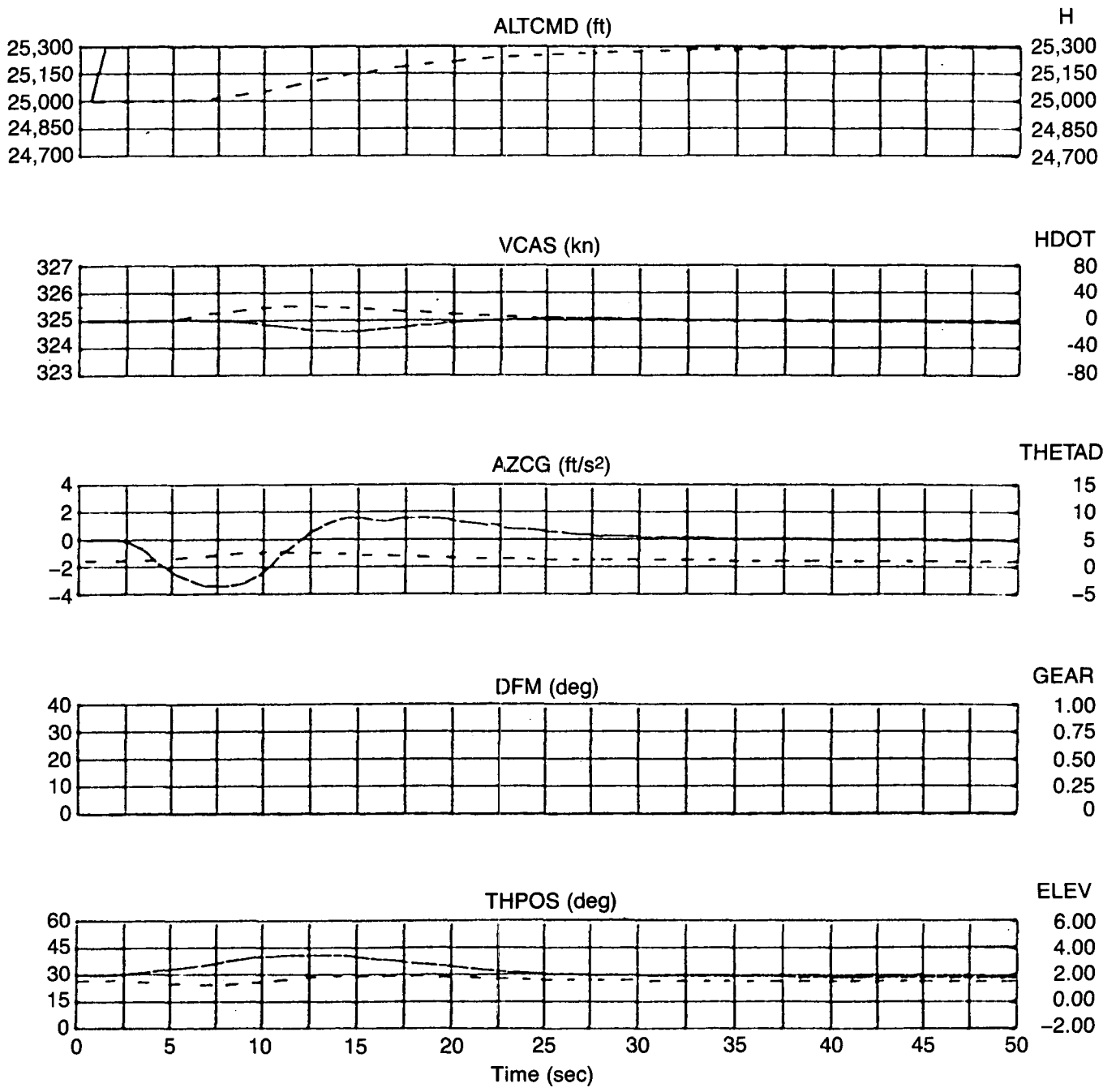

Figure 45. Altitude Control Mode: 325 kn, 25,000 ft, $\Delta h = +300$ ft

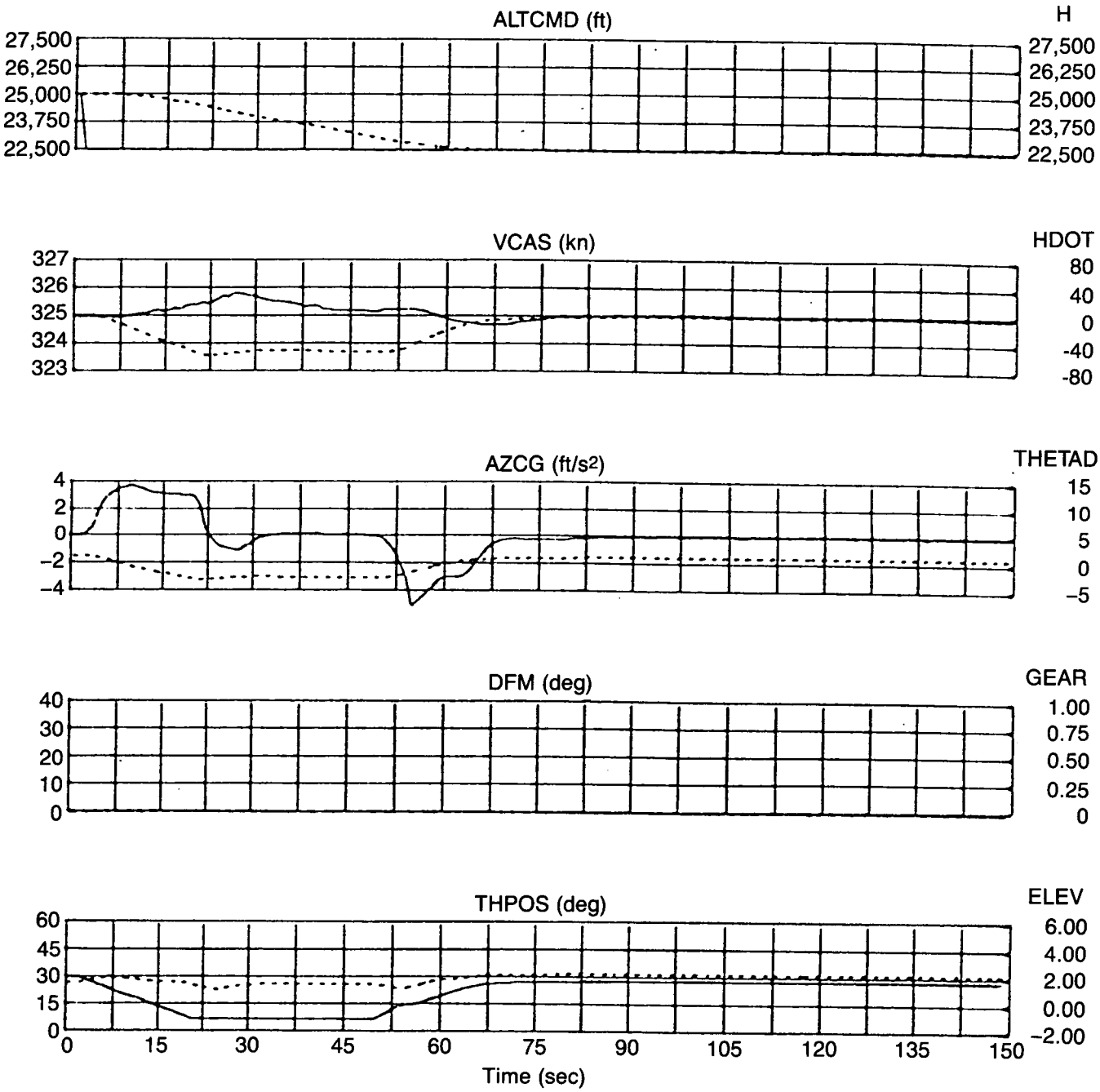

Figure 46. Altitude Control Mode: 325 kn, 25,000 ft, $\Delta h = -2{,}500$ ft

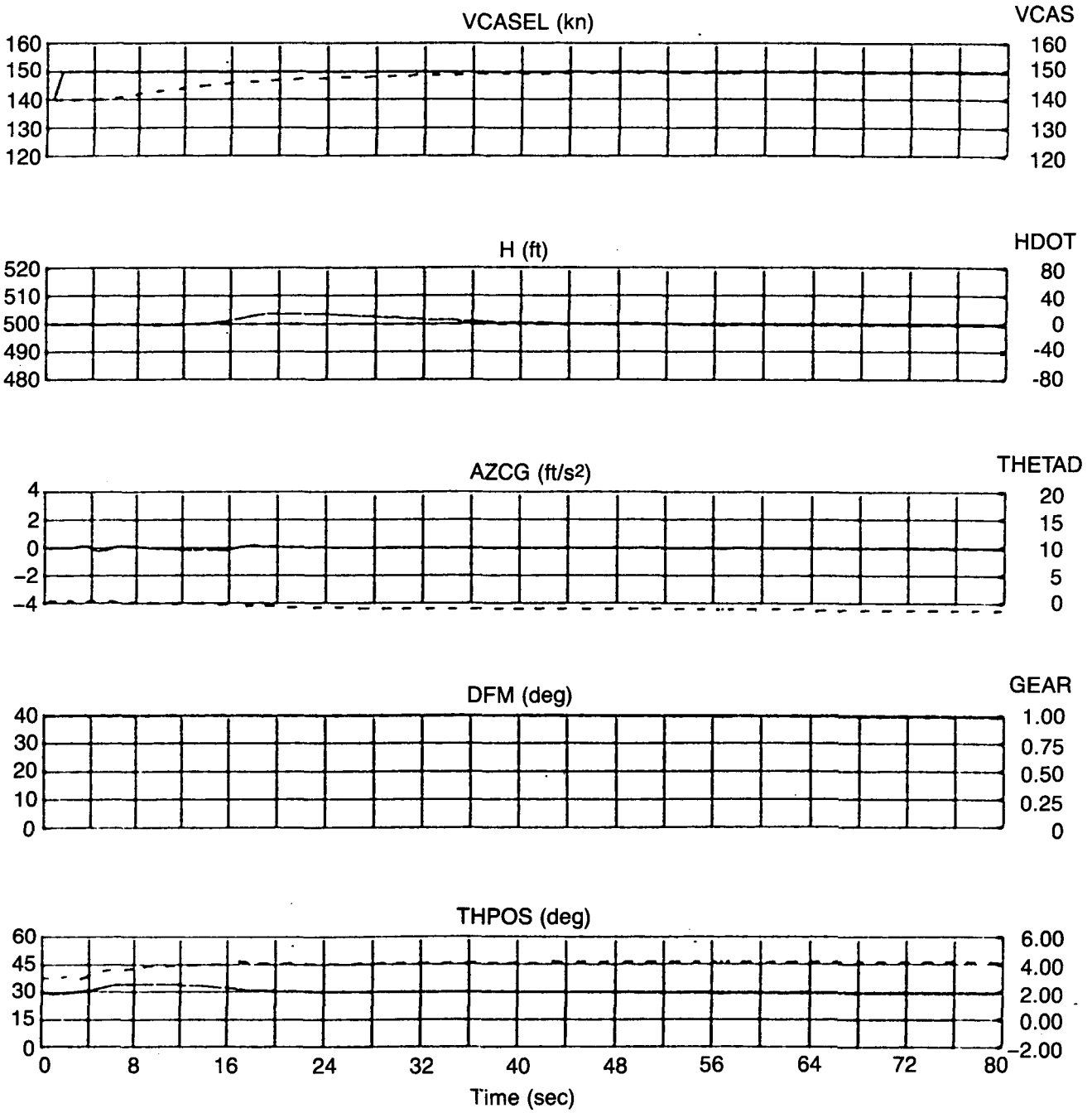

Figure 47. CAS Control Mode: 140 kn, 500 ft, FL = 40 deg, ΔV = +10 kn

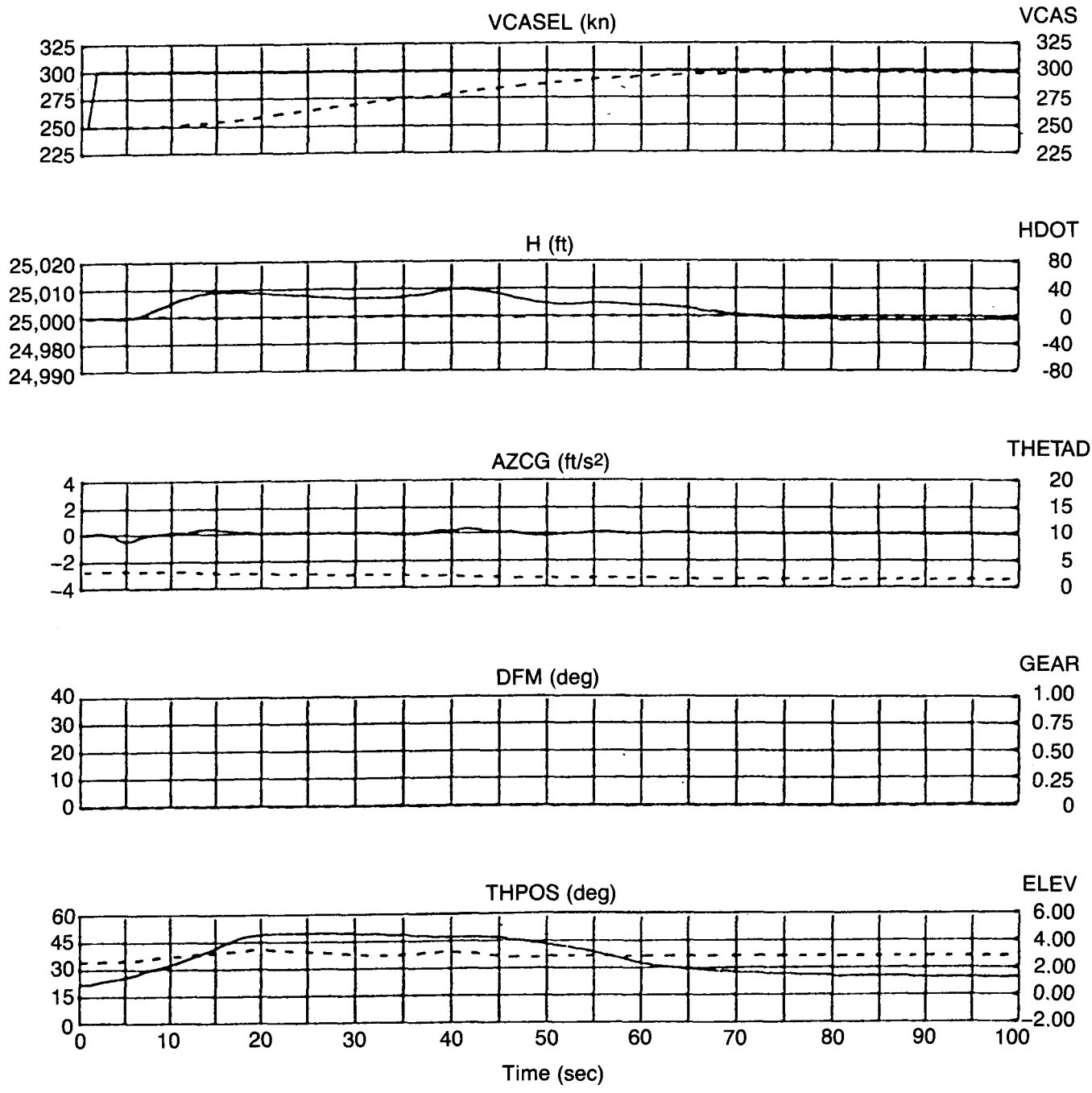

Figure 48. CAS Control Mode: 250 kn, 25,000 ft, FL = 0 deg, ΔV = +50 kn

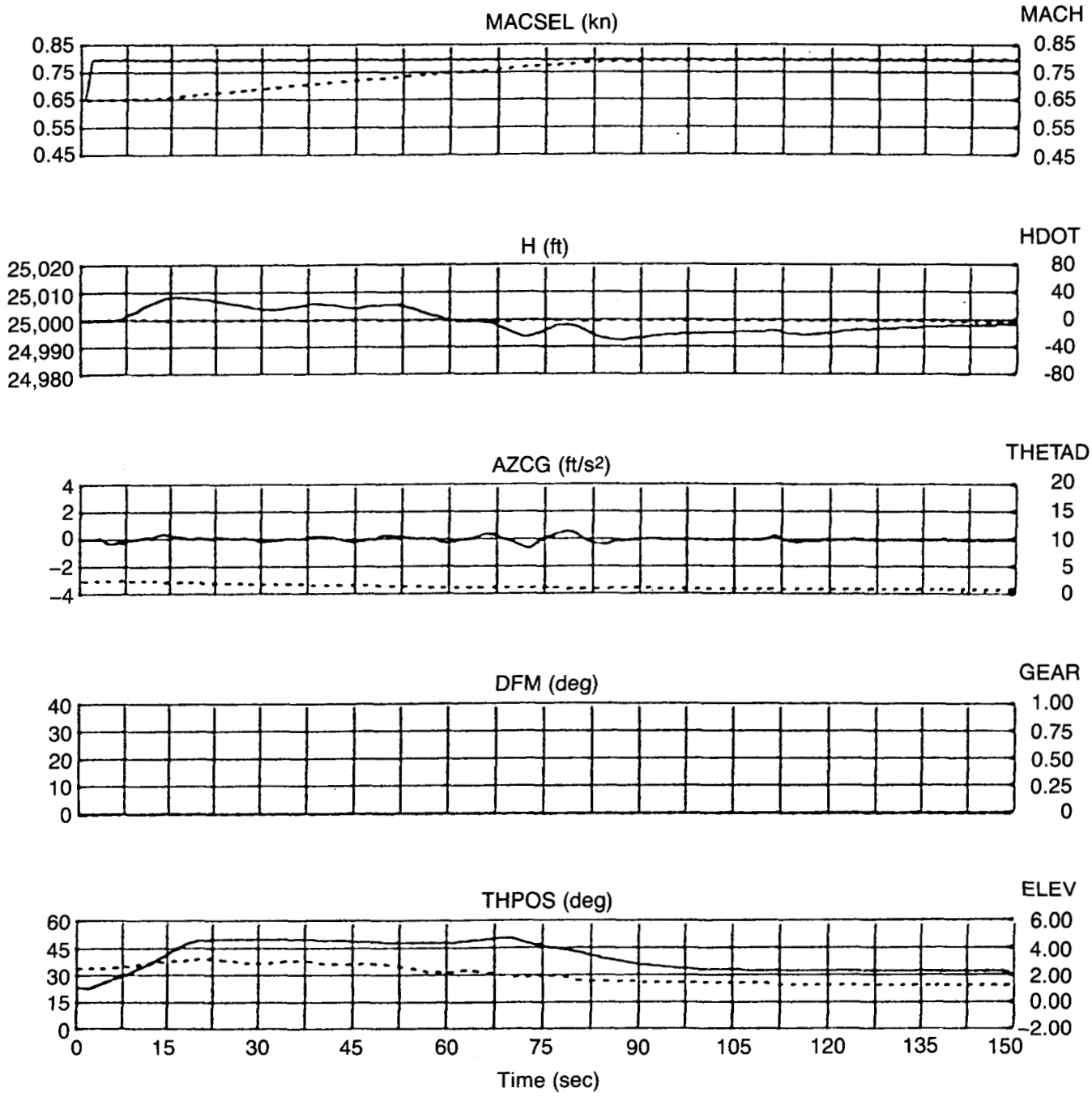

Figure 49. Mach Control Mode: M 0.65, 25,000 ft, $\Delta M = +0.15$

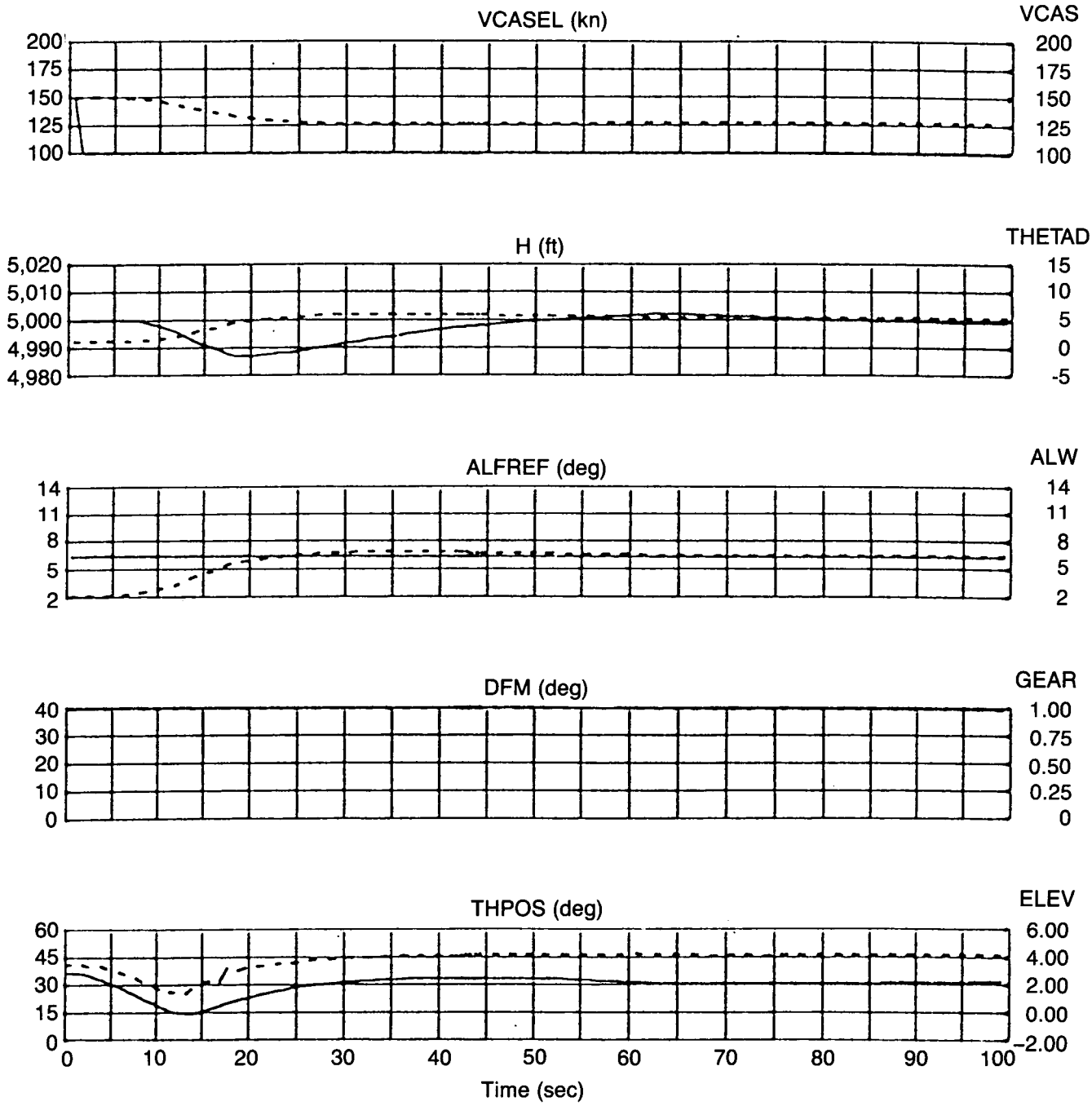

Figure 50. α Control Mode: 150 kn, 5,000 ft, 105,000 lb (31% CG, FL = 40 deg)

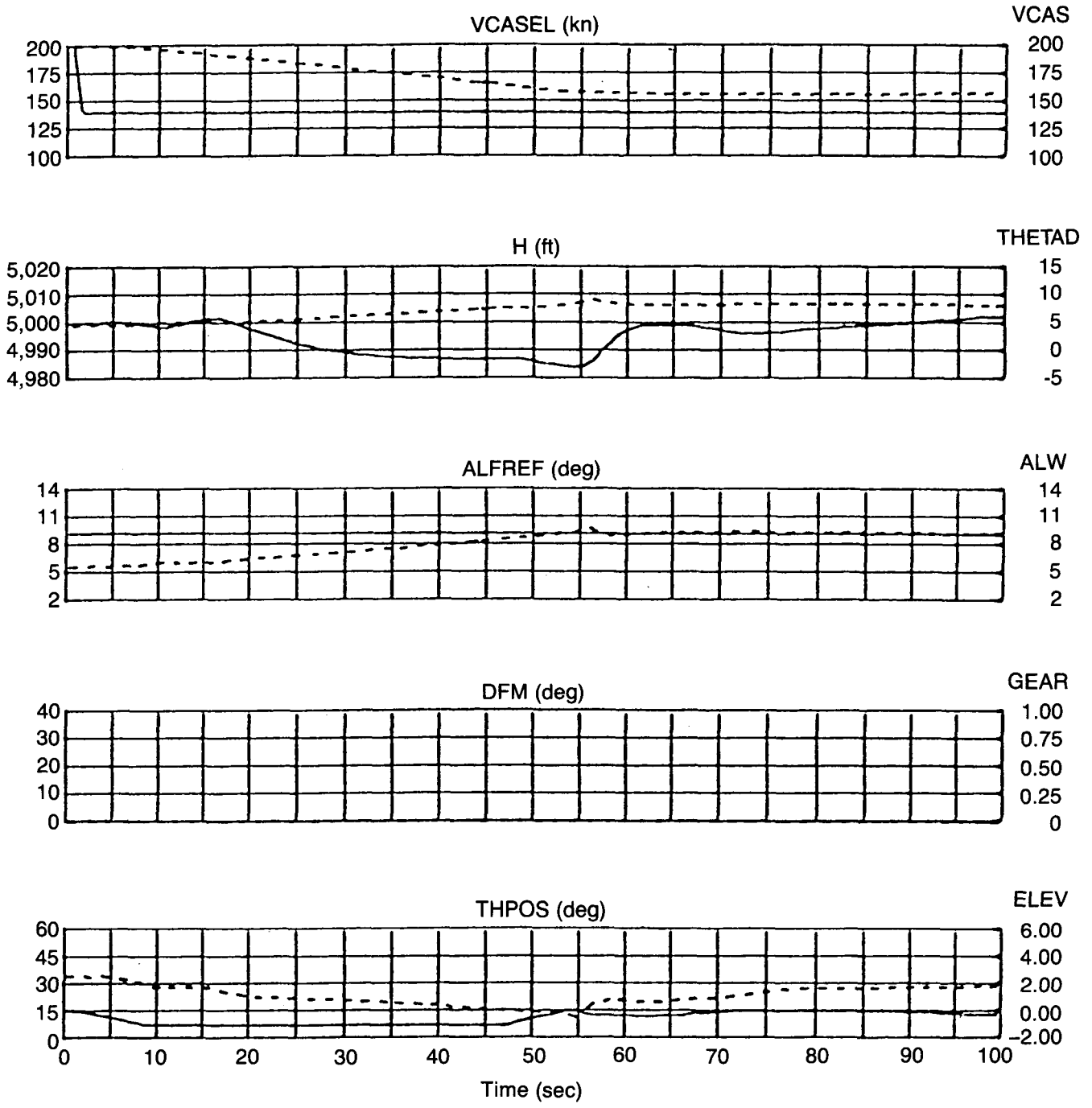

Figure 51. α Control Mode: 200 kn, 5,000 ft, 70,000 lb, 5% CG, FL = 0 deg

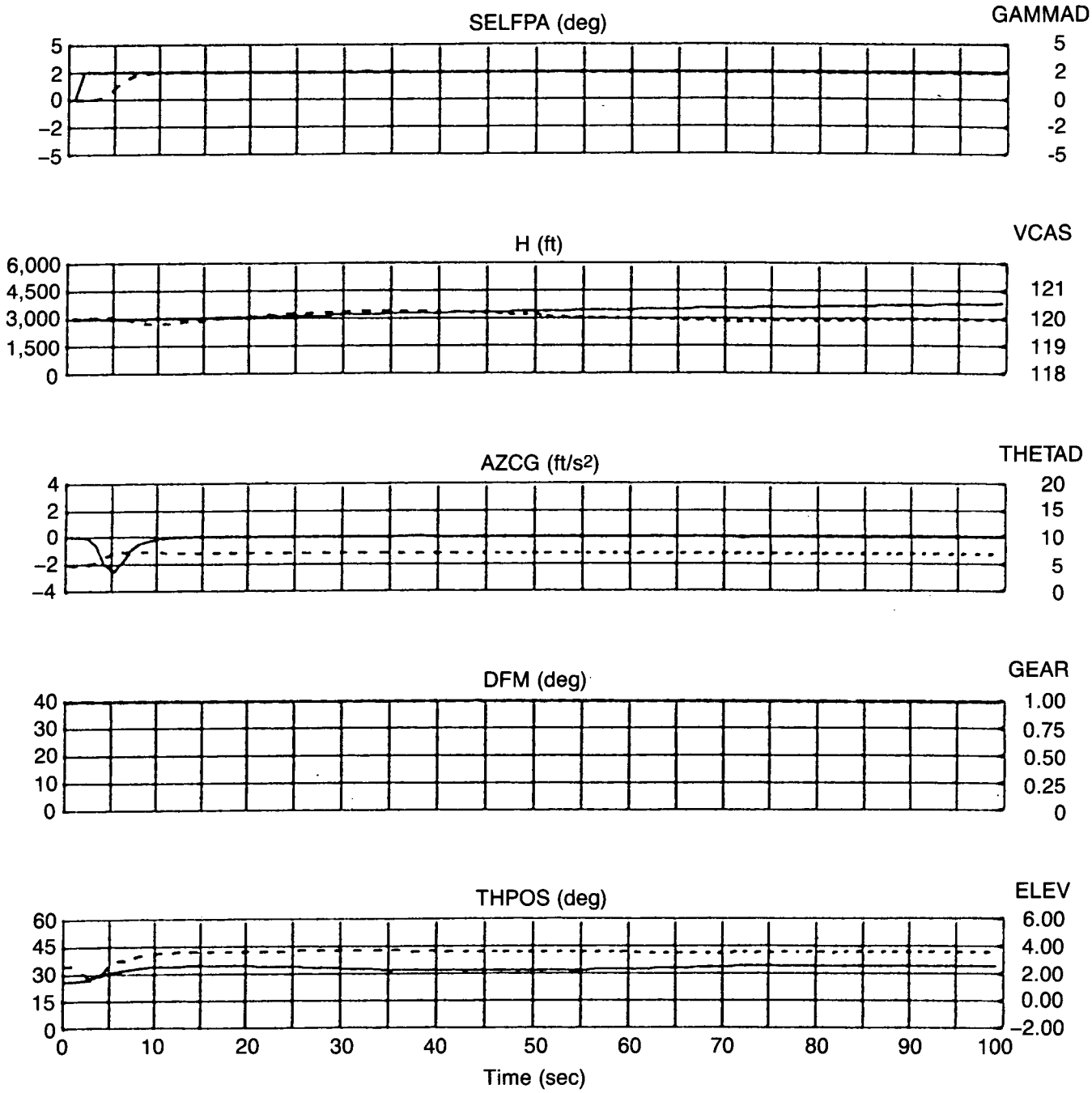

Figure 52. FPA Control Mode: 120 kn, 3,000 ft, FL = 40 deg, $\Delta\gamma$ = +2.5 deg

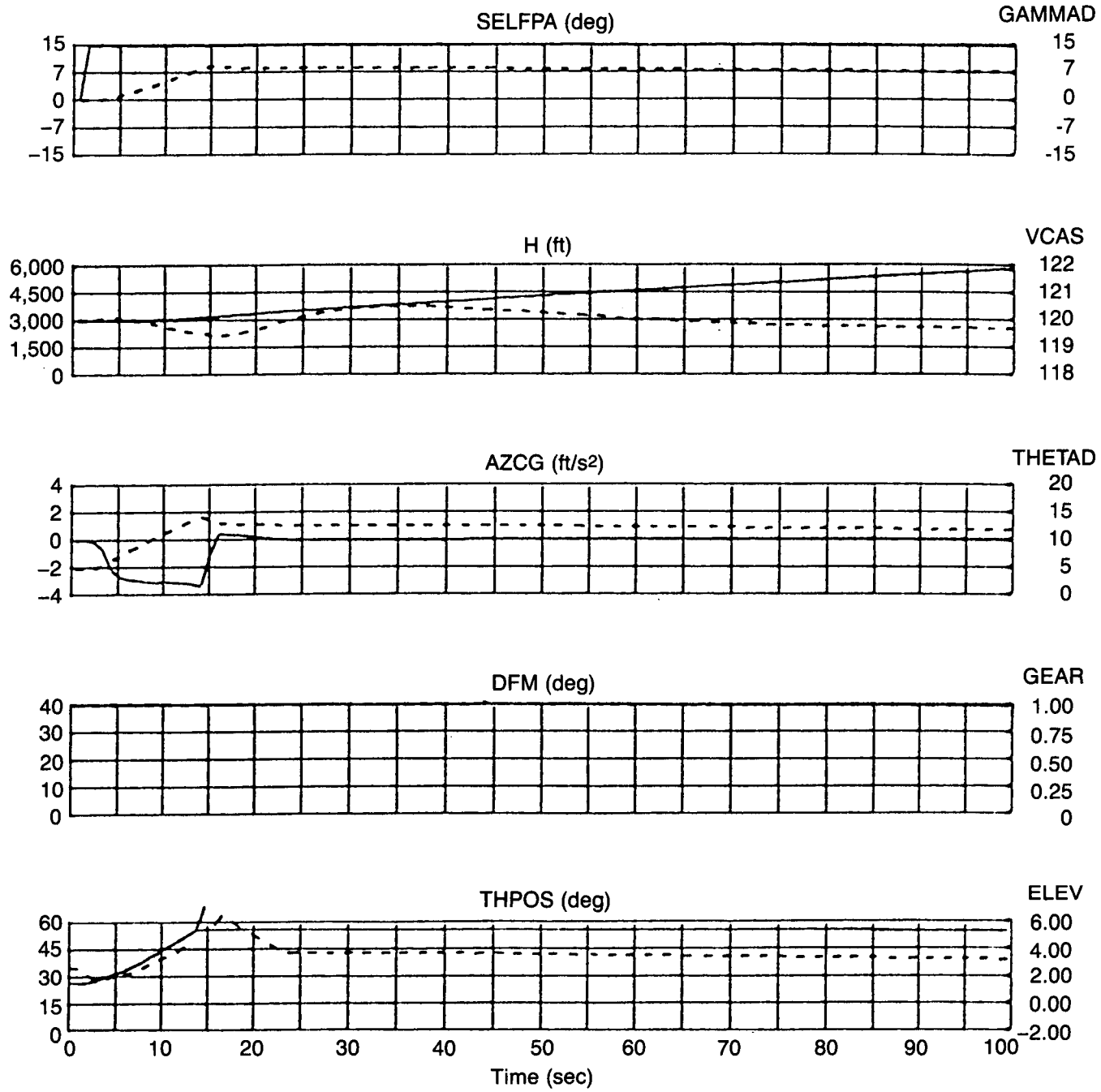

Figure 53. FPA Control Mode: 120 kn, 3,000 ft, $\Delta\gamma$ = +15 deg

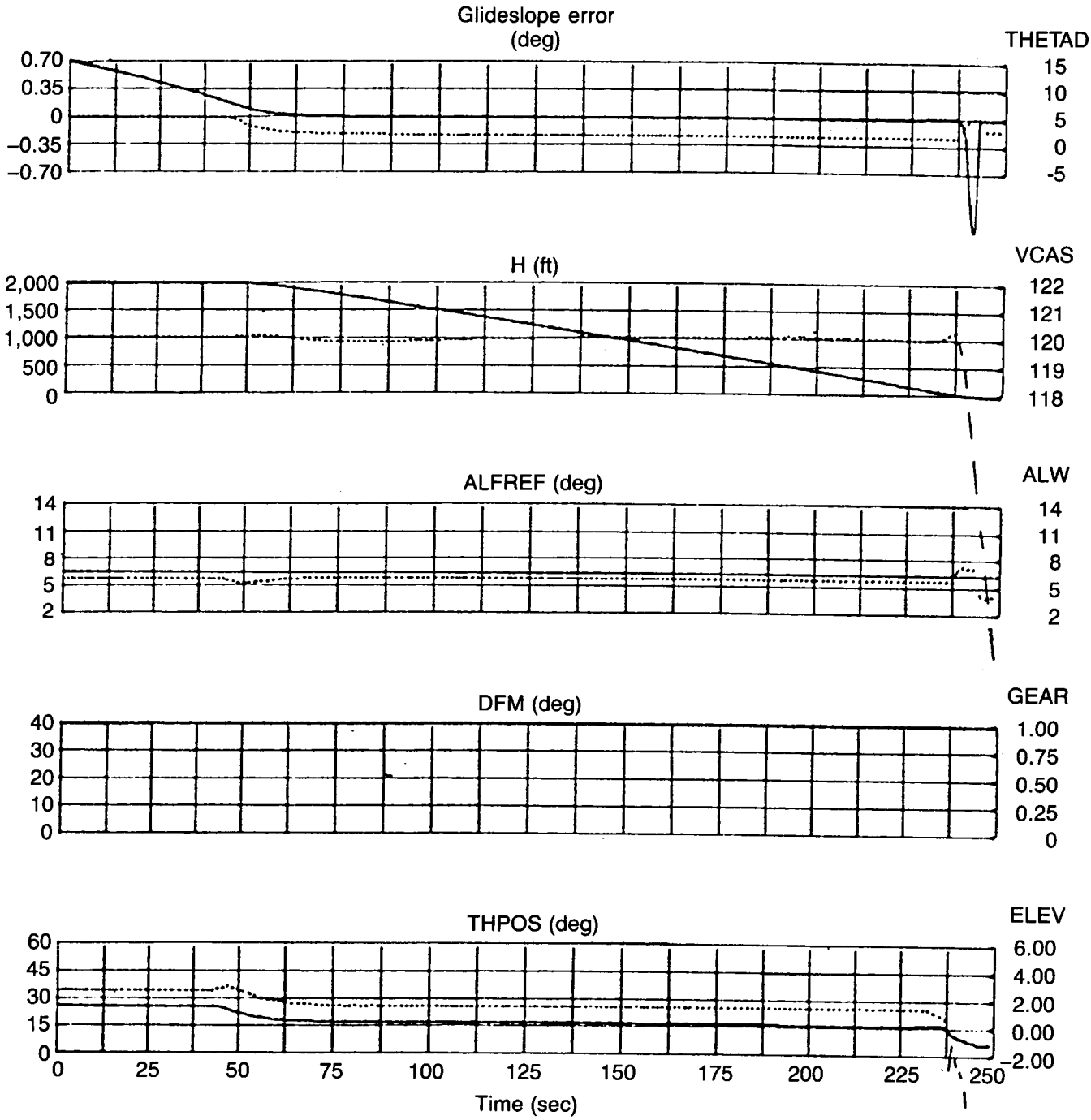

Figure 54. Glideslope Control Mode: H_0 = 2,000 ft, FL = 40 deg

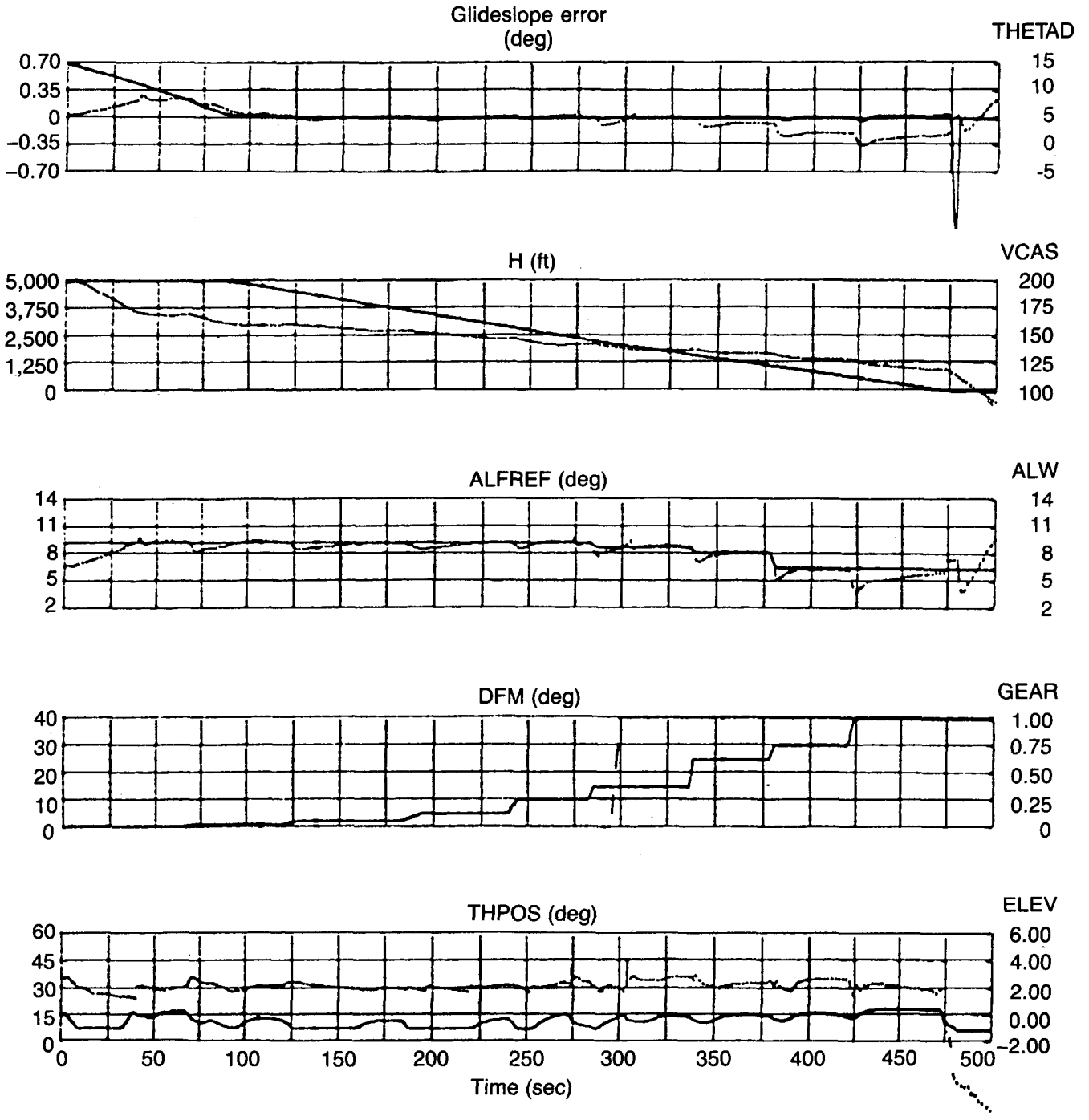

Figure 55. Glideslope Control Mode With Flap Extension and Touchdown

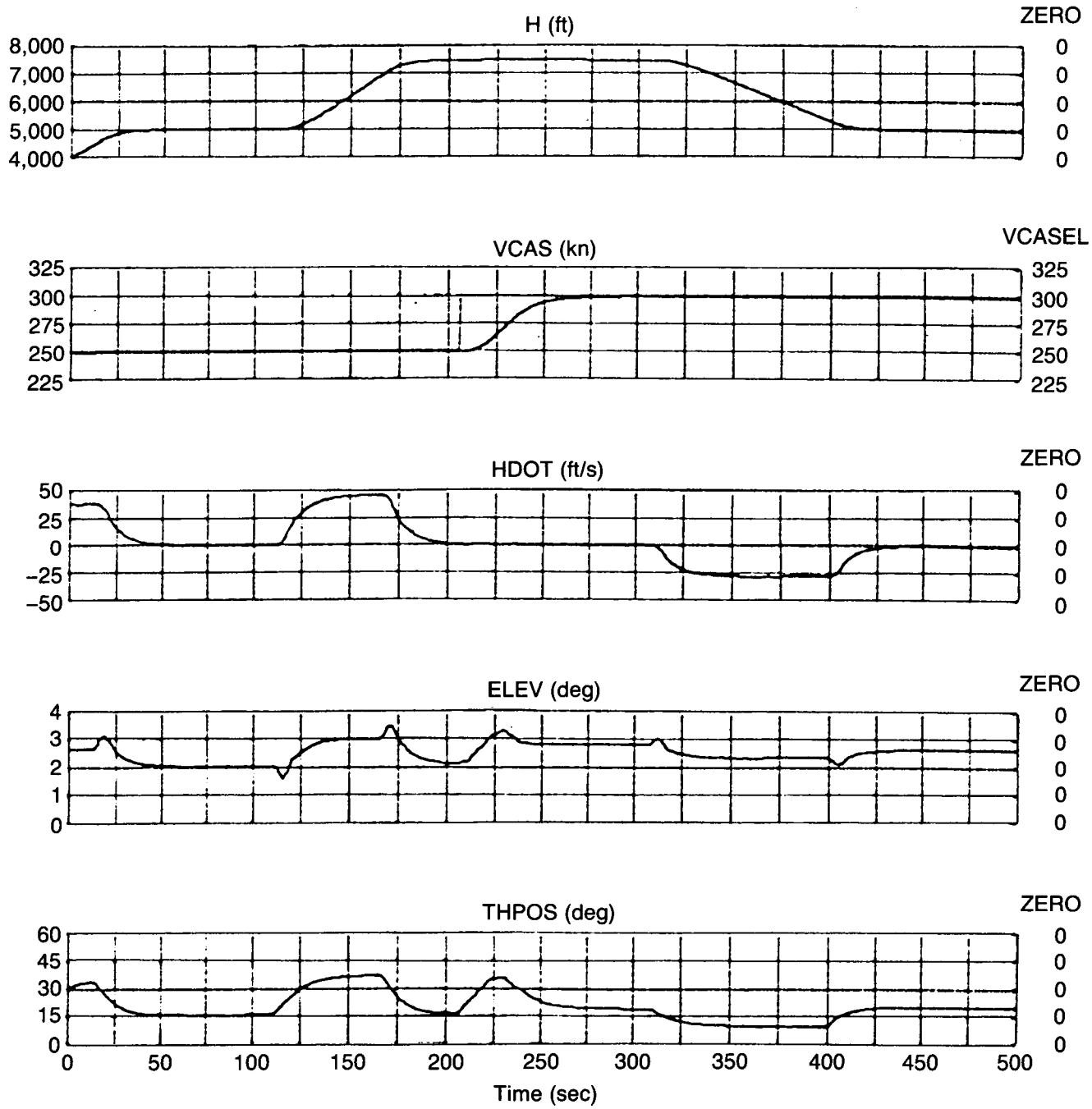

Figure 56. Vertical Path Mode

C-2

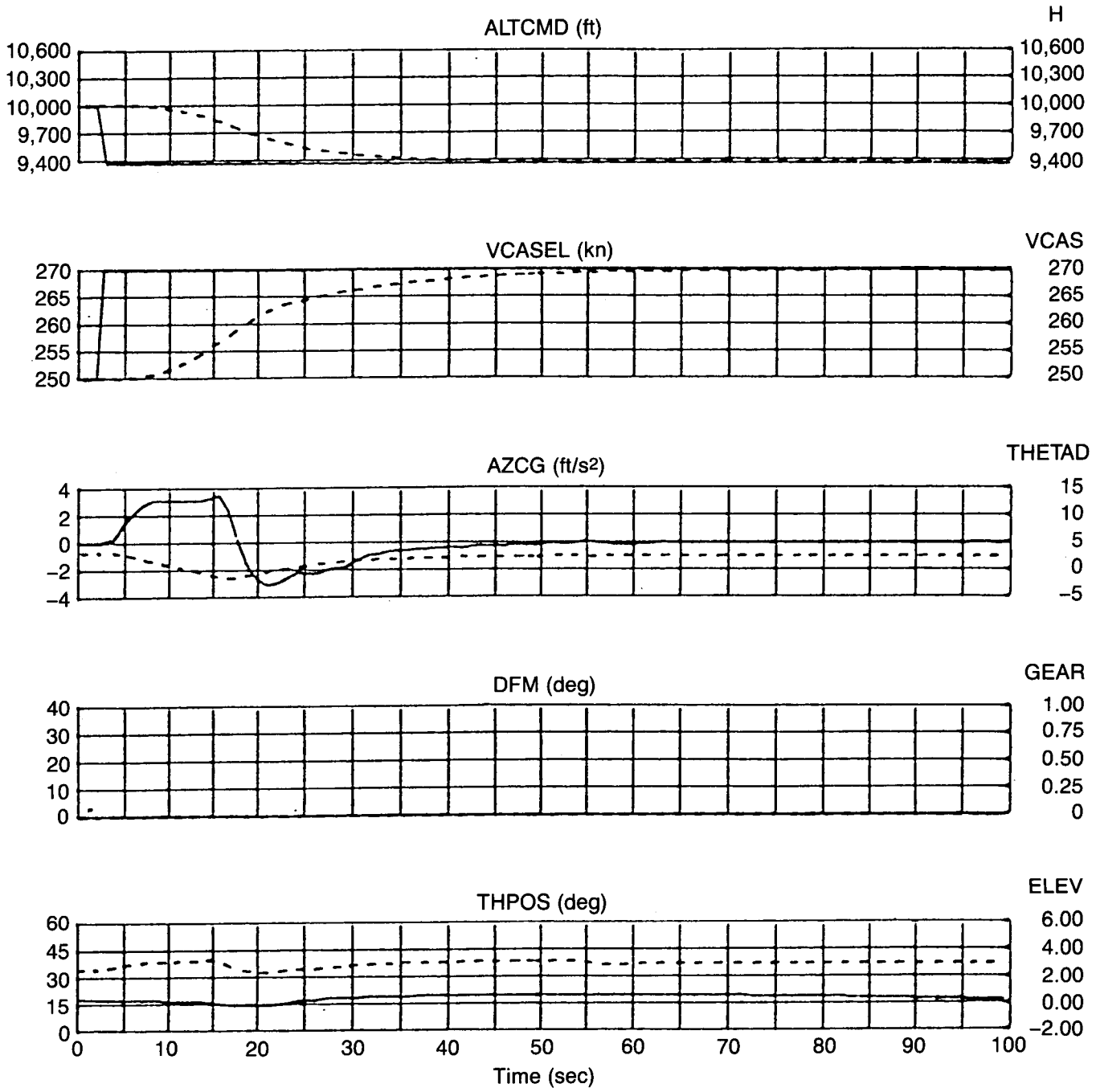

Figure 57. Double Maneuver ($\Delta\epsilon = 0$)

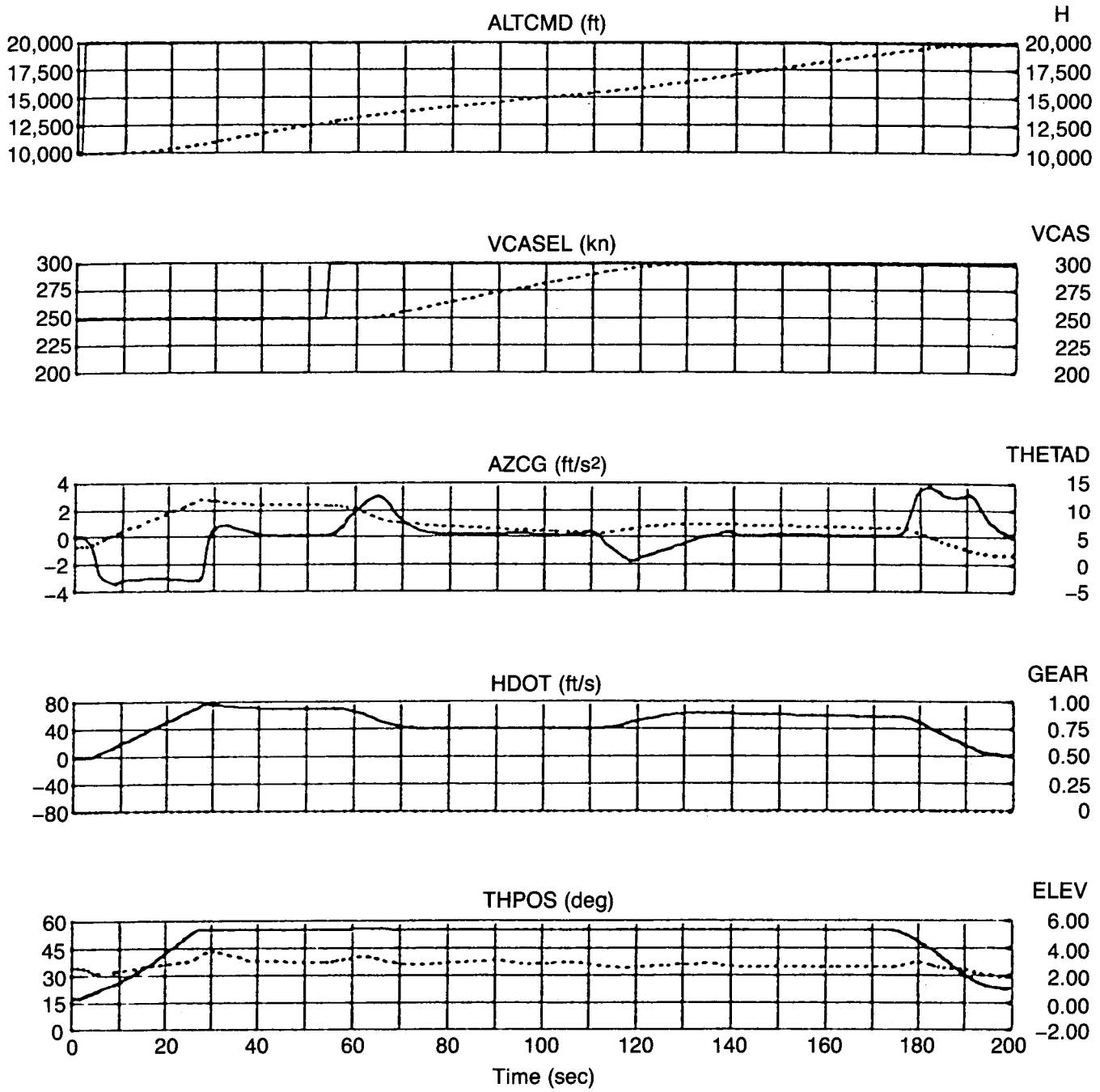

Figure 58. Climb and Accelerate Maneuver

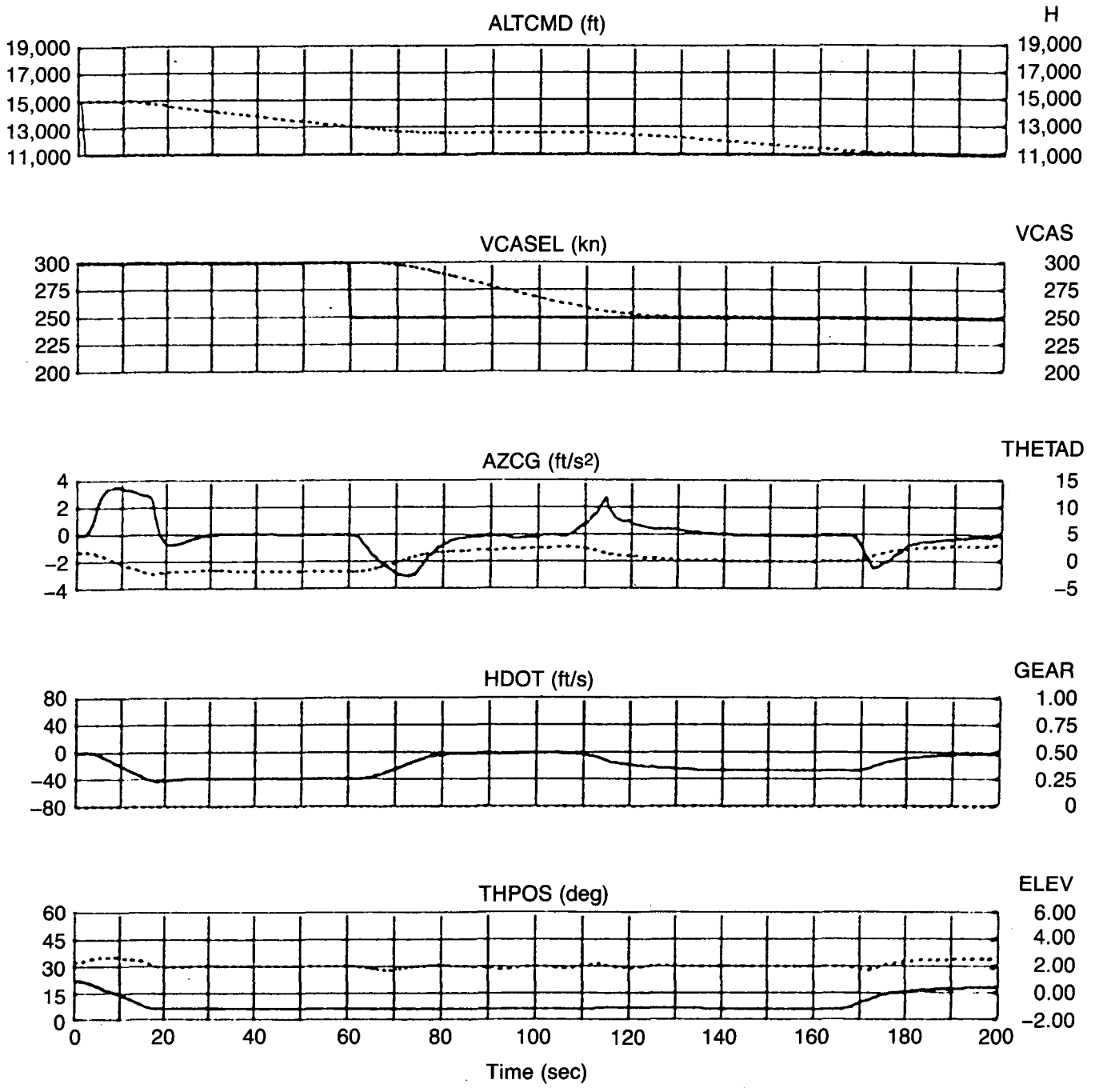

Figure 59. Descent and Deceleration Maneuvers

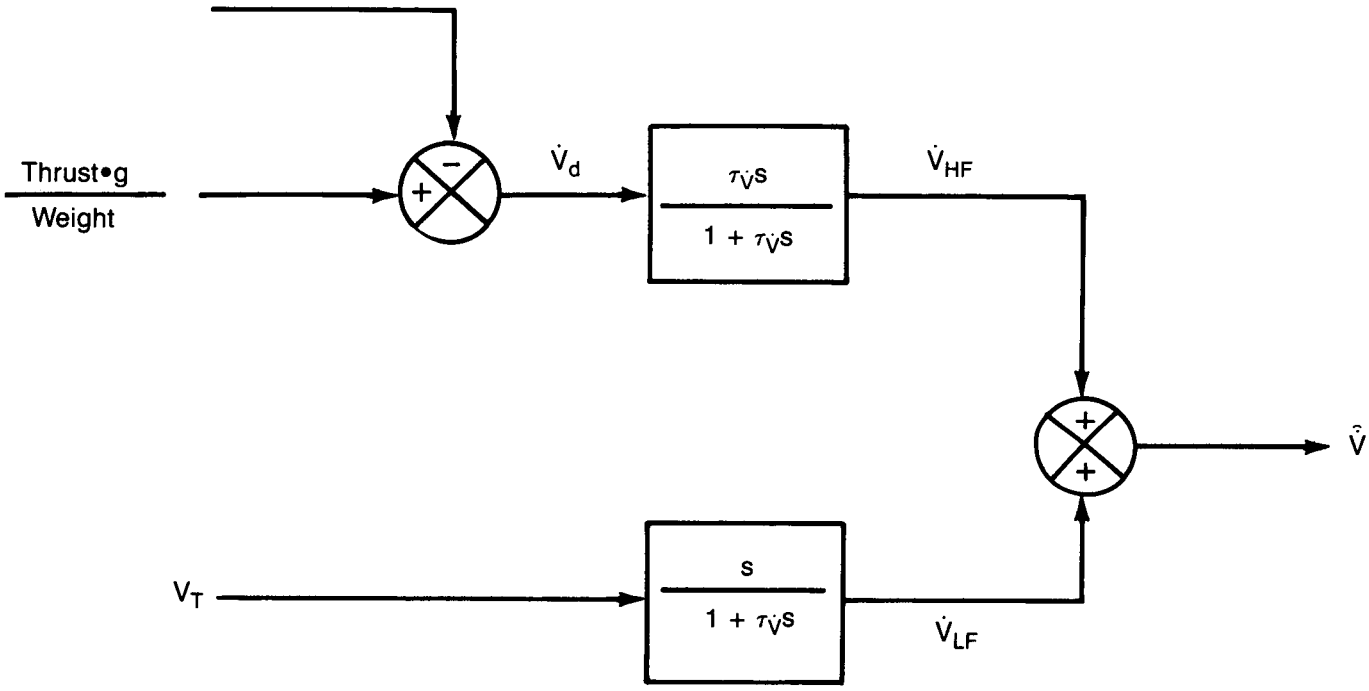

Figure 60. Complementary Filter To Provide Derivative Feedback Signal

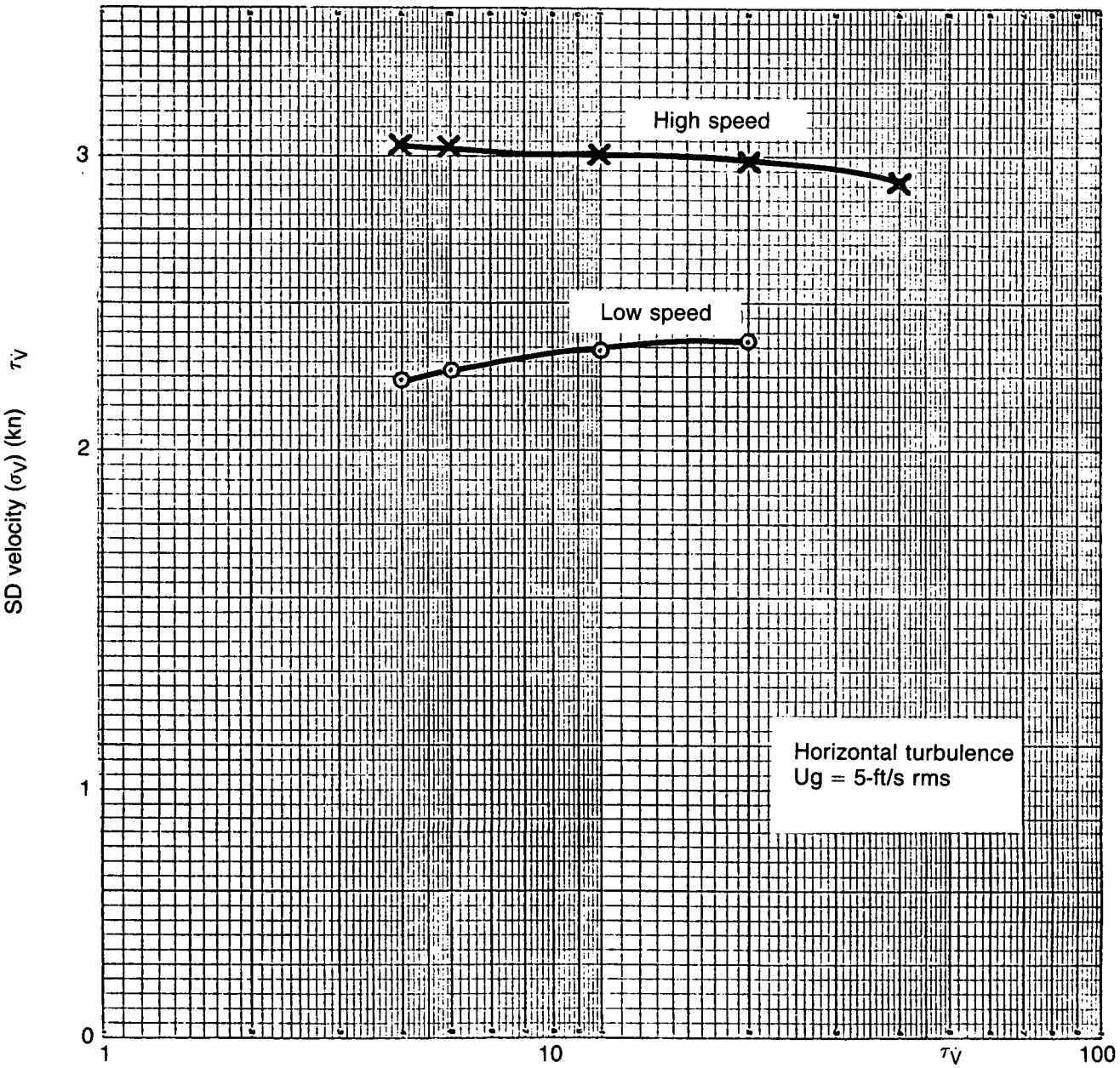

Figure 61. SD Velocity Against $\tau_{\dot{V}}$

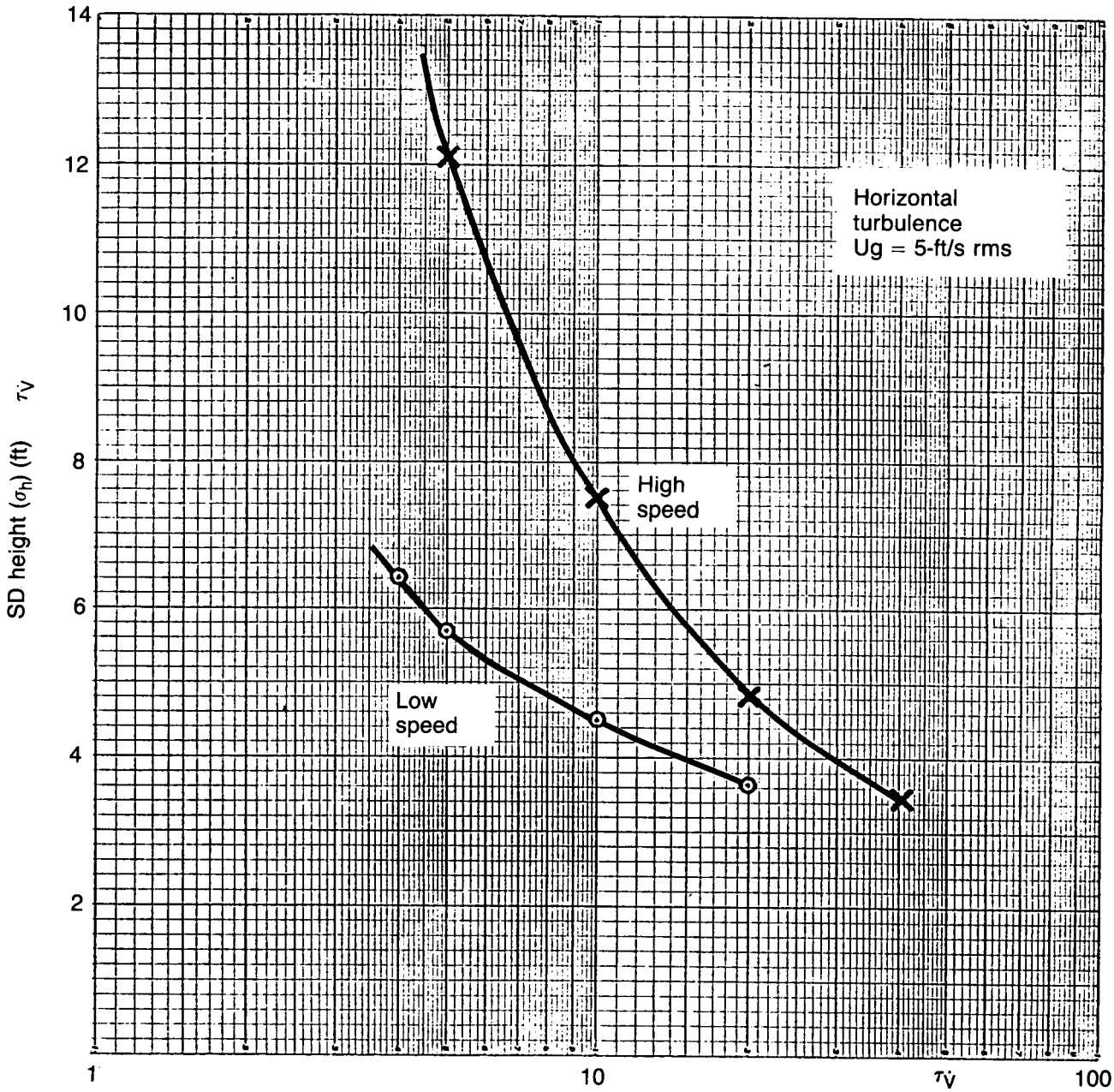

Figure 62. SD Height Against $\tau_{\dot{V}}$

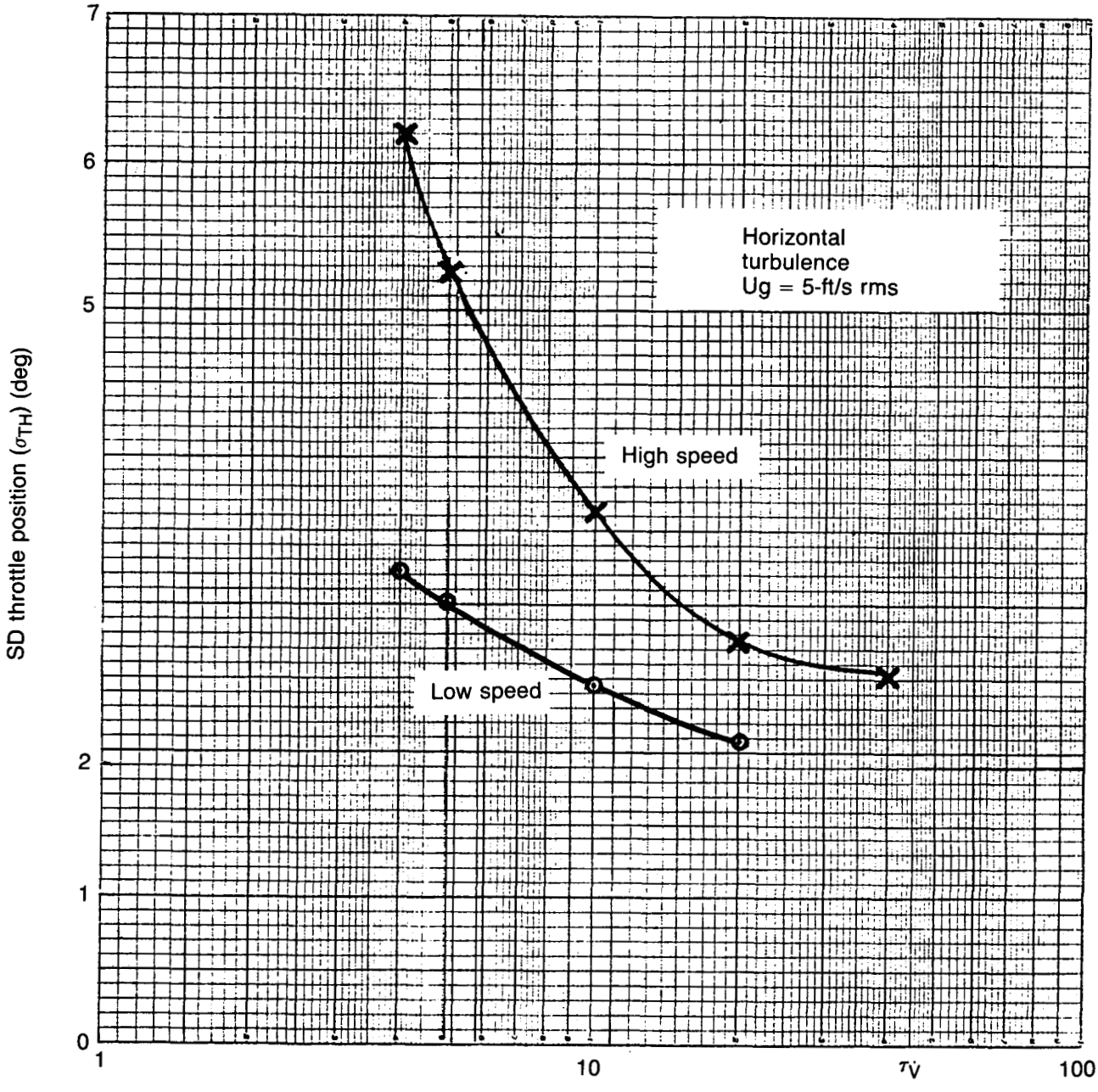

Figure 63. SD Throttle Position Against $\tau_{\dot{V}}$

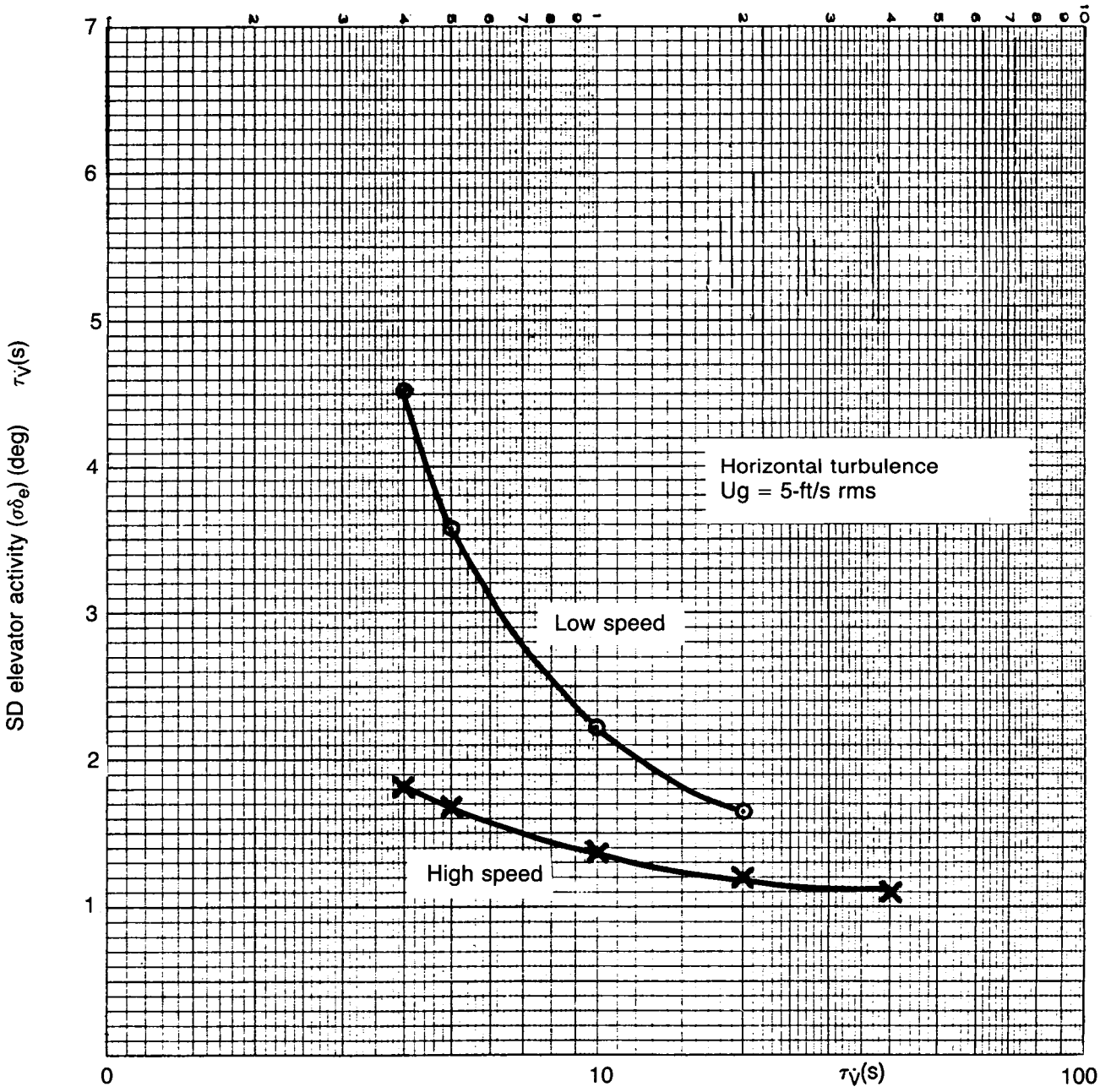

Figure 64. SD Elevator Activity Against $\tau_{\dot{V}}$

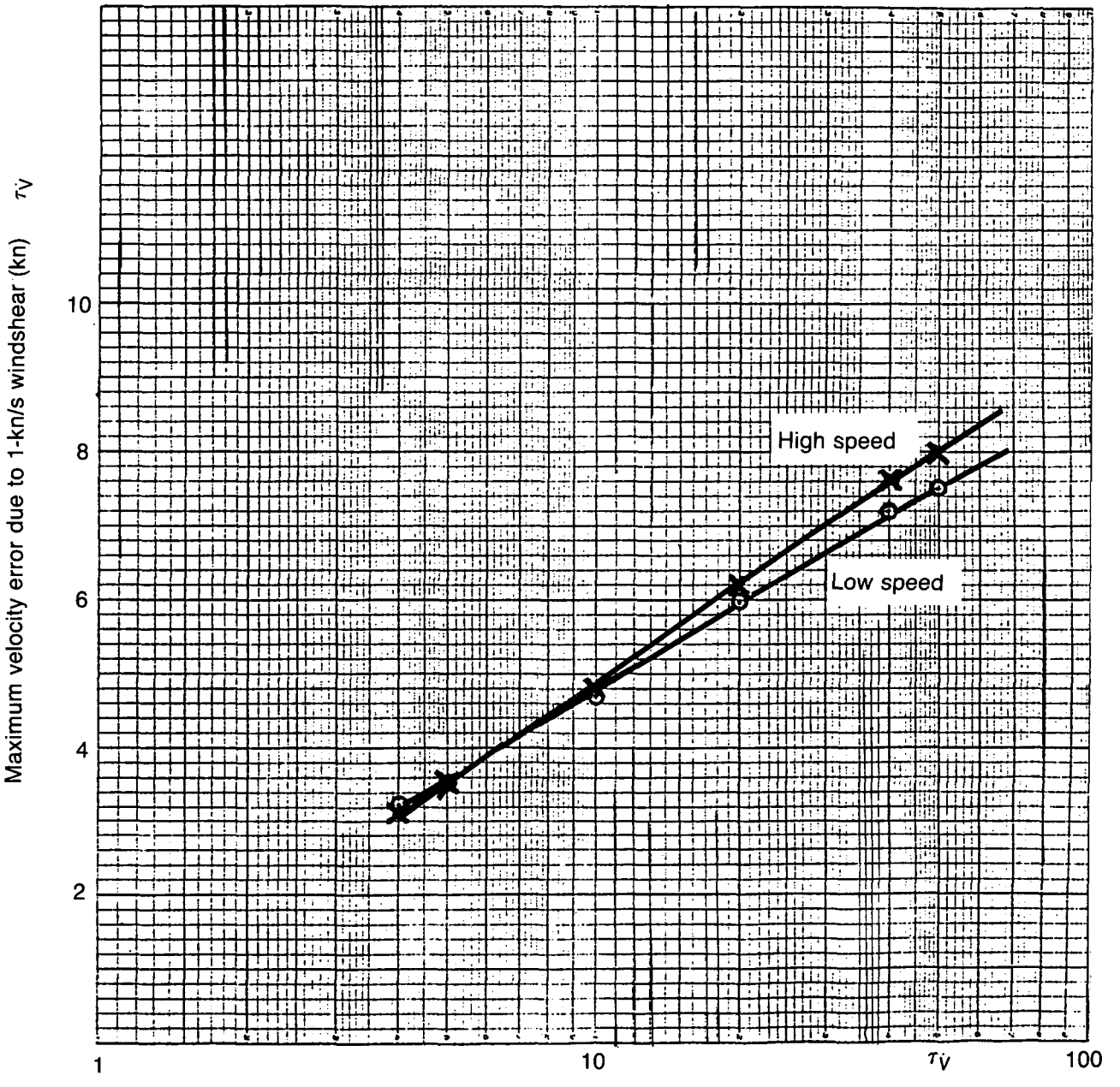

Figure 65. Maximum Velocity Error Due to Windshear Against $\tau_{\dot{V}}$

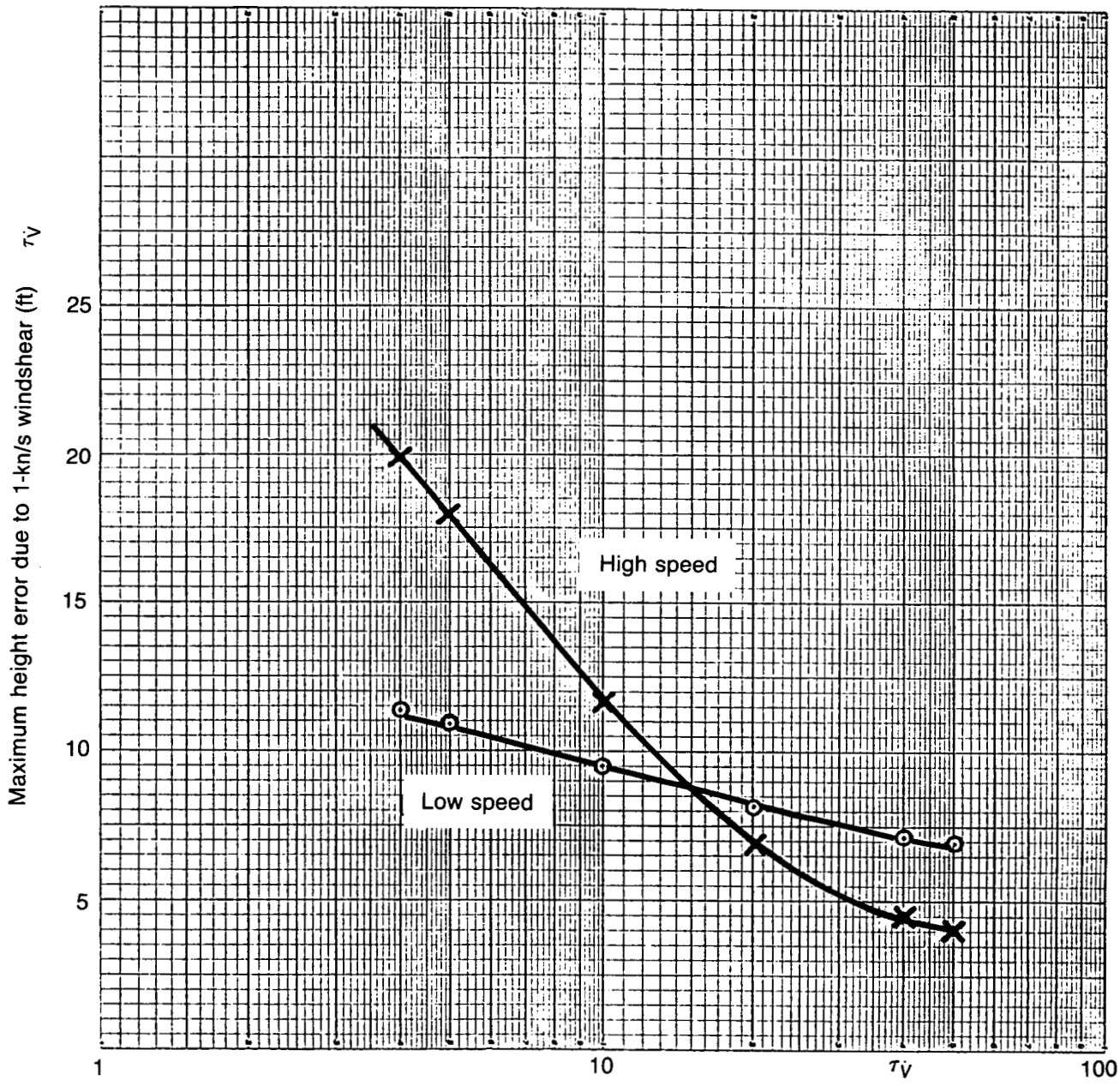

Figure 66. Maximum Height Error Due to 1-kn/s Windshear Against $\tau_{\dot{V}}$

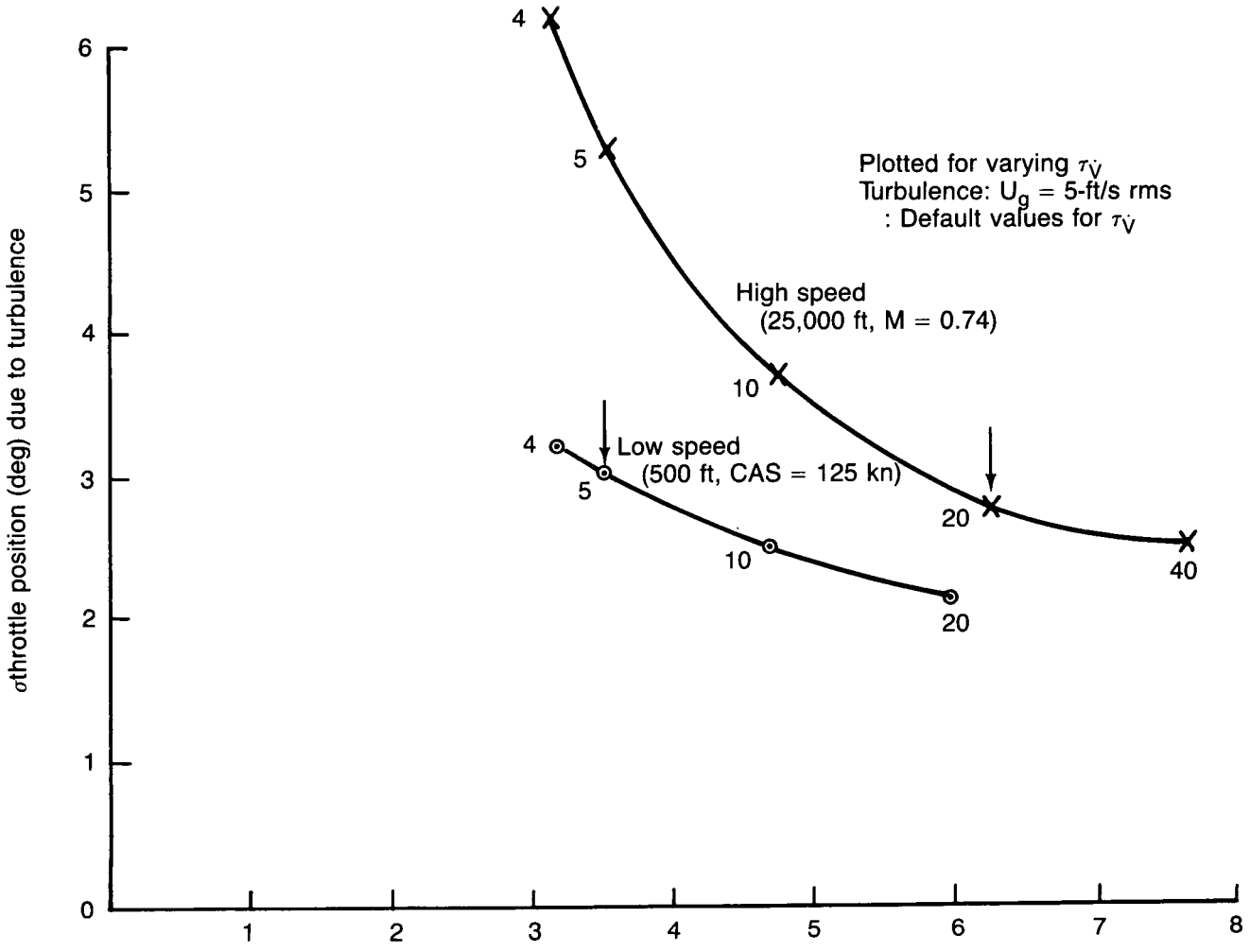

Figure 67. Maximum Velocity Error Due to 1-kn/s Windshear (kn)

1. Report No.	2. Government Accession No.	3. Recipient's Catalog No.
NASA CR-4131		

4. Title and Subtitle	5. Report Date
Integrated Autopilot/Autothrottle Based on a Total Energy Control Concept: Design and Evaluation of Additional Autopilot Modes	April 1988
	6. Performing Organization Code
7. Author(s)	8. Performing Organization Report No.
Kevin R. Bruce	
9. Performing Organization Name and Address	10. Work Unit No.
Boeing Commercial Airplane Company P.O. Box 3707 Seattle, WA 98124	505-45-33-04
	11. Contract or Grant No.
	NAS1-16300
	13. Type of Report and Period Covered
12. Sponsoring Agency Name and Address	Contractor Report
National Aeronautics and Space Administration Langley Research Center Hampton, VA 23665-5225	14. Sponsoring Agency Code

15. Supplementary Notes

NASA Langley Technical Monitor: J. F. Creedon
Boeing Technical Supervision: A. A. Lambregts
Boeing Contract Manager: R. L. Erwin, Jr.

16. Abstract

An integrated autopilot/autothrottle system was designed using a total energy control design philosophy. This design ensures that the system can differentiate between maneuvers requiring a change in thrust to accomplish a net energy change.

This report defines the system design, the development of the system, and a summary of simulation results.

17. Key Words (Suggested by Author(s))	18. Distribution Statement
Integrated Autopilot/Autothrottle Total Energy Control Autopilot Design	Unclassified-Unlimited Subject Category 08

19. Security Classif. (of this report)	20. Security Classif. (of this page)	21. No. of Pages	22. Price
Unclassified	Unclassified	112	A06

FORM 0005

For sale by the National Technical Information Service, Springfield, Virginia 22161

NASA-Langley, 1988